DISSERTATION / DOCTORAL THESIS

Titel der Dissertation /Title of the Doctoral Thesis

„Hybrid asymptotics and numerics of traveling water waves“

verfasst von / submitted by

Dipl.-Ing. Dominic Christian Amann, BSc

angestrebter akademischer Grad / in partial fulfilment of the requirements for the degree of

Doktor der Naturwissenschaften (Dr. rer. nat.)

Wien, 2021 / Vienna 2021

Studienkennzahl lt. Studienblatt / degree programme code as it appears on the student record sheet:	UA 796 605 405
Dissertationsgebiet lt. Studienblatt / field of study as it appears on the student record sheet:	Mathematik
Betreut von / Supervisor:	Univ.-Prof. Dipl.-Ing. Dr. Otmar Scherzer
Betreut von / Supervisor:	Konstantinos Kalimeris, Privatdoz. BA PhD

Abstract

Based on well-established analytical approaches, we study numerical methods to compute traveling water waves, which for example model Tsunami waves on the open sea. This category of waves, also known as steady periodic waves, are only affected by gravity and can be considered in a two dimensional framework. We are interested in their key properties like wave height and for which parameter sets such waves can be formed. Of particular interest are vorticity, which measures the local rotation of the fluid velocity, and the existence and position of stagnation points, which are points where the horizontal fluid velocity is equal to the wave speed of propagation. Our numerical outcomes are in agreement with the existing analytical results and in some cases, they lead to speculation of further analytical properties of waves.

This cumulative thesis is split into three parts. First, we present some of the more recent numerical approaches to compute traveling waves as well as the corresponding results. We give a short overview of their analytical background and discuss the similarities and limitations, in particular related to vorticity and stagnation points.

In the second part we analyze a numerical continuation approach, where we compute families of solutions starting from linear approximations of small amplitude waves. Numerical examples illustrate the performance of the algorithm for flows of constant vorticity, where we compare the results with known literature. We extend this approach from existing findings to compute new qualitative and quantitative results considering the characteristics of the water waves both for constant and variable vorticity.

Finally, the last part of the thesis considers a constructive algorithm based on asymptotic expansions for waves without stagnation points. We present a numerical implementation of this algorithm, which was previously only considered analytically, that verifies the analytical results and, indeed, computes large amplitude waves. Furthermore, we introduce a modification of the existing analytical procedure, which allows the computation of waves with variable vorticity.

Zusammenfassung

Basierend auf etablierten analytischen Methoden, untersuchen wir numerische Methoden zur Berechnung von wandernden Wasserwellen, welche beispielsweise Tsunami-Wellen auf offener See modellieren. Diese Klasse von Wellen, auch genannt periodische dauerhafte Wellen, werden von der Erdanziehungskraft beeinflusst und sind zweidimensional. Wir betrachten deren Kerneigenschaften, beispielsweise Höhe, und unter welchen Voraussetzungen solche Wellen existieren und entstehen können. Von besonderem Interesse ist die Wirbelstärke, eine Maßeinheit für lokale Rotation der Fluidgeschwindigkeit, sowie Flautepunkte, das sind Punkte im Fluid, an denen die horizontale Geschwindigkeit mit der Wellengeschwindigkeit übereinstimmt. Unsere numerischen Erkenntnisse stimmen mit bestehenden analytischen Resultaten überein und in führen in manchen Fällen zu Spekulationen über neue analytische Eigenschaften der Wellen.

Diese kumulative Arbeit setzt sich aus drei Teilen zusammen. Zunächst betrachten wir einige aktuelle numerische Verfahren zur Berechnung von wandernden Wasserwellen und deren Resultate. Wir geben einen Überblick über die Verfahren und deren analytische Grundlagen, ihre Gemeinsamkeiten und Limitationen, insbesondere bezüglich der betrachteten Wirbelstärke und ob Flautepunkte berücksichtigt werden können oder nicht.

Im zweiten Teil analysieren wir ein numerisches Fortsetzungsverfahren, bei dem wir gesamte Familien von Lösungen, ausgehend von linearen Approximationen von Wellen mit geringer Höhe, berechnen. Die Leistungsfähigkeit des Ansatzes wird mit Hilfe von numerischen Beispielen für konstante Wirbelstärke, für welche Ergebnisse aus der Literatur vorliegen, illustriert. Wir erweitern das Verfahren, insbesondere die Handhabe nahe Flautepunkten, was zu neuen Ergebnissen von Wellen mit konstanter und nicht konstanter Wirbelstärke führt.

Schlussendlich betrachten wir im letzten Teil ein konstruktives Verfahren basierend auf einer asymptotischen Expansion für Wellen ohne Flautepunkte. Wir präsentieren für diesen Ansatz, der zuvor nur analytisch betrachtet wurde, eine numerische Implementierung, die die analytischen Ergebnisse bestätigt und zur Berechnung von Wellen mit größer Wellenhöhe geeignet ist. Abschließend erweitern wir sowohl das analytische als auch das numerische Verfahren, was die Betrachtung von nicht konstanter Wirbelstärke ermöglicht.

Acknowledgments

I want to thank, first of all, both my advisors Otmar Scherzer and Konstantinos Kalimeris, for their advise and unwavering support and encouragement. I thank my RICAM coworkers who made me feel welcome at all times and the office and IT staff who always had time and expertise to help with any problem. Thank you also to Andreas Binder and MathConsult for their support and the opportunity to work there.

Lastly, I thank my family, friends and in particular Elisabeth, for enriching my life in uncountable ways.

Funding: The author is supported by the project *Computation of large amplitude water waves* (P 27755-N25), funded by the Austrian Science Fund (FWF), the Johann Radon Institute for computational and applied mathematics (RICAM), MathConsult GmbH and the State of Upper Austria.

Contents

1 Introduction

Water waves and their characteristics have been studied for centuries and continue to be a research field that raises much interest. One reason for the vastness of the field is the variety of possible questions, as well as the importance of understanding the related physical phenomena. One may be interested in surface patterns, maximal amplitudes, flow patterns below the water surface, the influence of obstacles like ships or to predict when wave breaking occurs. Furthermore, waves, as they occur on the open sea, can develop for a variety of reasons, from internal waves that are caused by water layers with different densities, to planetary waves that are governed by the pull of the moon and the earth's rotation. Lastly, waves can change their behavior drastically with their scale or the considered regime. For example, consider a wave that is caused by a disturbance somewhere in the ocean, then it travels as a steady wave across the sea before it reaches shallow coastal lands where it finally breaks. These three phases, while being interconnected, have to be considered separately, the problems of interest are in general too complex and can't be described by a single all-encompassing model.

The starting point of all further considerations is the construction of such a model, a system of equations describing the underlying physical processes. Understanding the problem is important in deriving the model, as it helps to decide which physical parameters can be safely neglected and which ones are relevant. This model can then be studied or used to do numerical simulations, two tightly interconnected fields that both have to be considered to gain a more complete understanding of the problem.

Theoretical considerations can prove existence, uniqueness, regularity and other properties of waves in different regimes. Linear approximations are a well established tool for studying many water-wave questions. Due to the non linear nature of waves, in particular those of moderate and large amplitude we are interested in, such linear approaches are not sufficient and other techniques, such as asymptotic expansions or favorable reformulations, are necessary.

These results, such as regularity, enable us to apply numerical computation schemes to the model. We can compute features of interest, such as maximal amplitudes of waves, or verify that the model is in agreement with experimental data. Furthermore, numerical simulations can lead to new questions and theories to be studied. The insight gained by both theoretical and experimental considerations can motivate improved models that better depict the physical phenomenon.

In this work we consider traveling water waves, different possible models and their properties as well as how they can be computed numerically. Traveling waves are also called steady periodic waves and are wave trains, see Figure 1.1, that are only affected by gravity. The source of such waves are local disturbances of the level water

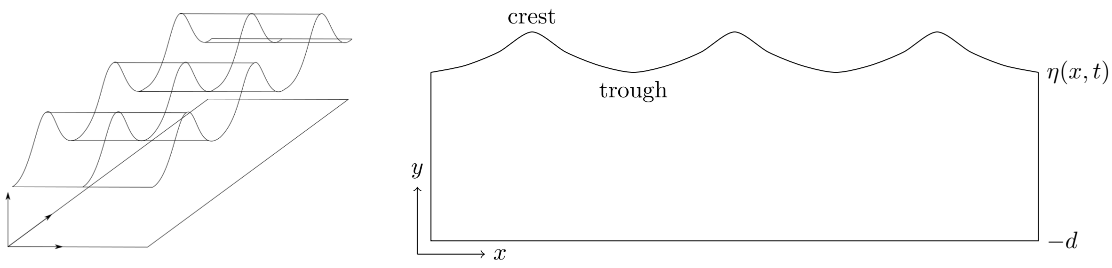

Figure 1.1: Traveling water wave

which is then restored by gravitational forces. Examples for such gravity waves are wind waves, where the sea has been locally raised by the wind, and Tsunamis. Thus, to better prepare for such waves, it is of importance to better understand their key properties, like maximum speed or amplitude or for which parameter set they can form. For a general introduction and studying of water waves, where also other waves such as solitons or breaking waves are considered, we refer to [14, 47].

1.1 Governing equations of traveling water waves

In this section we present a derivation of the governing equations for traveling water waves as well as some of their key properties and we justify the assumptions we make. While some of these equations stay true for more general waves, traveling water waves have some characteristics that simplify the model problem considerably.

The core problem is to determine the fluid velocity $\mathbf{u}$ and the free surface η of the wave. Traveling waves are **two dimensional**, which means their shape is identical orthogonal to the direction of propagation, and travel at a constant speed c. It is therefore sufficient to analyze a vertical cross-section of the flow, parallel to the direction of wave propagation and a two dimensional velocity field $\mathbf{u} = (u, v)$. For the considered large waves at open sea, we furthermore assume a flat bed at depth $-d$, see Figure 1.1, where the depth is chosen such that the free surface oscillates around zero. The highest part of the wave is called the crest and the lowest part is denoted as trough.

We assume the water to be a continuum and **incompressible** with constant density ρ. Let V be a bounded domain with piece wise C^1 surface ∂V. Since mass cannot be created or destroyed, the rate of change of mass in V must be equal to the flow across its border ∂V, that is

$$\frac{d}{dt}\int_V \rho d\mathbf{x} = -\int_{\partial V} \rho \mathbf{u} \cdot \mathbf{n} ds_X$$

with fluid velocity $\mathbf{u}$ and outward unit normal vector $\mathbf{n}$. Due to the constant density, the term on the left hand side is zero and the Gauss law gives us

$$0 = \int_V \nabla \cdot \mathbf{u} d\mathbf{X}.$$

Since this holds for any volume V we get the equation of mass conservation

$$\nabla \cdot \mathbf{u} = 0. \tag{1.1}$$

Next we consider Newton's law of motion, again in a domain V with a piece wise C^1 boundary ∂V. It states that the rate of change of momentum, which is mass times acceleration, is equal to the applied force plus the rate of flow across ∂V. Traveling water waves are **gravity waves** which means that the only external force is gravity, that is $\mathbf{F} = (0, -g)$ with a positive constant g. Furthermore, we assume the medium to be **inviscid**. Then, the force acting on the fluid is the result of gravity, which acts on the whole domain, and pressure P, which acts across the surface

$$\int_V \rho \mathbf{F} d\mathbf{X} - \int_{\partial V} P \mathbf{n} dS_X.$$

Rewriting this, using the divergence theorem, enables us to write down Newton's law of motion

$$\int_V \rho \frac{d}{dt} \mathbf{u} d\mathbf{X} = \int_V (\rho \mathbf{F} - \nabla P) d\mathbf{X},$$

where $\frac{d}{dt}\mathbf{u}$ is the total derivative of $\mathbf{u}$. This holds true for every domain V, which gives, after expanding the total derivative, the Euler equation of motion

$$\frac{\partial}{\partial t}\mathbf{u} + (\mathbf{u} \cdot \nabla)\mathbf{u} = -\frac{1}{\rho}\nabla P + (0, -g). \tag{1.2}$$

The considered traveling water wave problem has two boundaries, the free surface ξ and the flat bottom. The kinematic boundary condition states that the boundary of the fluid is always made up of the same particles. Let the boundary surface be described by the equation $S(\mathbf{X}, t) = 0$, then the kinematic boundary condition is formulated as $\frac{DS}{Dt} = \frac{\partial S}{\partial t} + u\frac{\partial S}{\partial X} + v\frac{\partial S}{\partial y} = 0$ with the fluid velocity $\mathbf{u} = (u, v)$. At the free surface we have $S(\mathbf{X}, t) = y - \xi(X, t)$ and at the flat bottom $S(\mathbf{X}, t) = y + d$, which gives us

$$v = \xi_t + u\xi_X \quad \text{on } y = \xi(X, t), \tag{1.3}$$
$$v = 0 \qquad\qquad \text{on } y = -d. \tag{1.4}$$

The dynamic boundary condition describes the effect of the atmosphere on the water surface. We assume **negligible surface tension**, which means that this effect is modeled by the constant atmospheric pressure P_{atm} acting on the surface

$$P = P_{\text{atm}} \quad \text{on } y = \xi(X, t) \tag{1.5}$$

Equations (1.1)–(1.5) fully describe the considered problem but can be simplified by eliminating the time variable. This is done by considering a moving reference frame $(x, y) := (X - ct, Y)$ which gives us a time independent free surface function

$\eta(X-ct) := \xi(X,t)$. This yields the mathematical formulation for the traveling wave problem to find the fluid velocity $\mathbf{u}$ and free surface η

$$
\begin{aligned}
\nabla \cdot \mathbf{u} &= 0 && \text{in } d < y < \eta(x), && (1.6)\\
\frac{\partial}{\partial t}\mathbf{u} + (\mathbf{u}\cdot\nabla)\mathbf{u} &= -\frac{1}{\rho}\nabla P + (0,-g) && \text{in } d < y < \eta(x), && (1.7)\\
v &= (u-c)\eta_x && \text{on } y = \eta(x), && (1.8)\\
v &= 0 && \text{on } y = -d, && (1.9)\\
P &= P_{\text{atm}} && \text{on } y = \eta(x). && (1.10)
\end{aligned}
$$

The occurring constants are summarized in table 1.1. In the remainder of this section we present two properties of the flow that are of significance for the presented computation methods, vorticity and flow reversal.

Constant	Description
d	mean depth of the domain
ρ	fluid density
g	gravitational constant
P_{atm}	atmospheric pressure
c	wave speed

Table 1.1: Constants

Vorticity, defined as the curl of $\mathbf{u}$, measures the local rotation of fluid velocity. The vorticity has significant influence on the mathematical analysis of the wave problem, the current inside the fluid domain, and the surface wave pattern. An important property is that flows with zero vorticity, also called irrotational flows, preserve their irrotationality over time. One possible source of irrotational flows is the existence of non-uniform flat surface flows *prior* to the wave formation. An illustration of the impact of vorticity, see [17, 18], is that periodic traveling waves with a flat bed, constant vorticity and no flow-reversal must be symmetric if the wave profile is monotone between successive crests and troughs. This means that an underlying non-uniform current of constant vorticity does not break the symmetry of irrotational wave trains. A general discussion of the physical implications of rotational flow can be found in [14] and [73].

The assumed absence of **flow reversal** mentioned above means that that the wave speed is greater than the horizontal velocity everywhere inside the wave, that is $u < c$. The wave speed is defined as the ratio of wavelength to wave period, which is the time it takes for two consecutive crests to pass a fixed point. This is an important assumption in the derivation of many models presented in this work, such as the one discussed in Chapter 3 and 4. A consequence of this assumption is that **stagnation points**, those are points where the horizontal velocity is equal to the wave speed, cannot be modeled by these formulations. Wave breaking, where the horizontal fluid velocity even exceeds the wave speed, is also excluded from considerations by this assumption. Stagnation points are an important limit case and even though we can't compute waves that include them, by computing waves close to stagnation and studying their properties, we can make conclusions about when and where they appear. In particular, the effects of a given vorticity on the existence and position of stagnation points is of interest.

1.2 Contribution

The goal of this thesis is two-fold. Firstly, we derive and study a numerical continuation and an asymptotic expansion scheme for the system (1.6)–(1.10). Secondly, we give an overview of and contextualize some approaches for the computation of traveling water waves with a focus on numerical computations.

As already stated there exists a vast body of work that relates to traveling water waves. Before we present some approaches in more detail, we give a short overview on some recent works related to traveling water waves. In [69], a shape optimization approach for η, that modifies the stream formulation such that it allows for non flat bottom, is presented. One main contribution of this work was the consideration of a non smooth surface η, which allows for waves with peaks. An integral formulation and its numerical solutions are considered in [55, 56]. In [46] the constant vorticity case for shallow water waves (those are waves that are long in relation to their depth) is studied by modifying the Korteweg-de Vries equation. The existence of solution for general vorticity with a fixed mean depth is presented in [40] by introducing and studying a novel formulation of the problem. A whole field of study in itself is the relationship of the pressure at the bottom and the form of the wave surface. The existence, uniqueness and form of such mappings under different assumptions is studied in [41, 52, 62].

1.2.1 Methods

The contributions presented in this work concern an analytical reformulation of (1.6)–(1.10) as derived in [22]. First, we introduce the stream function

$$\psi_x = -v, \qquad \psi_y = u - c$$

which is defined up to a constant. Let $\gamma = \Delta\psi$ be the vorticity which can be understood as the non zero part of the curl for a fluid with zero velocity in the third dimension. Due to the boundary condition (1.9) ψ is constant on the flat bottom and the boundary condition (1.8) simplifies to the statement that the tangential derivative of ψ along η is zero, thus ψ is constant at the free surface. Setting the additive constant of the stream function such that ψ is 0 at the bottom, the value of ψ at the free surface becomes

$$-p_0 = -\int_{-d}^{\eta(x)} (u(x,y) - c)dy$$

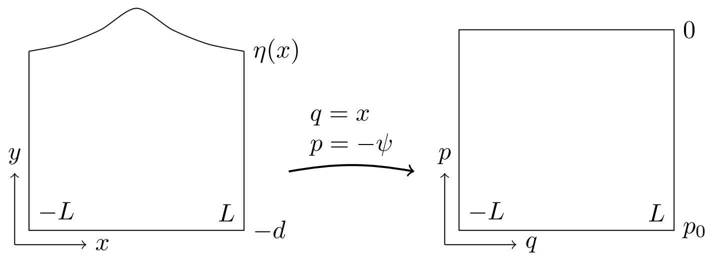

Figure 1.2: Dubreil-Jacotin transformation

which does not depend on x, for a proof see [21], and is called the relative mass flux. Now, the system can be reformulated as the free boundary problem

$$\begin{aligned} \Delta\psi &= \gamma && \text{in } -d < y < \eta(x), \\ |\nabla\psi|^2 + 2g(y+d) &= Q && \text{on } y = \eta(x), \\ \psi &= 0 && \text{on } y = \eta(x), \\ \psi &= -p_0 && \text{on } y = -d, \end{aligned}$$

where Q is a constant that incorporates the athmospheric pressure and the hydraulic head derived from the Euler equation (1.7). It is a constant that can be used to describe the branches of solution we will compute.

In a second step, one major difficulty of this problem, the free boundary, can be eliminated by applying a semi-hodograph transformation, namely the Dubreil-Jacotin transformation, see Figure 1.2 [31]. Introducing the mapping $q = x$ and $p = -\psi$ and considering the height function $h = y + d$ in the mapped domain, the free surface problem is reformulated as a nonlinear fixed-domain system of equations. Then, the problem is to determine $Q \in \mathbb{R}$ and a periodic, even function h satisfying

$$(1 + h_q^2)h_{pp} - 2h_p h_q h_{qp} + h_p^2 h_{qq} - \gamma(-p)h_p^3 = 0 \quad \text{in } R, \tag{1.11}$$

$$1 + h_q^2 + (2gh - Q)h_p^2 = 0 \quad \text{for } p = 0, \tag{1.12}$$

$$h = 0 \quad \text{for } p = p_0. \tag{1.13}$$

for a fixed rectangle domain R, constant p_0 and given vorticity function γ. Note that the mean depth d does not appear in this formulation, but it can be recovered by

$$d = \frac{1}{2L}\int_{-L}^{L} h(q,0)dq.$$

We note that this transformation requires the assumption that there is no flow reversal in the fluid, that means the velocity of fluid particles must everywhere be slower than the wave speed c. This assumption also excludes stagnation points, which are defined as points where the two velocities are equal, thus the fluid particle stays at the same spot of the wave. Other works that considered this formulation or derivations thereof are [6, 28, 46, 64].

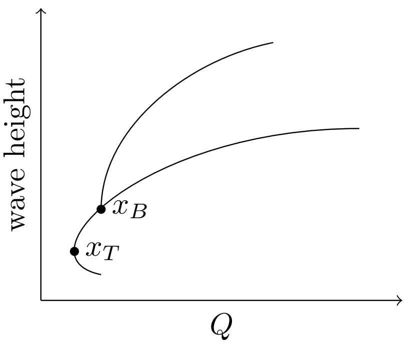

Figure 1.3: Bifurcation

Note that the system of equations (1.11)-(1.13) can have multiple solutions or none at all depending on the choice of the parameter parameter Q, thus we study the solutions by implementing analytical and numerical techniques established in **bifurcation** theory. By varying the parameter Q one can find connected curves of solutions, see Figure 1.3. Note that similar bifurcation considerations for the original problem (1.6)–(1.10) are possible, then the bifurcation parameters could for example be d or P_{atm}. Points of particular interest are turning points, where there are no solutions below a certain value Q_T, but multiple solutions above, and bifurcations points, where multiple solutions branches meet. One important branch of solutions we consider are waves whose flow occurs in streamlines which are parallel to the flat bottom, the so-called **laminar waves**. These flows, which have a flat surface η, can be computed analytically and form the starting point for many computational considerations. In this work we are interested in genuine waves, namely in waves with non-zero amplitude, in contrast to the above-mentioned laminar waves. To bifurcate to a branch of non-laminar waves, one must find the location of the bifurcation point as well as a good initial guess for the non-laminar wave to ensure convergence to a solution on the correct branch.

Chapter 2, published in [4], presents several schemes on how to solve (1.6)–(1.10) numerically in more detail. The discussed algorithms include two schemes based on a Dubreil-Jacotin transformation, a numerical continuation approach [6, 50, 51, 71] and an asymptotic expansion approach [5, 20, 48], as well as a non-local formulation [2, 7, 29, 39] and a conformal mapping approach [10, 58, 64]. All approaches solve their over determined systems by fixing all but one parameter of the equation, the free parameter can be varied to continue along the solution branch.

In Chapter 3, published in [6], we analyze a numerical continuation approach for the above described mathematical formulation, enriched with techniques appropriate to overcome some particular obstacles of this problem such as turning points, bifurcation points and stagnation points. The idea of reconstructing the bifurcation branch via numerical continuation techniques was introduced in [51].

The presented improvements include incorporating analytical results obtained in [22] such as the the explicit position of the bifurcation point, which is the starting point of our iterative numerical scheme. For different distributions of vorticity, this is obtained analytically through the methodology of [22], [21] and [49]. To bifurcate from the laminar wave and compute non-laminar flows, we use the favorable direction found analytically in [22], [20] and [49], for the different cases of vorticity. We further implemented these analytical results in order to realize numerical schemes for determining the bifurcation points and directions for general distributions of vorticity.

We use the flexibility of the numerical continuation scheme, such as variable step-size for the predictor, adaptive grid size for the numerical solution, and interchangeability of the continuation parameter, to derive an efficient and stable algorithm. The scheme is validated numerically against analytical data and by confirming expected convergence rates. Furthermore, adaptations of the numerical continuation technique that allow for the interchanging of the continuation parameter enable us to even use solutions for different model parameters, such as vorticity, as initial guesses. With this approach, we find new parts of the bifurcation diagram, i.e. to families of waves with novel characteristics.

Chapter 4, published in [5], discusses a different approach how to solve the nonlinear boundary value problem (1.11)–(1.13) that results from the partial hodograph transform. In [20] and [48], non-trivial solutions for this system were obtained analytically in the form of asymptotic expansions. A constructive algorithm was proposed for the computation of higher order terms of these asymptotic expansions. The above-mentioned algorithm provided a precise way to compute the expansions to all orders, but it involved tedious calculations, which limits computations to the first few order terms.

We provide a numerical implementation of the above algorithm, which allows us to numerically compute higher–order terms of the asymptotic expansions corresponding to waves of moderate and large amplitude. Central for this step is separation of variables which enables us to treat some terms analytically, thus only sets of 1D functions have to be computed numerically. For these, we present a numerical solution scheme and analyze it with respect to its unique solvability and convergence.

Finally, we extend the asymptotic expansion formulation presented in [48] to allow for non zero vorticity flows. This is done by introducing a novel transformation to the derivation of the model. These variable vorticity considerations are also extended to the numerical scheme.

1.2.2 Results and Achievements

In Chapter 3, we present an extension of a numerical continuation technique. We find agreement with already existing numerical results while observing additional wave characteristics close to stagnation. Previously, it was shown that below a critical vorticity γ_{crit}, this approach cannot compute waves of large height. We were able to circumvent certain critical stagnation points, thus finding new limiting waves near stagnation for constant vorticity, see Figure 1.4. Using this technique, we find different waves that share the same constant vorticity and both have a stagnation point at the bottom, see Figure 1.5. Furthermore, this technique indicates the existence of a wave that has two stagnation points, one at the crest and the second at the bottom below the crest, which is depicted in Figure 1.6. Lastly, the flexibility of the algorithm with

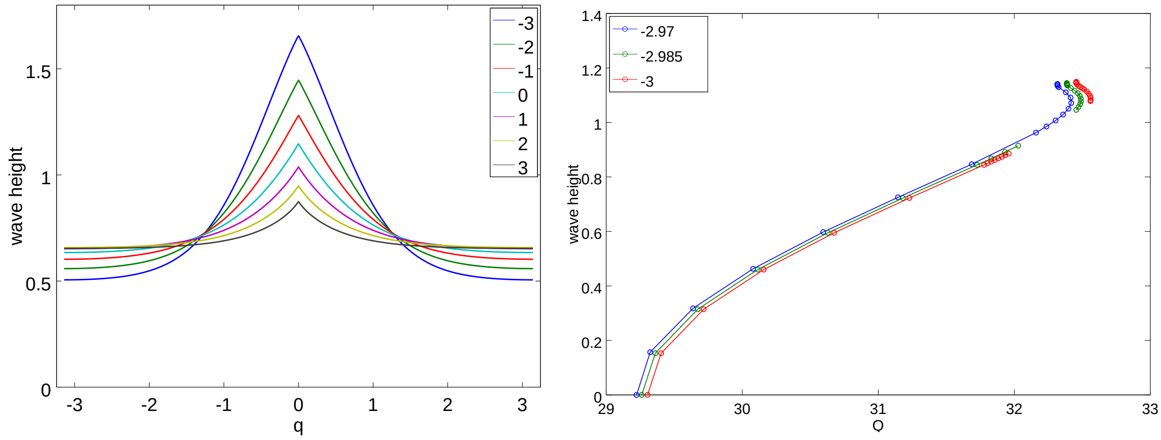

Figure 1.4: left: free surface of the maximal wave for different values of vorticity γ; right: bifurcation diagram for different values of γ, the gaps are due to stagnation points

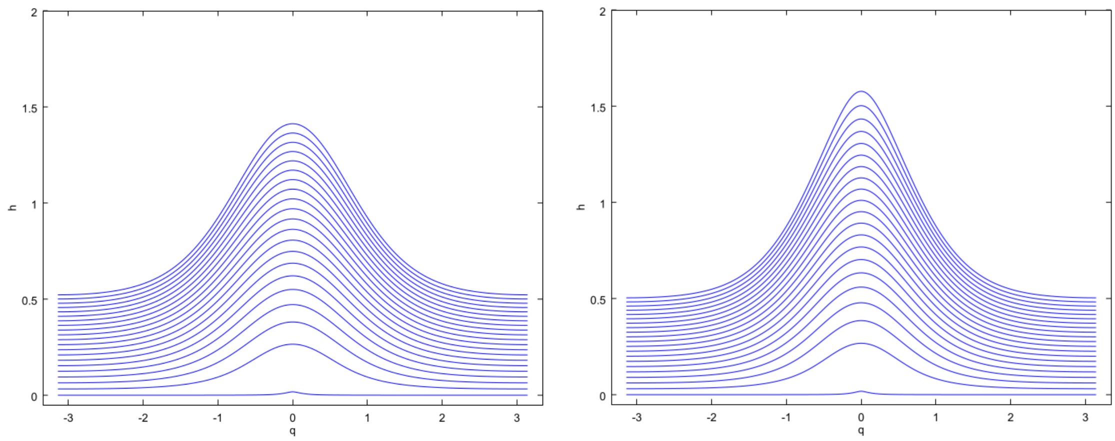

Figure 1.5: Streamlines for $\gamma = -3$ just below and above the gap.

regard to vorticity was shown, where we found waves of much larger amplitude with non-constant vorticity, see Figure 1.7 compared to existing numerical results.

In Chapter 4 we present and analyze a numerical computation scheme for an asymptotic expansion of the solution of the water wave problem. The performance of the numerical solver was verified and then used to compute much more expansion terms than was previously possible with the analytic approach, we were able to go from the first few terms to 31st term. Furthermore, modifications to the underlying asymptotic expansion where made to allow for variable vorticity, which was also realized with numerical experiments. Figure 1.8 for example shows wave profiles as well as the pressure at the flat bottom.

Chapter 2 contextualized the two presented approaches by presenting them alongside two other families of formulations and highlighting the similarities, advantages and drawbacks of each approach. Non local formulations, presented by means of the

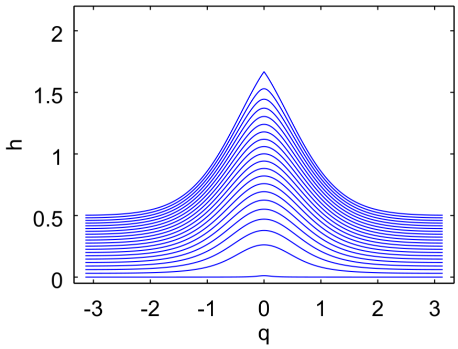

Figure 1.6: Streamlines of the maximal wave for $\gamma = -3.05$.

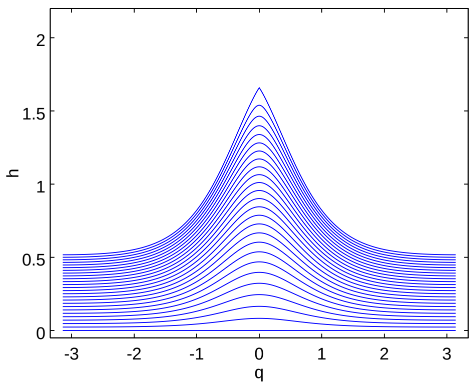

Figure 1.7: Streamlines of the maximal wave for $\gamma(-p) = -4\left(1 - \frac{p^2}{p_0^2}\right)$

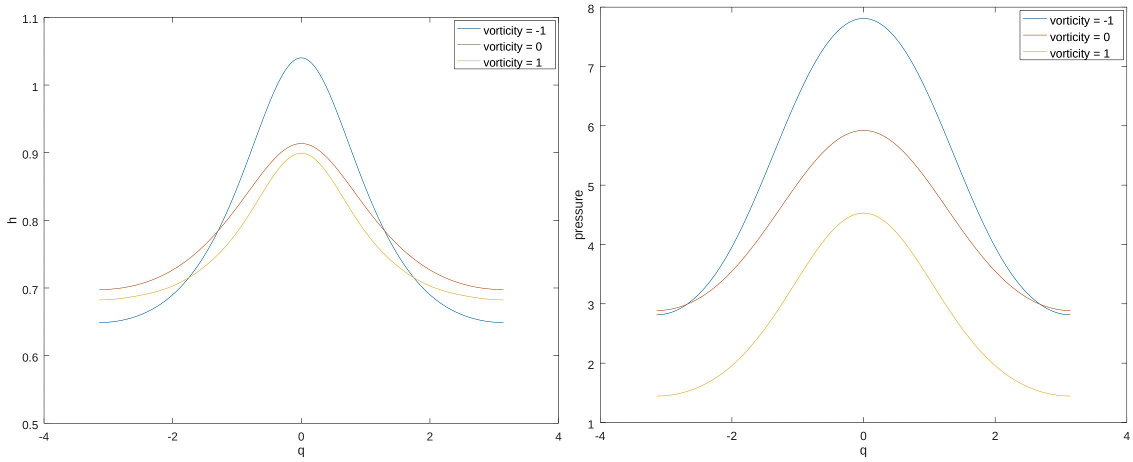

(a) Waveprofile

(b) Pressure at $p = p_0$

Figure 1.8: Comparison of three waves with constant but different γ. Waves are chosen such that the residual are similar, reference was $\gamma = 0$ with $Q = 22.05$.

example [29], allow for grid independent evaluation of streamlines and pressure even in the presence of stagnation points, but are more limited with regard to the considered vorticity compared to the approaches presented in Chapter 3 and Chapter 4. Conformal mappings, see for example [64], similarly, are not restricted by stagnation points and can be used to compute particle trajectory patterns, but are less flexible with respect to vorticity.

2 On recent numerical methods for steady periodic water waves

Dominic Amann

Abstract

The study of steady periodic water waves, analytically as well as numerically, is a very active field of research. We describe some of the more recent numerical approaches to computing these waves numerically as well as the corresponding results. The focus of this work is on the different formulations as well as their limitations and similarities.

2.1 Introduction

We consider steady water waves in two dimensions, travelling over a flat bottom with speed c and a free surface, under the influence of gravity. This means that in a frame moving along the wave with the same speed c, the velocity field, pressure and shape of the wave does not change over time. This model can be used to study plane waves by considering their cross section perpendicular to the wave crest. For a more detailed derivation of the model equations we refer to [14, 22].

This problem is governed by the Euler equations, find $u(x, y, t)$, $v(x, y, t)$ and $P(x, y, t)$ that solve

$$\begin{aligned} u_x + v_y &= 0 && \text{in } -d < y < \eta(x,t), \\ u_t + uu_x + vu_y &= -P_x && \text{in } -d < y < \eta(x,t), \\ v_t + uv_x + vv_y &= -P_y - g && \text{in } -d < y < \eta(x,t) \end{aligned} \tag{2.1}$$

with the free surface $\eta(x, t)$ and the depth d. The fluid domain is sketched on the left hand side of Figure 2.1. The boundary conditions for the pressure P and the velocity field (u, v) are the dynamic boundary condition

$$P = P_{\text{atm}} \quad \text{on } y = \eta(x,t) \tag{2.2}$$

which model the interaction on the free surface where negligible surface tension is assumed. Additionally we have kinematic boundary conditions, those are that the surface of the wave is always made up of the same particles and that the water can not penetrate the flat bottom. These boundary conditions are modelled by

$$v = \eta_t + u\eta_x \quad \text{on } y = \eta(x,t), \tag{2.3}$$

$$v = 0 \quad \text{on } y = -d. \tag{2.4}$$

Since we consider steady periodic waves, we introduce a frame moving at the constant speed c which removes the time variable from our system. The new system is

$$\begin{aligned} U_X + V_Y &= 0 && \text{in } -d < Y < \eta, \\ (U-c)U_X + VU_Y &= -\tilde{P}_X && \text{in } -d < Y < \eta, \\ (U-c)V_X + VV_Y &= -\tilde{P}_Y - g && \text{in } -d < Y < \eta \end{aligned} \tag{2.5}$$

where $(X,Y) = (x - ct, y)$ and $(U, V, \tilde{P})$ are the functions (u, v, P) transformed to the moving frame. The boundary conditions now read

$$\tilde{P} = \tilde{P}_{\text{atm}} \quad \text{on } Y = \eta, \tag{2.6}$$

$$V = (U-c)\eta_X \quad \text{on } Y = \eta, \tag{2.7}$$

$$V = 0 \quad \text{on } Y = -d. \tag{2.8}$$

Of particular interest are rotational waves, that means that the vorticity $\gamma = v_x - u_y$ is not zero. One reason for the importance of vorticity is its influence on the existence and position of stagnation points, these are points in the wave where the velocity of the fluid is equal to the wave speed c. For the effects that stagnation points have on the flow structure of wave see [78, 33, 32]. For example, waves with a non-smooth peak, such as the Stokes wave of maximal height, see [74], have a stagnation point at that peak.

In this work several schemes on how to solve (2.1)–(2.4) numerically are discussed. While there exists a large literature concerning this problem, see [28, 40, 65, 68], here some more recent approaches are presented. Section 2.2 presents two schemes based on a Dubreil-Jacotin transformation, a numerical continuation approach [6, 50, 51, 71] and an asymptotic expansion approach [5, 20, 48]. Section 2.3 discusses a non-local formulation [2, 7, 29, 39] and a conformal mapping approach [10, 58, 64] is presented in Section 2.4. The schemes have in common that in order to be able to solve their respective systems, they assume all but one of the parameters, like depth, vorticity or velocity, are fixed. The remaining parameter can be varied to continue along the solution branch.

A non-exhaustive list of further numerical schemes not included in this discussion are: in [69] a shape optimisation approach applied to a stream formulation that allows for a non-flat bottom is presented; [46] modifies the nonlinear shallow water equations to allow for constant vorticity and examines wave breaking; the papers [55, 56] study and compute periodic waves based on an integral formulation.

2.2 Dubreil-Jacotin transformation

Following the procedure described in [22] we define the stream function ψ by $\psi_x = -V$ and $\psi_y = U - c$. Then the system (2.5)–(2.8) can be reformulated as the equivalent system

$$\Delta\psi = \gamma(\psi) \quad \text{in } -d < y < \eta, \tag{2.9}$$
$$\psi = 0 \quad \text{on } y = \eta, \tag{2.10}$$
$$|\nabla\psi|^2 + 2g(y+d) - Q\psi = -p_0 \quad \text{on } y = -d, \tag{2.11}$$
$$\psi = 0 \quad \text{on } y = \eta. \tag{2.12}$$

Here Q is the hydraulic head, p_0 the relative mass flux and γ the vorticity function. In order to ensure that the vorticity is a function of ψ one has to assume

$$u < c \tag{2.13}$$

in the whole fluid domain. This condition excludes stagnation points since there it holds $u = c$.

One major difficulty with the original system as well as the stream formulation is the unknown free surface η. In [22, 71] a fixed domain formulation equivalent to (2.9)–(2.12) is discussed. The used coordinate transform known as the Dubreil-Jacotin transform, see [31], is illustrated in Figure 2.1. This transform exploits that ψ is constant both on the flat bottom and the free surface as well as strictly increasing inside the domain, note that this again makes use of the assumption (2.13). Introducing the fixed domain $R = \{(q,p) | -\pi < q < \pi; p_0 < p < 0\}$ and the height function $h = y + d$ where y depends implicitly on q and p, results in a new system of equations.

Hence instead of (2.9)–(2.12) the problem is now to find h and Q satisfying

$$\mathcal{H}[h] := (1 + h_q^2)h_{pp} - 2h_p h_q h_{qp} + h_p^2 h_{qq} - \gamma(-p)h_p^3 = 0 \quad \text{in } R, \tag{2.14}$$
$$\mathcal{B}_0[h, Q] := 1 + h_q^2 + (2gh - Q)h_p^2 = 0 \quad \text{for } p = 0, \tag{2.15}$$
$$\mathcal{B}_1[h] := h = 0 \quad \text{for } p = p_0 \tag{2.16}$$

for a given domain R and vorticity function γ. Due to assumption (2.13), the formulations presented in this chapter and all schemes based on the Dubreil-Jacotin transformation can not be used to compute waves with stagnation point.

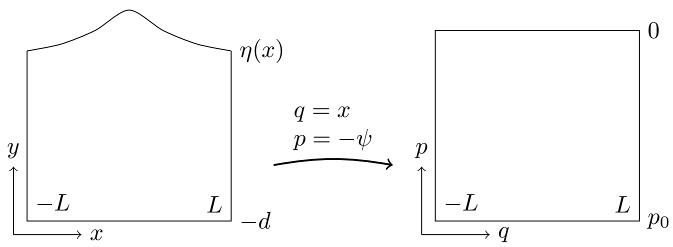

Figure 2.1: Dubreil-Jacotin transformation

A special family of solutions of these equations are the so called laminar waves. These solutions, defined in the fixed domain R, describe parallel shear flows that do not depend on the q variable and are denoted as H. In the case of linear vorticity the laminar waves are given by

$$H(p;\lambda) = \frac{2(p-p_0)}{\sqrt{\lambda - 2\gamma p} + \sqrt{\lambda - 2\gamma p_0}} \tag{2.17}$$

where the parameter $\lambda > 0$ is coupled to Q by the relation

$$Q = \lambda - \frac{4gp_0}{\sqrt{\lambda} + \sqrt{\lambda - 2\gamma p_0}}.$$

In general, there are no non-laminar waves in the neighbourhood of the laminar wave $(Q(\lambda), H(\lambda))$. For certain values of λ and thus Q, determined by the dispersion relation [49], a branch of non-laminar waves bifurcates from the family of laminar flows. These bifurcation points are denoted as λ_* and Q^* respectively.

While the schemes presented in Section 2.3 and 2.4 consider different system of equations and computational domains, the concepts of laminar branches and bifurcation of a branch of non-trivial waves remain the same.

2.2.1 Numerical continuation scheme

One straightforward approach is to discretise (2.14)–(2.16) with a second order finite difference scheme as was done in [6, 50, 51, 71]. The resulting system is underdetermined since the hydraulic head Q as well as the height function h are unknown. A numerical continuation scheme can be used to compute waves along the solution branch. This means introducing additional conditions to make the system determined and provide initial guesses based on previous solutions, the resulting system of nonlinear equations is solved with a Newton's method.

Finding the bifurcation point Q^* and the initial guess for the first non-trivial wave can be done by either computing eigenvalues of the linearised system, using analytical results [49] or employing other approaches such as the asymptotic expansion, see Section 2.2.2.

For numerical computations, wavelength λ and the relative mass flux p_0 have to be chosen. In the standard case of a given vorticity function γ the hydraulic head Q is the only free parameter which makes it the natural choice for the bifurcation parameter.

Note that other choices are valid and may be beneficial. For example consider the case of constant vorticity $\gamma = \gamma_0$, then one can fix Q and consider γ_0 as the bifurcation parameter. Given one solution, new waves can then be computed by varying γ_0 while Q remains fixed. This strategy was used in [6] to compute parts of the solution branch beyond a wave with stagnation points. This branch is not reachable by continuation with Q since there, the part of the branch that violates (2.13), can not be bypassed.

The biggest drawback of this approach is that, due to the assumption (2.13) of the Dubreil-Jacotin transform, waves with stagnation points are not modelled by (2.14)-(2.16). This manifests in an increasingly ill-condition Jacobian of the discretisation near stagnating waves. The advantage of this scheme are its ease of use and the big

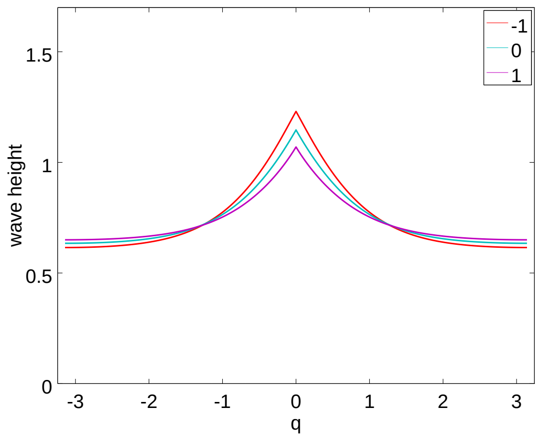

Figure 2.2: Free boundary of the limiting wave with vorticity $\gamma_\alpha(p) = \alpha(1 - \frac{p}{p_0})$ for $\alpha \in \{-1, 0, 1\}$

flexibility it has: no assumptions on the vorticity function γ are made, examples presented in [6, 50, 51] include piecewise constant and cubic vorticity with respect to the stream function; Figure 2.2 shows some examples of linear vorticity; The scheme is also flexible with regard to the model equation (2.1). Extensions, like periodic travelling equatorial waves [15, 63], that add earths rotation to the model, are straightforward to incorporate.

2.2.2 Asymptotic expansion

In the approach presented in [5] and based on [20, 48], one considers the fixed domain formulation (2.14)–(2.16) and finds asymptotic expansion of its solution around a bifurcation point.

Looking for q-independent solutions of (2.14)–(2.16) leads to the laminar flows H. Similarly, one can obtain solutions for the linearised problem with the approach

$$\hat{h}(q, p; b) = H(p, \lambda) + bm(q, p)$$

where $b \in \mathbb{R}$ and m is an even and 2π-periodic function in q. The unknown function m is chosen such that $\hat{h}$ is the solution of the linearised problem, that is

$$\mathcal{H}[\hat{h}] = \mathcal{O}(b^2), \quad \mathcal{B}_0[\hat{h}, Q] = \mathcal{O}(b^2), \quad \mathcal{B}_1[\hat{h}] = 0.$$

This linearised problem only has non-trivial solutions at bifurcation points, that is $(Q^*, H(\lambda_*))$. Those are either known analytically [49] for some vorticities or can be approximated numerically. A way to compute a better approximation of h would be to consider higher order approximations. As discussed in [20], adding more terms to $\hat{h}$ only yields solutions of the system up to second order. There exists no expansion $\hat{h}_3$ of third order that satisfies the system (2.14)–(2.16) up to third order, that is

$$\mathcal{H}[\hat{h}_3] = \mathcal{O}(b^4), \quad \mathcal{B}_0[\hat{h}_3, Q] = \mathcal{O}(b^4), \quad \mathcal{B}_1[\hat{h}_3] = 0.$$

This caveat was remedied in [48] by approximating not just the height function h but Q as well. For this introduce approximations of the pair (Q, h) by the polynomials in $b \in \mathbb{R}$

$$Q \approx Q^{(2N)}(b) \qquad := Q^* + \sum_{k=1}^{N} Q_{2k} b^k, \tag{2.18}$$

$$h(q,p;Q) \approx h^{(2N+1)}(q,p;b) := \sum_{k=0}^{2N+1} h_k(q,p) b^k \tag{2.19}$$

with coefficients $Q_{2k} \in \mathbb{R}$ and h_k defined as

$$h_{2k}(q,p) := \sum_{m=0}^{k} \cos(2mq) f_{2m}^{2k}(p), \tag{2.20}$$

$$h_{2k+1}(q,p) := \sum_{m=0}^{k} \cos((2m+1)q) f_{2m+1}^{2k+1}(p) \tag{2.21}$$

where $f_m^k \in C^\infty([p_0, 0])$ for all m, k. Note that the functions f_m^k only depend on p introduced by the Dubreil-Jacotin transformation. Let the wavelength, vorticity γ and relative mass flux p_0 be given. What remains to be computed are the constants Q_{2k} and functions f_m^k such that $(Q^{(2N)}, h^{(2N+1)})$ satisfies (2.14)–(2.16) up to $\mathcal{O}(b^{2N+2})$. The structure of $h^{(2N+1)}$, given by (2.19)–(2.21), can be exploited to considerably simplify this problem, as shown in [5]. Ultimately, what has to be solved is a series of one dimensional systems of differential equations which can be done numerically.

Due to the used Dubreil-Jacotin transformation, restriction (2.13) must be satisfied what in turn means this approach is limited to non-stagnation waves. The advantage of this scheme is its flexibility with regard to the vorticity, in particular non constant vorticity is possible, see [5]. This, together with the availability of analytical results for the first couple expansion terms [48], allows the use of this expansion as a very good initial guess for other approaches.

2.3 Non-local formulations

In [2], a new, non-local formulation of the Euler equations was presented which is based on the unified transform or Fokas method. While this approach allows for rotational waves, we present here the periodic irrotational case as was considered in [29]. In the irrotational case, that is $\gamma = 0$, the Euler equations can be formulated in terms of a velocity potential ϕ and become

$$\Delta\phi = 0 \qquad \text{in } -d < y < \eta \tag{2.22}$$

$$\phi_y = 0 \qquad \text{on } y = -d, \tag{2.23}$$

$$\eta_t + \phi_x \eta_x = \phi_y \qquad \text{on } y = \eta, \tag{2.24}$$

$$\phi_t + \frac{1}{2}\left(\phi_x^2 + \phi_y^2\right) + g\eta = \sigma \frac{\eta_{xx}}{(1+\eta_x^2)^{3/2}} \qquad \text{on } y = \eta \tag{2.25}$$

where σ denotes the constant surface tension and ρ is the density.

Introduce the velocity potential evaluated at the surface, see [80], as $q(x,t) = \phi(x,\eta(x,t),t)$ which leads to the dynamic boundary condition

$$q_t + \frac{1}{2}q_x^2 + g\eta - \frac{1}{2}\frac{(\eta_t + q_x\eta_x)^2}{1+\eta_x^2} = \sigma\frac{\eta_{xx}}{(1+\eta_x^2)^{3/2}}. \tag{2.26}$$

Additionally one gets a non-local equation

$$\int_0^L e^{-ikx}\{i\eta_t \cosh[k(\eta+d)] + q_x \sinh[k(\eta+d)]\}dx = 0, \quad t > 0 \tag{2.27}$$

where $k = k_n = \frac{2k\pi}{L}$ with $n \in \mathbb{Z} \setminus \{0\}$.

Starting from the set of equations (2.26)–(2.27) several modifications and generalisations can be made. Considerations include the constant vorticity case [7, 77], a variable bottom [2] and using a moving frame [29]. A hybrid of the novel formulation and an approach based on conformal mapping is presented in [39], where water waves with variable bottom are studied numerically.

For numerical considerations in the case of steady periodic water waves (2.26)–(2.27) can be reformulated as a single non-local equation only containing the unknown η, see [29]. The wave profile η is approximated by truncated Fourier series and the non-local equation discretised using a spectral collocation method. Then the problem to find solutions can be seen as a bifurcation problem for fixed wavelength and depth where the wave velocity c is the bifurcation parameter. To find a bifurcation point for which non-trivial solutions exist, the null space of the linearisation about the trivial wave is studied.

This approach allows for the computation of streamlines and pressure in the whole domain, independent of any grid. This holds true even in the presence of stagnation points when rotational waves are considered. For example, in [77] a wave with interior stagnation and a bottom pressure maxima which is not under the crest is presented.

Such non-local formulations are a very active research area, for some more related formulations see [61, 62, 77]. This, together with the easily available information about streamlines, wave form and pressure, make non-local formulations very effective. The main limitation is that the vorticity function has a larger impact on the formulation and is thus more restricted, in most cases to constant vorticity.

2.4 Conformal mapping and spectral collocation method

In the approach presented in [64], the constant vorticity case is considered as a superposition of a linear shear flow and a harmonic velocity potential. This leads to a system of equations similar to (2.22)–(2.25) but with an additional vorticity term, which is then non-dimensionalised. The manuscript [64] considers the case of periodic travelling waves with constant speed and introduces a frame moving along with wave speed c. Then the problem is to find the potential ϕ satisfying

$$\Delta\phi = 0 \quad \text{in } -1 < y < \eta \tag{2.28}$$
$$\phi_y = 0 \quad \text{on } y = -1, \tag{2.29}$$
$$-c\eta_x + (\phi_x - \gamma(\eta + b))\eta_x = \phi_y \quad \text{on } y = \eta, \tag{2.30}$$
$$-c\phi_x + \frac{1}{2}\left(\phi_x^2 + \phi_y^2\right) + \eta - \gamma(\eta + b)\phi_x + \gamma\psi = B \quad \text{on } y = \eta \tag{2.31}$$

where B is the Bernoulli constant, ψ is the streamfunction associated with ϕ and $b \in \mathbb{R}$ is a parameter of the background flow.

To solve this system, a conformal mapping such as given in [10, 58], that maps the uniform strip onto the wave domain, is considered. In the uniform strip domain, a flat domain of unknown depth, the solution of the Laplace equation is analytically known. It is ensured that this solution satisfies the dynamic and kinematic boundary conditions using a spectral collocation method. For a sketch of the involved domains see Fig 2.1, where reversely the fluid domain was mapped onto a rectangle domain.

To compute a first non-laminar wave the irrotational case of small amplitude, for which good approximations are available, is considered. More waves along the solution branch can be computed using a continuation scheme with previous solution as initial guess. For continuation parameters, [64] studies two cases. In the first case, the depth and wave height H are fixed and the continuation parameter is the wavelength λ. In the second case, the depth and wavelength are fixed and either the vorticity γ or the steepness parameter $\frac{H}{\lambda}$ are varied.

This approach can be used to compute waves with stagnation points as well as wave characteristics such as streamlines, stagnation points, particle paths and the pressure. The results presented in [64] include waves with up to three interior stagnation points and waves with switched pressure maxima and minima at the bottom opposed to the irrotational case. The various continuation schemes allow for the detailed study of interactions between parameters and wave characteristics. The biggest restriction of this approach is that it is limited to constant vorticity.

3 A numerical continuation approach for computing water waves of large wave height

Dominic Amann, Konstantinos Kalimeris

Abstract

We analyze an algorithm for the calculation of travelling water waves in flows with constant and variable vorticity. The algorithm is based on numerical continuation techniques, which are suitably adapted to the water wave problem. Numerical examples illustrate the performance of the algorithm for flows of constant vorticity, where the results are compared with the literature. We observe agreement with already existing results, but we also have some new qualitative and quantitative results considering the characteristics of the water waves both for constant and variable vorticity.

3.1 Introduction

We are studying two-dimensional waves travelling at constant speed c, for different vorticities. This problem has practical interest because it is related with the detection of non-uniform underlying currents from the surface wave pattern. The characterization 'travelling' means that in a two-dimensional frame moving with the constant speed c, the flow pattern — and, in particular, the shape of the surface of the fluid — does not change over time. Two-dimensionality means that the waves propagate in a fixed horizontal direction and the flow presents no variation in the horizontal direction orthogonal to the direction of wave propagation. For this reason, it suffices to analyse a vertical cross-section of the flow, parallel to the direction of wave propagation. To model sea waves of large amplitude the assumptions of inviscid flow in a fluid of constant density are appropriate and the effects of surface tension are negligible – see the discussion in [14].

It is worth highlighting the physical importance of flows with vorticity in modelling wave-current interactions; general discussions of the physical implications of rotational flow may be found in the references [14] and [73]. Recent studies have pointed out that periodic travelling waves which propagate at the surface of water with a flat bed in a flow of constant vorticity must be symmetric if no flow-reversal occurs and if the wave profile is monotone between successive crests and troughs, see [17, 18]. This means that an underlying non-uniform current of constant vorticity does not break the symmetry of irrotational wave trains. Thus, following this formulation, we make the assumption of no flow-reversal in this work: In the absence of flow reversal, the approach developed in [19] ensures the real-analyticity of all the streamlines; see also the discussion in the survey [36]. In contrast to this, the available results on regularity for flow reversal (case in which critical layers appear) are merely of class C^∞, see the results in [26].

Prior to the establishment of any analytically rigorous mathematical results, numerical investigations for large amplitude waves with vorticity, were initiated by the seminal papers [68] and [28] for the infinite, and finite, depth cases respectively. Indeed, due to significant technical complications, rigorous mathematical analysis establishing the existence of large amplitude water waves has only recently been achieved. In the case of irrotational waves this was achieved by the work of Toland and collaborators (where [9, 72] represent nice surveys of this topic), and for waves with vorticity, following the seminal paper [22], the existence of large amplitude waves was established for various physical generalisations in [41, 43, 57, 79].

In this work, we follow the analytical formulation derived in [22], and reviewed in several other works, see for example [71, 21]. In this approach, the curve of solutions is extensively analyzed and a crucial ingredient is the existence of a branch of the bifurcating diagram, which contains flows beneath genuine waves[1]. In particular, this branch starts from a special laminar solution, the existence of which is connected with the so-called *dispersion relation*; this curve may be continued, using arguments from bifurcation theory, to a global continuum which contains at the limit a flow with a stagnation point. The characteristic of the latter wave is that its horizontal velocity approaches the constant speed of propagation c, being related to waves of maximal amplitude, hence providing the analogue to the Stokes' extreme wave. Computations which are based on this approach are performed in [51, 50], with several interesting results which agree with the relevant analytical predictions. Among the most important results of those works we point out the following: The stagnation can occur, not only at the crest, but also at the point on the bottom directly below the crest. Along the bifurcation curve, for fixed relative mass flux[2] p_0, the amplitude of the wave is increasing, the depth d varies only slightly and the hydraulic head[3] Q has (in general) one turning point. Furthermore, the waves of maximal amplitude are obtained at the end of the bifurcation curve and the maximal amplitude is an increasing function of $|p_0|$, in the case of constant vorticity. Finally, the shapes of the streamlines of the extreme waves depend on the vorticity, which is a result observed also in several numerical works and indicates the importance of the effect that the vorticity has on the features of water waves.

In our work, we analyze a numerical continuation approach tailor-made for the

[1] In the sense that they are not of zero amplitude.
[2] The flux p_0 is defined in (3.9).
[3] This quantity, being indicative of the total mechanical energy of the wave, is defined in (3.12).

above described mathematical formulation, enriched with techniques appropriate to overcome some particular obstacles of this problem (turning points, bifurcation points and stagnation points). The idea on reconstructing the bifurcation branch described in [22], via numerical continuation techniques, was introduced in [51]. In our algorithm, among other techniques which are described in more detail in section 3.4, we make explicit usage of analytical results obtained in [22] — instead of evaluating numerically the relevant features, through the solution of an eigenvalue problem. In more detail:

- The explicit position of the bifurcation point, which is the starting point of our iterative numerical scheme is obtained analytically through [22], [21] and [49] for different cases of vorticity.
- Starting from the above point, the favourable direction for the numerical continuation, which will lead to the reconstruction of the branch containing the non-laminar flows (as opposed to the trivial one), is obtained analytically in [22], [20] and [49], for the different cases of vorticity.
- The careful refining of the mesh described in section 3.4 allows for the computation of waves closer to stagnation than the ones obtained in [51].
- The adaptation (described in section 3.3) of the numerical continuation technique on this formulation of the water wave problem allows the systematic study of the main features of the wave and the improvement of the algorithm; as examples we note the adaptation of the step-size in the 'predictor stage' of our method and the interchange of the continuation parameter.

This has as a result an efficient and inexpensive algorithm, which, additionally, gives rise to new parts of the interesting branch of the bifurcation diagram, i.e. to families of waves with novel characteristics, see for example Section 3.4.2. Furthermore, we find agreement with already existing numerical results while observing additional characteristics close to stagnation, which in some cases is important enough to give an additional understanding on the solutions of the problem. Finally, in order to show the generality of our algorithm, we compute some cases of continuous and non-constant vorticity; this results in, also, an interesting family of water waves, which is depicted in Figures 3.23-3.24.

We find worth-mentioning a series of computational works, for example [59, 76, 77, 62, 39], which are based on a different mathematical formulation of the problem. In particular, they are based on the analysis of [29, 2]; see also [7, 38] and [37] for extending the latter work in a domain with fixed and moving bottom, respectively. One can observe that our computational results are in qualitative agreement with results of the above-mentioned works.

In the recent work [64] an extensive numerical study of periodic travelling water waves is made. This work is based on a conformal mapping which is described also in [10, 58] and their results are obtained through a combination of analytical techniques and spectral methods. This approach has the advantage over our work that the computation of waves with stagnation points (both on the boundary and in the interior) are possible. On the other hand this approach treats only the case of constant vorticity; one could find potential on extending this work to general vorticity using the analysis of [78] and [33]. Our approach, although having the disadvantage on stagnation points, provides results for more general distributions of vorticity; as an example we provide some examples in section 3.4.3. Moreover, our computation reveals some interesting behaviour of the pressure for a particular family of waves which is discussed in Section 3.4.2 and it is novel, up to our knowledge. Even though that for waves that do not have stagnation points there is qualitative agreement between our work and the above-mentioned one, the most interesting cases of that work involves waves with internal stagnation (which we do not compute). Finally, the rigorous and *exact* correspondence of these two formulations – the conformal mapping used in [64] and the semi-hodograph transformation used in [22] and here – is still an open question.

The paper is organised as follows: In section 3.2, we make a brief review of the mathematical formulation of the problem. In section 3.3, we present the numerical continuation method, which we employ in order to compute the water waves along the bifurcating curves. In section 3.4, we present the numerical results of the above procedure and we discuss the special characteristics of the waves, depending on the different values of constant vorticity. Moreover, in order to show the generality of our algorithm, we present the relevant results for some case that the vorticity is not constant; in these examples the vorticity varies linearly, as well as quadratically, with respect to the stream function. In particular, we illustrate the wave profiles, as well as other characteristics such as the velocity profile and the pressure throughout the fluid. The knowledge of these flow characteristics is very useful in qualitative studies, see [13, 24]. Moreover, in practice information on the state of the sea surface is often gathered from subsurface pressure and/or velocity measurements; we refer to the discussions in [11, 12, 16, 41, 52, 62].

3.2 The basic equations and terminology

In this section we present the governing equations for periodic two-dimensional travelling water waves in flows of constant and variable vorticity over a flat bed.

Let us denote the height function of the wave above the flat bottom by $h(q, p)$. This function satisfies the nonlinear boundary value problem, defined by (3.1)-(3.3). We omit here the derivation of (3.1)-(3.3) from the physical problem which was described in the Introduction. Instead, for the derivation of the constitutive equations (3.1)-(3.3) and the mathematical formulation of the problem we refer to [22, 71] for a detailed construction, to [21, 51] for an extended review and to [20, 48] for a brief review.

Definition 1. The constitutive equations for the height function $h(q, p)$, which is even and $2L$-periodic in q, are the following:

$$(1+h_q^2)h_{pp} - 2h_p h_q h_{qp} + h_p^2 h_{qq} - \gamma(-p)h_p^3 = 0 \quad \text{in } R, \tag{3.1}$$

$$1 + h_q^2 + (2gh - Q)h_p^2 = 0 \quad \text{for } p = 0, \tag{3.2}$$

$$h = 0 \quad \text{for } p = p_0, \tag{3.3}$$

where R is the rectangle defined by

$$R = \{(q,p) : \ -L < q < L, \ p_0 < p < 0\}. \tag{3.4}$$

Moreover, the free boundary of the wave is given by the expression $h(q,0)$.

In this equation γ denotes the vorticity as defined in (3.7), which is assumed a known function, being indicative of underlying currents. Vanishing vorticity is the property typical of uniform currents and a constant vorticity characterizes linearly sheared currents. We also recall that g is the gravitational constant of acceleration, and p_0 is the relative mass flux as defined in (3.9), and it is a constant, too. The parameter Q is called the hydraulic head, it plays an important role in the profile of the waves, and is defined in (3.12).

For the justification of the q evenness and periodicity of the water waves we refer to the discussion in [17, 18]. Moreover, without loss of generality, me make the assumption that the crest is at $q = 0$ and the trough at $q = L$. Thus, we define the wave height as the maximal variation of the oscillations of the free surface, given by

$$a := \max_{q\in[-L,L]} h(q,0) - \min_{q\in[-L,L]} h(q,0) = h(0,0) - h(L,0). \tag{3.5}$$

Following the methodology of [48], below we provide the sufficient terminology for the fundamental boundary value problem (3.1)-(3.3).

Basic terminology

In the description of the physical problem in the Introduction, we emphasized the fact that we are studying two-dimensional waves travelling at constant speed c. Moreover, we made the assumption of no flow-reversals and no surface tension.

We denote:

- The free boundary of the wave by

$$S = \Big\{(x,y) : -L < x < L \text{ and } y = \eta(x)\Big\},$$

- The flat bottom by

$$B = \Big\{(x,y) : -L < x < L \text{ and } y = -d\Big\},$$

  with $d > 0$, for the normalized wavelength $2L$.

- The velocity field of the flow by
$$\Big(u(x,y), v(x,y)\Big),$$
with $(x,y) \in \mathcal{D}$, where
$$\mathcal{D} = \Big\{(x,y) : -L < x < L \text{ and } -d < y < \eta(x)\Big\}.$$

- The pressure in the fluid by $P(x,y)$, with $(x,y) \in \mathcal{D}$. Neglecting the effects of surface tension we impose that the water pressure is constant on S, $P(x,\eta(x)) = P_{atm}$, where P_{atm} is the atmospheric pressure.

The assumption of no flow-reversals, which also excludes stagnation point throughout the fluid domain, is formulated as the condition
$$u < c \quad \text{throughout the fluid.} \tag{3.6}$$

Let us recall the following definitions:

- The vorticity of the flow is defined by
$$\gamma := u_y - v_x. \tag{3.7}$$
Furthermore, we define the following function
$$\Gamma(p) := \int_0^p \gamma(-s)ds, \tag{3.8}$$
which is useful for describing other quantities of the problem.

- The relative mass flux[4] is defined by
$$p_0 := \int_{-d}^{\eta(x)} \Big(u(x,y) - c\Big)\, dy < 0, \tag{3.9}$$
which in fact is independent of x, see [21]. Moreover, condition (3.6) shows that p_0 is negative. This relation shows that the amount of water passing any vertical line is constant throughout $\mathcal{D}$.

- The stream function $\psi(x,y)$ is defined as the unique solution of the differential equations
$$\psi_x = -v, \qquad \psi_y = u - c \text{ in } \overline{\mathcal{D}}, \tag{3.10}$$
subject to
$$\psi(x,-d) = -p_0\ . \tag{3.11}$$

[4]The terminology 'relative' is due to the fact that $(u-c)$ is the relative horizontal velocity of the flow, with reference to the moving frame at speed c.

- The hydraulic head, which is *constant* throughout the fluid, and denoted by Q, is defined by

$$Q := (u-c)^2 + v^2 + 2g(y+d) + 2(P - P_{atm}) + 2\Gamma(-\psi), \tag{3.12}$$

  where Γ was defined in (3.8). Indeed, it is proven in [22] and in [21], that the expression

$$\frac{(u-c)^2 + v^2}{2} + gy + P + \Gamma(-\psi)$$

  is a constant throughout $\mathcal{D}$, thus the expression in (3.12) is constant, too; this is a form of conservation of energy.

The Dubreil-Jacotin transformation, see Figure 3.1, maps the unknown domain $\mathcal{D}$ to the rectangle R, defined in (3.4). The independent variables as they appear in the Dubreil-Jacotin transformation [31] are

$$q = x, \qquad p = -\psi.$$

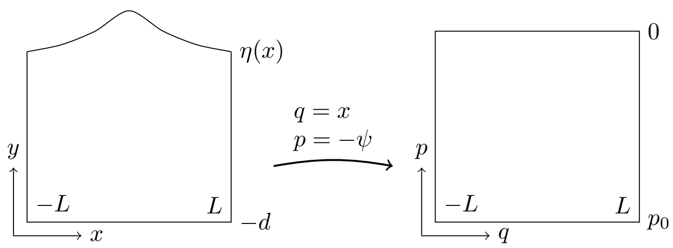

Figure 3.1: Dubreil-Jacotin transformation

Finally, we recall that:

- The height function $h(q,p)$ is defined by

$$h := y(q,p) + d, \tag{3.13}$$

  where y is assumed to depend implicitly on new semi-Lagrangian $q, p-$variables.

- The velocity field is given by

$$(c-u, v) = \left(\frac{1}{h_p}, -\frac{h_q}{h_p}\right). \tag{3.14}$$

- The water pressure is given by

$$P = P_{atm} - \frac{1 + h_q^2}{2h_p^2} - gh - \Gamma(p) + \frac{Q}{2}, \tag{3.15}$$

  with Γ being defined in (3.8).

- The coordinates are chosen such that the mean-water level is located at $y = 0$; then $\int_{-L}^{L} \eta(x)dx = 0$ and accordingly, from the definition of h, the mean-depth of the fluid is recovered by the expression

$$d = \frac{1}{2L} \int_{-L}^{L} h(q,0)dq. \tag{3.16}$$

Remark 1. The mean-depth of the fluid can only be recovered *a posteriori* following bifurcation from the standard Dubreil-Jacotin formulation of the water wave problem – indeed, in [51] it was shown that the depth d varies along the bifurcation continuum; similar results are presented also here in Figure 3.15.

A novel approach to overcome this issue was initiated in [41, 42]. Based on this formulation one may proceed through a similar numerical continuation technique and compute families of non-laminar water waves of fixed depth, where the relative mass flux p_0 will be varying. We consider this a very fruitful approach in order to see, among other interesting features, how the variation of the quantity p_0 will affect important characteristics of waves. In our opinion, a systematic numerical study of this formulation, can be presented independently of the current work and certainly deserves an article of similar length of this one. Recalling that in our computations, waves of maximal amplitude are obtained at the limiting points of the bifurcation curve, we observe that maximal amplitude increases as $|p_0|$ increases. For a brief overview on the influence of p_0 on the wave characteristics we refer to Remark 2 in Section 3.4.2.

3.3 Numerical Continuation

Discretization of (3.1)–(3.3) leads to a system of nonlinear equations

$$F(\theta, \mathbf{h}) = \mathbf{0} \tag{3.17}$$

with a given mapping $F : \mathbb{R} \times \mathbb{R}^N \to \mathbb{R}^N$ and unknowns $\mathbf{h} \in \mathbb{R}^N$ and $\theta \in \mathbb{R}$. To overcome the two major problems in solving (3.17), the underdetermined system and the need for a good initial guess, we employ a numerical continuation strategy. We consider the case that at least one solution is known and the goal is to compute additional solutions. Parametrization of the solution curve and fixing the step size results in a well defined problem and the known solutions are used to predict an initial guess. As a corrector we use a Newton algorithm to solve the system of nonlinear equations.

This section gives a short introduction into this topic, putting it in a more general frame, but also giving some specific details of the problem, where needed. For a more elaborate study we refer to [3, 30].

3.3.1 Predictor Corrector method

Let $\mathcal{C}$ be the set of all pairs satisfying (3.17) and $(\theta_k, \mathbf{h}_k) \in \mathcal{C}$ a known solution, then the problem is to find a new solution

$$F(\theta_{k+1}, \mathbf{h}_{k+1}) = \mathbf{0}.$$

Since this is an underdetermined system we first have to find an additional equation. Assume that a parametrization of the solution curve $\mathcal{C}$ in a neighbourhood of $(\theta_k, \mathbf{h}_k)$ is given such that

$$\begin{aligned} F(\theta(s), \mathbf{h}(s)) = 0 \quad &\text{for } |s| < s_0, \\ \theta(0) = \theta_k \quad \text{and} \quad &\mathbf{h}(0) = \mathbf{h}_k, \end{aligned}$$

for some $s_0 > 0$. Using the equation $\mathfrak{p}(\theta, \mathbf{h}, s) = 0$ to describe the above parametrization, we can append this to (3.17) for a fixed step size s resulting in

$$\begin{pmatrix} F(\theta_{k+1}, \mathbf{h}_{k+1}) \\ \mathfrak{p}(\theta_{k+1}, \mathbf{h}_{k+1}, s) \end{pmatrix} = \begin{pmatrix} \mathbf{0} \\ 0 \end{pmatrix}. \tag{3.18}$$

The existence and uniqueness of a solution to (3.18) depends on the choice of $\mathfrak{p}$ and the solution set $\mathcal{C}$. We now discuss two choices for $\mathfrak{p}$ and properties of the resulting systems.

Parametrization of $\mathcal{C}$ by θ is called natural parametrization and equates to fixing the value of θ. The corresponding function is

$$\mathfrak{p}(\theta, \mathbf{h}, s) = \theta - (\theta_k + s). \tag{3.19}$$

In a similar way, instead of θ we can choose any entry of $\mathbf{h}$ as parameter. Let i be an index of $\mathbf{h}$, then the so called local parametrization is given by

$$\mathfrak{p}(\theta, \mathbf{h}, s) = \mathbf{h}[i] - (\mathbf{h}_k[i] + s).$$

Figure 3.2 shows both these parametrizations on a bifurcation diagram that plots $(\theta, \mathbf{h}[i])$ for all solutions in $\mathcal{C}$. Additionally to $\mathcal{C}$ the line of all pairs $(\theta, \mathbf{h})$ satisfying $\mathfrak{p}(\theta, \mathbf{h}, s) = 0$ is also plotted, the solution we seek is the intersection of these two lines. The existence and uniqueness of such an intersection depends on $\mathcal{C}$ and the choice of s. In the example $\mathcal{C}$ has a turning point in θ, so there exists no solution pair that satisfies the natural parametrization if s is too large. Indeed, if the current solution is exactly on the turning point, there exists no $s_0 > 0$ such that (3.19) describes a parametrization of $\mathcal{C}$. In such a case, one way to proceed with the numerical continuation is by parametrizing with respect to another characteristic such that the bifurcation curve does not have a turning point, in the given example $\mathbf{h}[i]$.

For our model problem (3.1)–(3.3) it proved most effective to parametrize by the entry of $\mathbf{h}$ corresponding to the highest point of the wave. The considered solution curves $\mathcal{C}$ are monotonous in this parameter and thus have no turning points with respect to this parametrization.

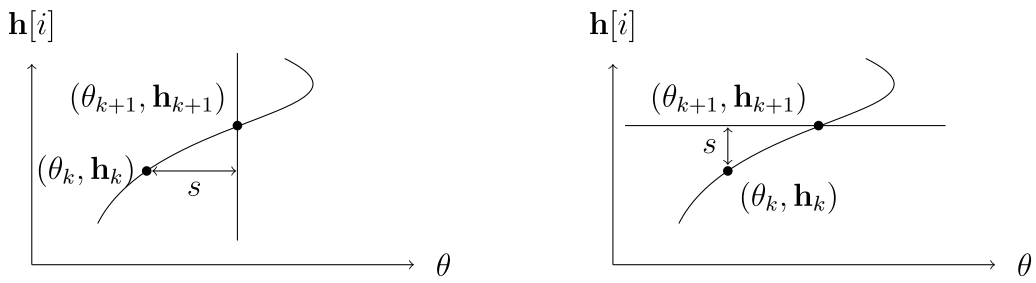

Figure 3.2: Natural and local parametrization

The predictor is the initial guess for the Newton scheme and will be denoted as $(\theta_{k+1}^{(0)}, \mathbf{h}_{k+1}^{(0)})$. Of the many predictors described in literature we only briefly introduce two, the trivial and secant predictor

$$(\theta_{k+1}^{(0)}, \mathbf{h}_{k+1}^{(0)}) := (\theta_k + s^{(0)}, \mathbf{h}_k),$$
$$(\theta_{k+1}^{(0)}, \mathbf{h}_{k+1}^{(0)}) := (\theta_k, \mathbf{h}_k) + s^{(0)}(\theta_k - \theta_{k-1}, \mathbf{h}_k - \mathbf{h}_{k-1}).$$

The value $s^{(0)}$ is chosen such that the parametrization equation is satisfied.

3.3.2 Bifurcation and turning points

Along the solution curve $\mathcal{C}$, two kind of points are of special interest. A turning point is illustrated in Figure 3.2 and means that locally there are two solutions below some value of θ and none above or vice versa. A point along $\mathcal{C}$ where two or more solution branches intersect is called a bifurcation point.

Let $(\theta_k, \mathbf{h}_k)$ be a solution of (3.17). The point is called regular if the Jacobian $(F_\theta | F_\mathbf{h}) \in \mathbb{R}^{N \times N+1}$ has full rank N. Near a regular point, $\mathcal{C}$ can be uniquely described by a one dimensional branch of solutions [30].

The full rank condition implies that at a regular point it must hold either rank$F_\mathbf{h} = N$ or rank$F_\mathbf{h} = N - 1$ and $F_\theta \notin$ range$(F_\mathbf{h})$. In the first case the branch of solution near $(\theta_k, \mathbf{h}_k)$ can be parametrized by θ [3]. The second case describes the situation of a turning point in θ, so even though $\mathcal{C}$ can be uniquely parametrized, θ is not the proper parameter. At last, if a point is not a regular point, then at least two branches of solutions intersect at this point.

While traversing along the bifurcation curve, it is important not to miss bifurcation points, we restrict our considerations to simple bifurcation points. For this we define a test function τ with the properties that $\tau(\theta^*, \mathbf{h}^*) = 0$ on a bifurcation point and $\tau(\theta^+, \mathbf{h}^+)\tau(\theta^-, \mathbf{h}^-) < 0$ if the two points are separated by a bifurcation point. One choice for a test function is the sign of the determinant of the Jacobian

$$\tau(\theta, \mathbf{h}) := \operatorname{sign}\left(\det\left(F'(\theta, \mathbf{h})\right)\right),$$

which is readily available if the linear system appearing in the Newton algorithm is solved via LU–decomposition. This and other test functions, such as the eigenvalue of smallest magnitude, are discussed in [67].

3.3.3 Bifurcation from the laminar flow

The numerical continuation method assumes that at least one solution of (3.17) is given. How to find this solution is problem–dependent and often includes a certain choice for the value of θ to facilitate the solution of the resulting system. Here we discuss how this can be done for the equations (3.1)–(3.3) arising from travelling water waves.

First we consider solutions H that are q-independent and correspond to parallel shear flows. These solutions $H(p)$ are called laminar waves and solve

$$\begin{aligned} H_{pp} - \gamma(-p)H_p^3 &= 0 \quad \text{in } R, \\ 1 + (2gH - Q)H_p^2 &= 0 \quad \text{for } p = 0, \\ H &= 0 \quad \text{for } p = p_0. \end{aligned}$$

For general vorticity, the laminar flow is given by

$$H(p;\lambda) = \int_{p_0}^{p} \frac{1}{\sqrt{\lambda - 2\Gamma(s)}} ds,$$

where λ satisfies the relation

$$Q = \lambda + 2g \int_{p_0}^{0} \frac{dp}{\sqrt{\lambda - 2\Gamma(p)}},$$

with Γ defined by (3.8). For some vorticity functions, for example $\gamma(p)$ constant or linear, solutions of this system are known analytically [20, 22, 49].

The above formulae give, not only one, but many solutions, in particular, we define the curve that contains the laminar flows

$$\mathcal{T} = \left\{ (Q(\lambda), H(p;\lambda)) : \lambda > 0 \right\}.$$

However, if we are to compute nonlaminar solutions, we need more information. Indeed, in [22] it was proven that near this curve, as the parameter λ varies, there are generally no genuine waves, except at some critical values $\lambda = \lambda_*$, which can be determined by the following procedure.

Define the linearized height function $h_L = H + bm$ with $b \in \mathbb{R}_+$ and m chosen such that h_L solves (3.1)–(3.3) up to an error of order $\mathcal{O}(b^2)$. This leads to the linearized system

$$\begin{aligned} m_{pp} + H_p^2 m_{qq} &= 3\gamma H_p^2 m_p \quad && \text{in } R, \\ gm &= \lambda^{3/2} m_p && \text{for } p = 0, \\ m &= 0 && \text{for } p = p_0, \end{aligned}$$

with the appropriate periodicity conditions in the q variable. For general values of $\lambda > 0$ the linearized system will only have the trivial solution $m \equiv 0$. In order to obtain non-trivial solutions $m(q, p)$ of the above system we make usage of the so-called ‘dispersion relation’; for the water waves this is a consistency relation which is determined by the critical bifurcation values of the parameter $\lambda = \lambda_*$, see [14, 22]. For some choices of vorticity, including constant and linear, the dispersion relation as well as analytical forms for m are known [20, 49]. Moreover, in [22] it was proven that $\big(Q(\lambda_*), H(p; \lambda_*)\big)$ is a bifurcation point on the curve $\mathcal{T}$, from where a curve that contains non-laminar flows arises, with Q being the global bifurcation parameter. This reads as a mapping $Q \mapsto h(q, p; Q)$ such that $h_q \not\equiv 0$ unless $h = H(p; \lambda_*)$. Furthermore, this curve may be continued, using arguments from analytic global bifurcation theory [9], to a global continuum which contains at the limit a flow with a stagnation point; such a flow is analogous to the Stokes’ wave of greatest height, or Stokes’ extreme wave, in the irrotational setting [9, 14]; we denote the value of the bifurcating parameter at this flow by $Q = Q_M$.

Let b be fixed, then h_L is a predictor for a solution on the bifurcation branch. Note that a too small b will urge the corrector to converge to a laminar wave while a too big b can result in a diverging corrector step. In our experience, the choice $b = s$ with a small enough s leads to convergence to the nonlaminar branch.

Higher than first order approximations for h are known [20, 48] but a first order expansion is sufficient to bifurcate from the curve of laminar flows.

3.4 Numerical results

For the numerical examples, we fix the values of the parameters

$$g = 9.8, \qquad L = \pi, \qquad \text{and} \qquad p_0 = -2.$$

This choice of parameters is made accordingly to the one in [50]; we make this choice for allowing the comparison with the results displayed therein. From the particular choice of parameters the one that is of interest is the choice of the value of the relative mass flux p_0. We refer to the discussion in Remarks 1 and 2, for the influence of the choice of other values of p_0.

As in [50, 51] we discretize the system (3.1)–(3.3) by a second order finite difference scheme resulting in a system of nonlinear equations of the form (3.17). Instead of discretizing the whole domain $[-\pi, \pi] \times [p_0, 0]$ we exploit that h is an even function and only consider $[-\pi, 0] \times [p_0, 0]$, reducing the computational cost. In the interior and at the boundary $q = -\pi$, we used central schemes to approximate the derivatives of h. In order to be able to do this we expanded the solution beyond the left border by mirroring along $q = -\pi$. This procedure was motivated by the periodicity of h and the expected regularity at $q = -\pi$. At the border $q = 0$ such regularity assumptions are not satisfied, in particular close to a stagnation point, so we used backward difference schemes in q and a central scheme in p. Vice versa, we used a forward scheme in p and a central scheme in q on the top of the boundary.

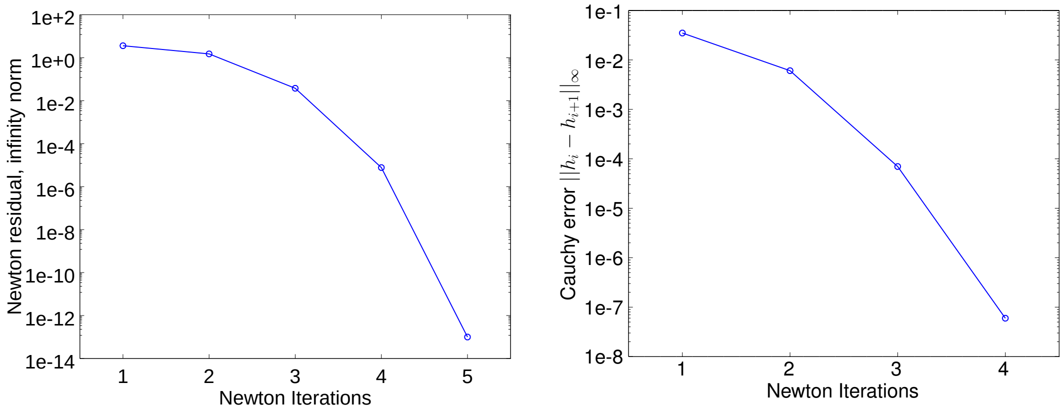

(a) Cost functional

(b) Cauchy error

Figure 3.3: Newton Iterations.

The described algorithm was implemented using PETSc [8] for assembling and solving the non-linear systems. The computational domain is discretized by a equidistant 400×400 grid and then additionally refined where stagnation points and thus weaker regularities are expected. From theoretical [23] and numerical [50, 51] results and tests with equidistant grid points we know that the first encountered stagnation point is below the crest of the wave either on the top or on the bottom. To account for both these cases, we refine at the top and the bottom which results in a mesh with 460×580 grid points. At the expected stagnation points the mesh size is 8 times smaller than it was for the equidistant grid.

Moreover, for the case of constant vorticity, in [50, 51], a critical (numerical) value of the parameter γ appears, denoted as γ_{crit}, which distinguishes the above two cases. In particular, if $\gamma > \gamma_{\mathrm{crit}}$ the stagnation point appears in the top, whereas, if $\gamma < \gamma_{\mathrm{crit}}$, the stagnation point appears at the bottom of the fluid[5]. The computed waves, in this section, demonstrate different characteristics below and above a critical vorticity which is, for the above choice of parameters, $\gamma_{\mathrm{crit}} \approx -2.971$. We emphasize the fact that we obtain, also, some new qualitative results, compared with [50]; these are discussed in Section 3.4.2.

The natural choice for the bifurcation parameter θ is Q when we assume all other parameters to be fixed. For most of our computations we used this parameter. Note that for waves of constant vorticity we can alternatively fix Q and choose γ to be the bifurcation parameter. This choice can be beneficial and we will discuss one such case in Section 3.4.2.

Considering the validation of our algorithm, we first illustrate the performance of the corrector step to solve (3.18), for which we employ a Newton algorithm and stop when the residual is below 10^{-12}. Figure 3.3 shows for one exemplary wave the residual of the cost function (3.18) and the Cauchy error where we compare two solution of two

[5]Here, we have taken into consideration the difference of the sign of the vorticity between the above references and our work.

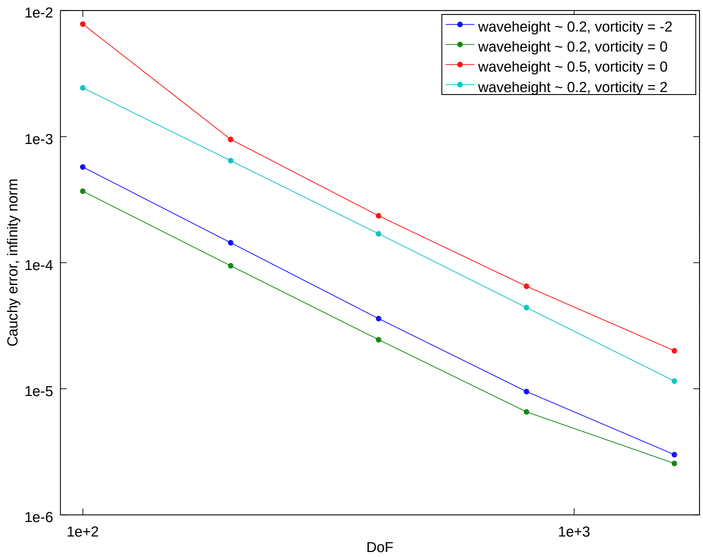

Figure 3.4: The Cauchy error $||h_N - h_{N/2}||_\infty$ for several vorticities and wave heights.

successive Newton steps. We note that this strategy is in accordance with the common practice in the error analysis of this problem, see for example [77]. Furthermore, we have performed the same error tests for some example (laminar flow), for which we have the a priori knowledge of the analytical expression of the solution. The results show the same behaviour of our algorithm as in Figures 3.3.

The number of necessary Newton steps depends on various factors, mainly the predictor model and the step size. We used the secant predictor which reduced the necessary Newton steps in contrast to the trivial predictor in most cases by one to two. While smaller step sizes decrease the necessary Newton iterations, the need for more predictor-corrector steps far outweighs the savings in Newton steps. On the other hand, too large step sizes can lead to a diverging corrector step, either because of a bad initial guess or an unsolvable system. One strategy that works well for most computations is an initial step size $s \approx 0.1$ which is multiplied by a factor $\frac{1}{3}$ if the corrector step does not converge. The number of necessary Newton steps for the presented results is between 4 to 6 once on the non-laminar branch and 7 to 9 for the bifurcation from the laminar branch.

Figure 3.4 shows the Cauchy error for different values of constant vorticity and wave height. Here the Cauchy error is the difference of two solutions h_N and $h_{N/2}$ where the sub index denotes the degrees of freedom used to discretize the free boundary. A decreasing Cauchy error indicates that the computed approximation is mesh independent. We see that the Cauchy error behaves similarly for all four considered cases and only varies in the absolute value. Note that for the irrotational case ($\gamma = 0$) the wave height 0.5 is already 97.7% of the maximal observed wave height and close to the stagnating wave.

These results support the claim that the algorithm presented in [51, 50], which our work is based on, provides a reliable way to compute waves of large amplitude and

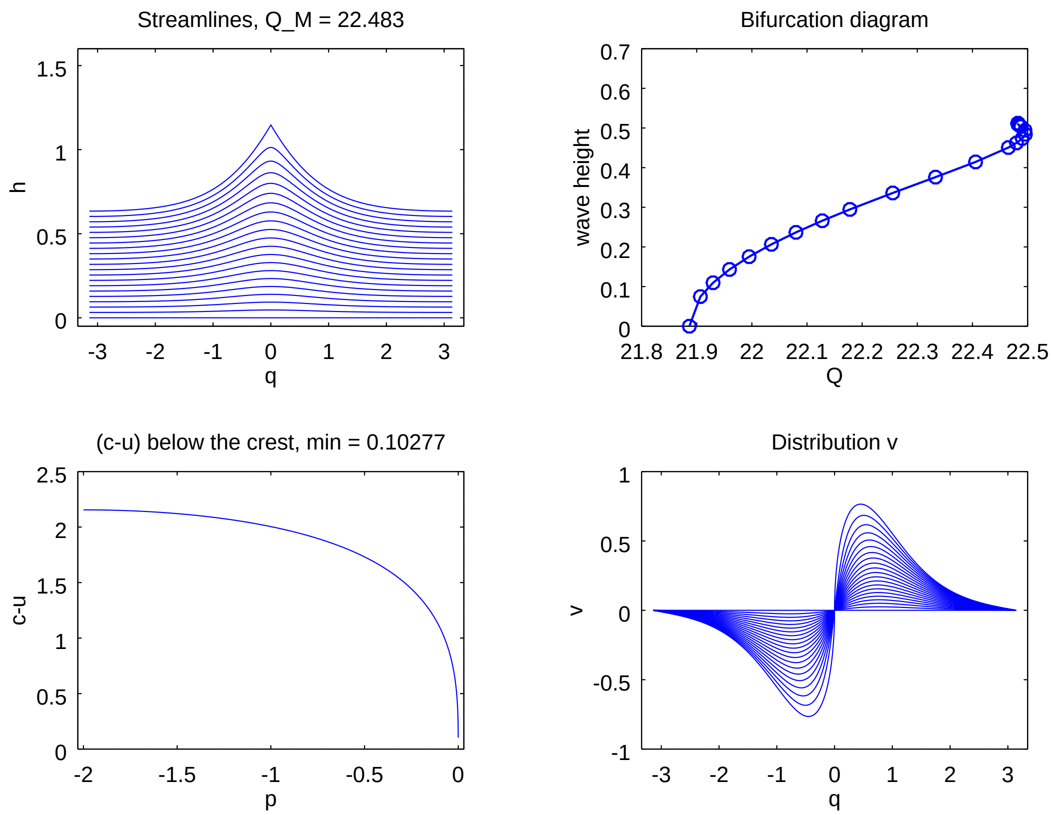

Figure 3.5: The Stokes' wave for $\gamma = 0$ (obtained at $Q = Q_M$) and its bifurcation diagram.

our improvements, like finer grading of the mesh, lead to a better approximation, thus allowing for computations closer to stagnating waves. Choosing the residual threshold 10^{-12}, in accordance[6] with other numerical studies on water waves [55, 56], ensures that solving the non-linear system does not introduce dominant errors. Being not the main scope of this work to present an algorithm performing with substantially better accuracy on computing the well studied (irrotational) Stokes' wave, we construct an algorithm which improves on [51, 50] and is quite general in the computation of waves with non-constant vorticity.

3.4.1 Vorticity above the critical value

Recall that the linearized height function

$$h_L(q, p) = H(p) + bm(q, p)$$

is, for a proper step size $b = s$, a predictor for a solution on the non-laminar branch.

[6]The deviation of the Bernoulli constant in [55] is of the order 10^{-10} while in our computations it is of order 10^{-12}.

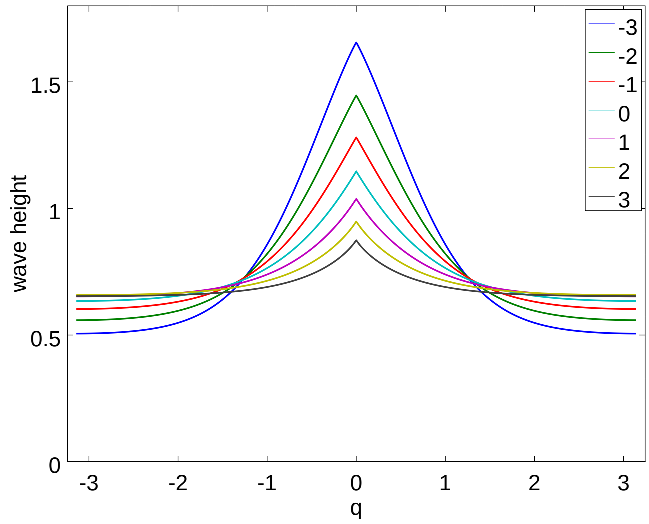

Figure 3.6: The free boundary of maximal waves (obtained at $Q = Q_M$) for different values of constant vorticity.

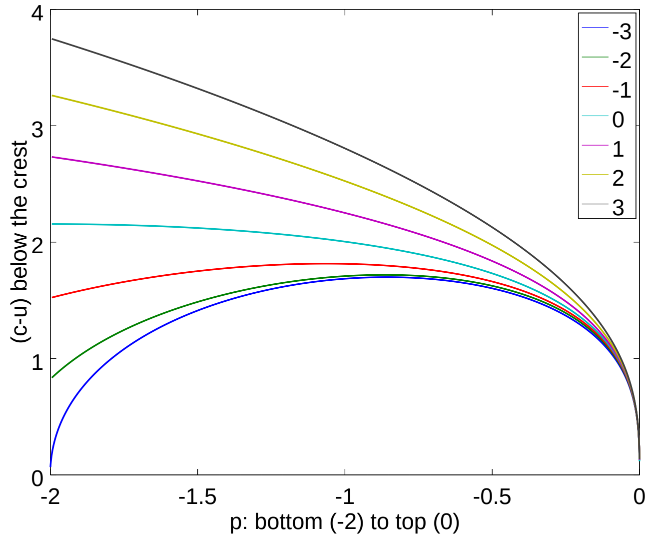

Figure 3.7: For different values of constant vorticity: The horizontal part, $(c - u)$, of the velocity field, on the vertical line below the wave crest, for maximal waves (obtained at $Q = Q_M$).

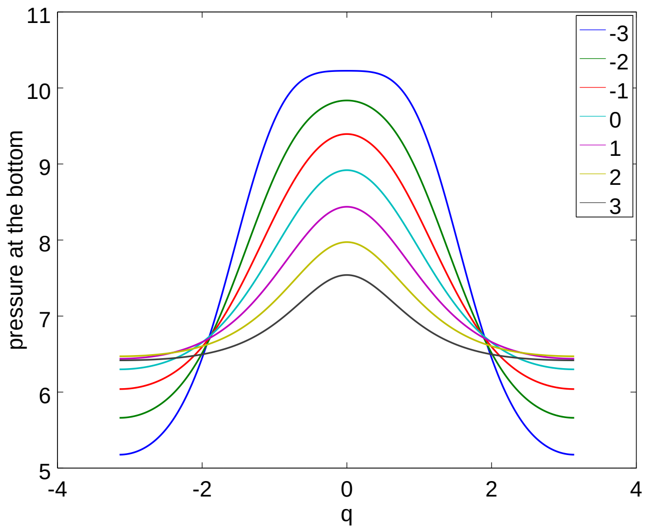

Figure 3.8: For different values of constant vorticity: The pressure at the flat bottom , for maximal waves (obtained at $Q = Q_M$).

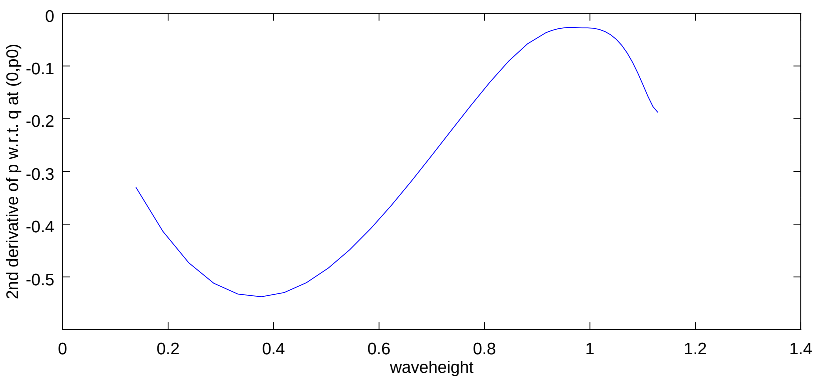

Figure 3.9: The value of $P_{qq}(0, p_0)$ along the bifurcation curve for $\gamma = \gamma_{\text{crit}}$.

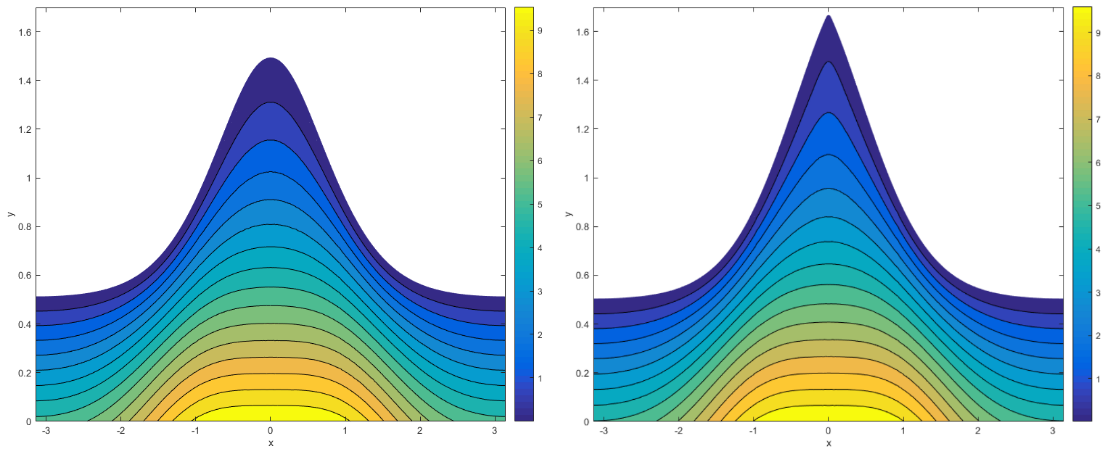

(a) $\gamma = \gamma_{\text{crit}}$ at Q_G

(b) $\gamma = \gamma_\ell$ at Q_M

Figure 3.10: Contourplot of the pressure in the physical domain.

Referring to [22, 48], for constant vorticity,

$$\gamma(-p) \equiv \gamma,$$

the laminar solution is given by

$$H(p) = \frac{2(p - p_0)}{\sqrt{\lambda_* - 2\gamma p} + \sqrt{\lambda_* - 2\gamma p_0}}, \quad p_0 \leq p \leq 0,$$

where λ_* satisfies the dispersion relation

$$\frac{\lambda}{g - \gamma\sqrt{\lambda}} + \tanh\left(\frac{2p_0}{\sqrt{\lambda} + \sqrt{\lambda - 2p_0\gamma}}\right) = 0.$$

Furthermore, the function $m(q, p)$ is given by

$$m(q,p) = \frac{\sqrt{\lambda_* - 2p_0\gamma}}{\sqrt{\lambda_* - 2p\gamma}} \sinh\Big(H(p)\Big) \cos q, \qquad p_0 \leq p \leq 0, \quad -\pi \leq q \leq \pi.$$

Thus, now, we can perform the numerical continuation approach that was described above, using as an initial guess the linearized height function. For $\gamma > \gamma_{\text{crit}}$ the first observed stagnation point appears at the top of the wave. Such a stagnation point breaks the proposed algorithm since it violates the assumption $c - u > 0$ and leads to weaker regularity of h. As a stopping indicator we choose the minimum of $c - u$ which measures how close to a stagnation we are. We denote a wave as a stagnating wave once $c - u$ reaches 5% of its initial value at the laminar wave H. The magnitude of this threshold is in accordance with the literature, and in general smaller in our computation, allowing us to compute waves closer to stagnation and of larger wave

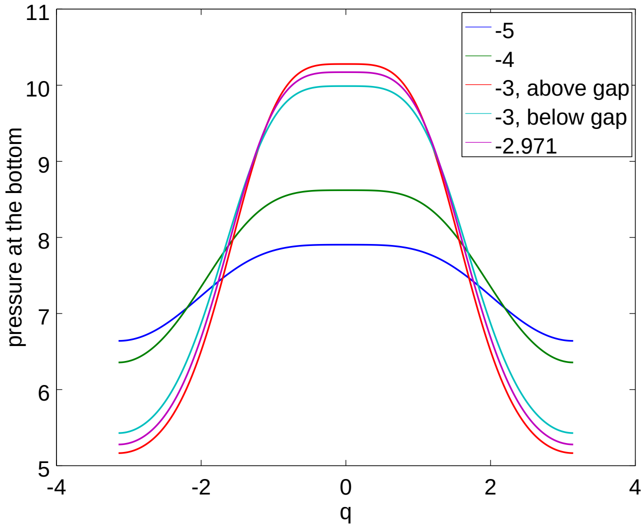

Figure 3.11: Pressure at the flat bottom for the maximal wave of $\gamma = -4, -5$, directly below and above the gap for $\gamma = -3$ and Q_G for $\gamma = \gamma_{\text{crit}} = -2.971$.

height. We recall here, that once the profile of the wave $h(q, p)$ is computed, then the quantity $c - u$ is readily available by equation (3.14).

Since all waves for $\gamma > \gamma_{\text{crit}}$ show the same characteristic we only discuss one example in detail and give some remarks on the influence of γ. Figure 3.5 shows the famous Stokes' wave of greatest height, i.e. the limiting wave for $\gamma = 0$, which is obtained for $Q = Q_M$. At first we present a plot of the streamlines, which show the characteristic 120° degree angle occurring at the stagnation point at the wave crest; each streamline is defined by $[p = \text{constant}]$, with this constant taking values in the interval $[p_0, 0]$. With the same technique, we depict v, which is the vertical part of the velocity field, given by (3.14). Finally, we plot the bifurcating curve $\mathcal{C}$ for which we observed two turning points in Q, which is a novel characteristic of $\mathcal{C}$. It is interesting that the second picture in Figure 3.5 concurs with a quite surprising conjecture stating that, of all regular irrotational waves, whereas the wave of greatest height is indeed the highest travelling wave, it does not actually maximise other physical quantities inherent to such waves: it is not the fastest, or most impulsive, or most energetic (as represented here by Q). This was also first observed by way of numerical investigations, cf. [65].

The appearance of two turning points in Q and a monotonously increasing wave height along the solution curve is observed for all constant vorticities $\gamma > \gamma_{\text{crit}}$. The value of γ does have a significant influence on the stagnating waves. Indeed, in Figure 3.6 we present the profiles for the waves of maximal amplitude which are obtained for the value of hydraulic head $Q = Q_M$. We observe the following characteristics for the wave profile:

- The wave height decreases, as the vorticity γ gets larger.
- The shape of the wave changes with the vorticity; the crest becomes sharper and the trough wider and flatter as the vorticity increases. For some interesting

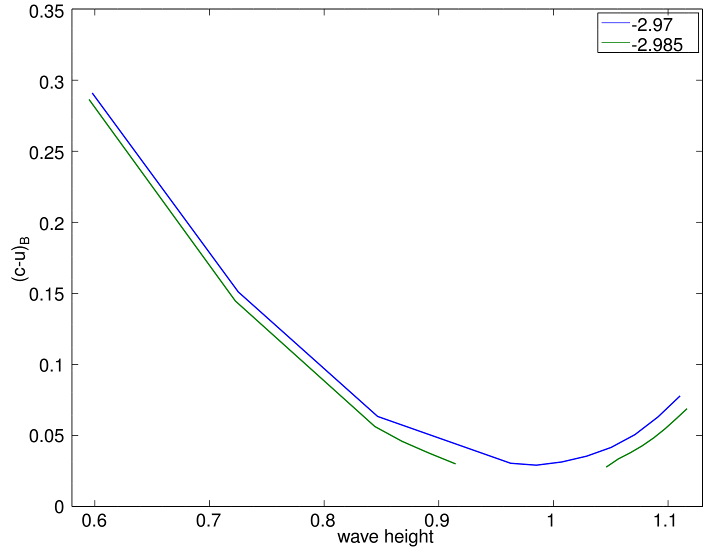

Figure 3.12: $(c-u)_B$ along the solution curve $\mathcal{C}$, parametrized by the wave height.

rigorous mathematical treatment of extreme waves, or wave with stagnation points, which possess an underlying vorticity we refer to [23, 75].

Furthermore, in Figure 3.7 we present the results for the speed $(c-u)$ below the crest, for the maximal waves obtained for each value of constant vorticity and whose wave profiles were presented in Figure 3.6, respectively; these results display qualitatively different distribution of the speed $(c-u)$ below the crest, which becomes more transparent closer to the bottom of the flow.

3.4.2 Critical vorticity and below

The presented procedure does not compute a maximal wave with a sharp angle at the top for all constant vorticities. In particular, if the vorticity is below γ_{crit}, it breaks down earlier. This behaviour was also observed in [50, 51] and attributed to a stagnation point at the bottom of the wave. An indication for this, is the value of $(c-u)$ at the bottom right below the crest which is close to zero, see Figure 3.7. This value is denoted by $(c-u)_B$, and is readily available, once the wave is computed, from the expression

$$(c-u)_B = \frac{1}{h_p\,(0, p_0)}.$$

A more detailed consideration revealed that for vorticities close to but greater than the critical value, $(c-u)_B$ has a minimum inside the bifurcation curve $\mathcal{C}$. Indeed, in Figure 3.12, we observe this behaviour of $(c-u)_B$ as a function of the continuation parameter, for two different values of vorticity. It is worth-mentioning that this

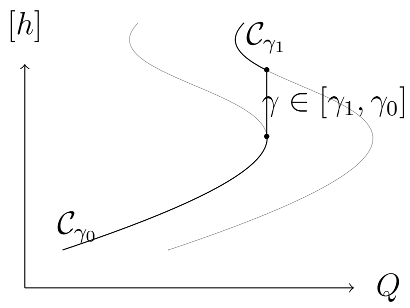

Figure 3.13: Numerical continuation via Q and γ combined

behaviour of $(c-u)_B$ is common for all constant vorticities we considered. This observation motivated the idea that for vorticities smaller than the critical value, $(c-u)$ at the bottom should increase after the presumptive stagnation point, and thus the corresponding wave be computable with the presented algorithm.

The major obstacle in computing these waves is that intermediate steps along $\mathcal{C}$ are not computable. Instead, we consider some γ_0 above the critical value and compute the solution with maximum value of Q along $\mathcal{C}_{\gamma_0}$. Then we fix Q and instead consider γ as the bifurcation parameter, looking for a solution for $\gamma_1 < \gamma_{\text{crit}} < \gamma_0$. Now we switch back to Q as the bifurcation parameter and compute the upper section of $\mathcal{C}_{\gamma_1}$, bounded above by the wave of maximal wave height and below by the wave with the stagnation point at the bottom. This procedure is sketched in Figure 3.13.

Numerical experiments show that this approach works and that waves with stagnation point at the top exist even for vorticities below the critical value, see Figure 3.14. The results also show that the non-computable section of $\mathcal{C}$ grows larger even for small changes in γ. We emphasize the fact that this section of $\mathcal{C}$ is bounded, below and above, by two values of the bifurcation parameter Q, which give two *different* waves with stagnation points at the bottom; in Figure 3.16 we observe that the second wave is larger and steeper. Soon, the computable upper section of $\mathcal{C}$ becomes too small and it is practically incomputable with this scheme; the last wave we could compute was at $\gamma = \gamma_\ell = -3.062$. In summary, the γ-continuation technique in the interval $(\gamma_\ell, \gamma_{\text{crit}})$, indicates the existence of waves that have a stagnation point on the free surface, for vorticities *below* the critical value and conjectures the existence of waves with stagnation points both at the crest and at the bottom, right below the crest. This becomes transparent in Figure 3.17, where we present the basic characteristics of the maximal water wave with vorticity close to γ_ℓ; note that in this figure we present only the upper (new) part of the bifurcating diagram in order to display more details of this.

We recall that the knowledge of the pressure at the bottom is important for reconstruction of the waves, both analytically and experimentally, and that the pressure is readily available by equation (3.15).

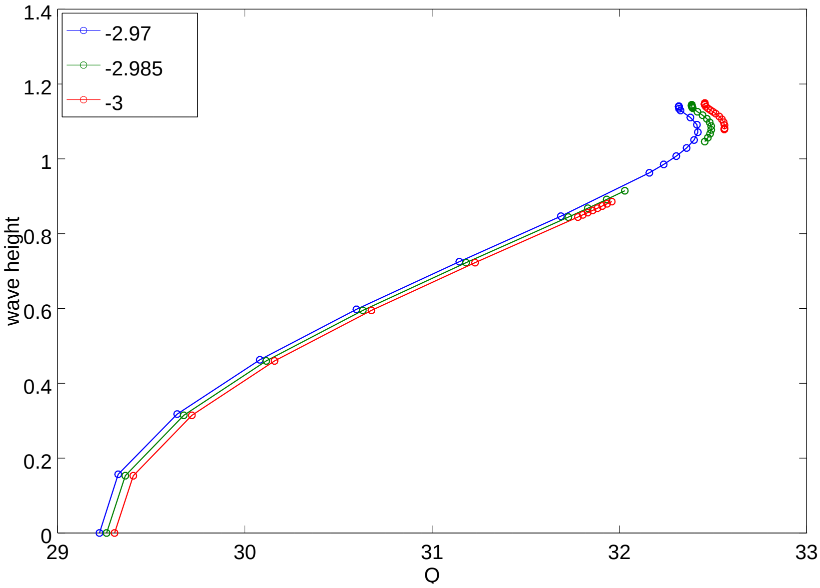

Figure 3.14: Bifurcation diagram for different values of constant vorticity in the interval $(\gamma_\ell, \gamma_{\text{crit}}]$.

We emphasize the fact that the pressure of the fluid displays a qualitative change for values of vorticity smaller than the critical value. Indeed, in Figure 3.8, where we depict the pressure of the fluid at the bottom, we see that when $\gamma < \gamma_{\text{crit}}$, the pressure at the point right below the crest displays a 'plateau' behaviour instead of a local maximum, which characterizes flows with $\gamma > \gamma_{\text{crit}}$. We observe this behaviour of the pressure at the bottom for the various numerical experiments that we have performed, and we have not included here for matters of brevity. An overview of these results is presented in Figure 3.11.

An indication of the occurrence of this 'plateau' can be given by studying the value of $P_{qq}(0, p_0)$, which should vanish; in Figure 3.9 we observe this behaviour of the quantity $P_{qq}(0, p_0)$ for $\gamma = \gamma_{\text{crit}}$, around the neighbourhood of the point on the bifurcation curve where the gap will appear, namely Q_G.

A more detailed analysis of the features of the pressure shows that, if $\gamma_\ell < \gamma < \gamma_{\text{crit}}$, then this behaviour occurs for the two waves which correspond to the endpoints of the gap in the bifurcation curve. In Figure 3.10 we depict two waves which display this 'plateau' for two different values of constant vorticity, i.e. $\gamma = \gamma_{\text{crit}}$ and $\gamma = \gamma_\ell$. It is worth noting that these waves were obtained for substantially different points on the bifurcation curve, namely Q_G and Q_M, resulting different features: the latter one has a stagnation point at the top whereas the first one has a smooth surface.

For vorticities $\gamma < \gamma_\ell$ we are only able to compute the lower section of $\mathcal{C}$. The last computable wave has a smooth surface and instead a very small value of $(c-u)$ at the bottom, indicating a stagnation point there, see Figure 3.18. Moreover, the pressure distribution at the bottom for the last computable wave displays the above mentioned 'plateau' behaviour.

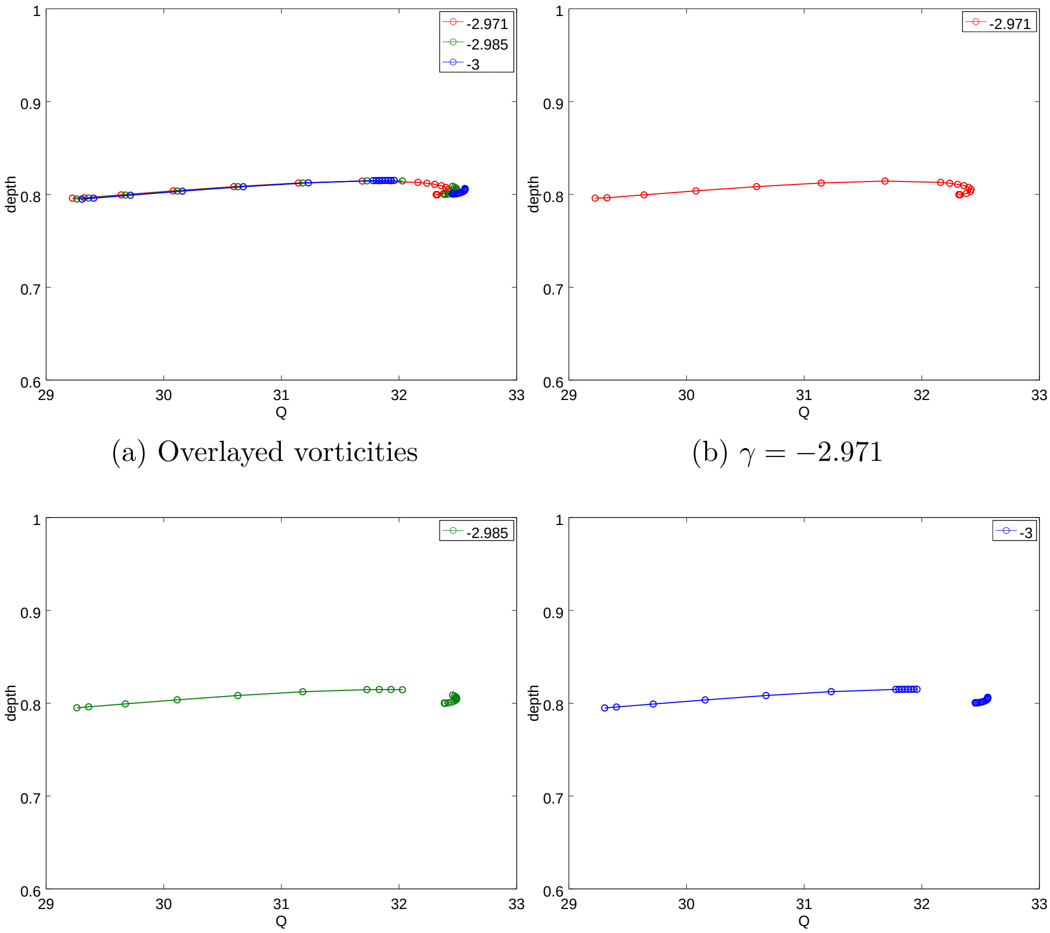

(a) Overlayed vorticities (b) $\gamma = -2.971$

(c) $\gamma = -2.985$ (d) $\gamma = -3$

Figure 3.15: Depth along the bifurcation curve for two vorticities with a gap and γ_{crit}

We note that the 'plateau' feature is also displayed for one value of constant vorticity in Figure 8 of [64], for a wave with a stagnation point at the bottom. Similar conclusions can be made by comparing Figures 6 and 7 of [77]. Our results indicate the existence of a family of waves which display the 'plateau' feature.

Gathering the results of the above procedure, for different values of constant vorticity, we display the wave height and average depth for maximal waves in Figure 3.19.

Remark 2. We observed that the value of γ_{crit} is increasing as $|p_0|$ increases. However, not for all values of p_0 we can find γ_{crit}. Considering the case $\gamma < 0$, and following the discussion of Section 3 in [22], for given p_0 there is a minimum value of γ for which a bifurcation point (and a bifurcation curve) exists; we denote this value by γ_m. Moreover, it is shown that as $|p_0|$ increases, γ_m approaches zero rapidly. There is some (large enough) value of $|p_0|$ for which the γ_{crit} is equal to γ_m. In our case this value is $|p_0| \approx 4.4$, and for values of $|p_0|$ larger than that, waves do not display the feature of critical vorticity. These results are in qualitative agreement with [51].

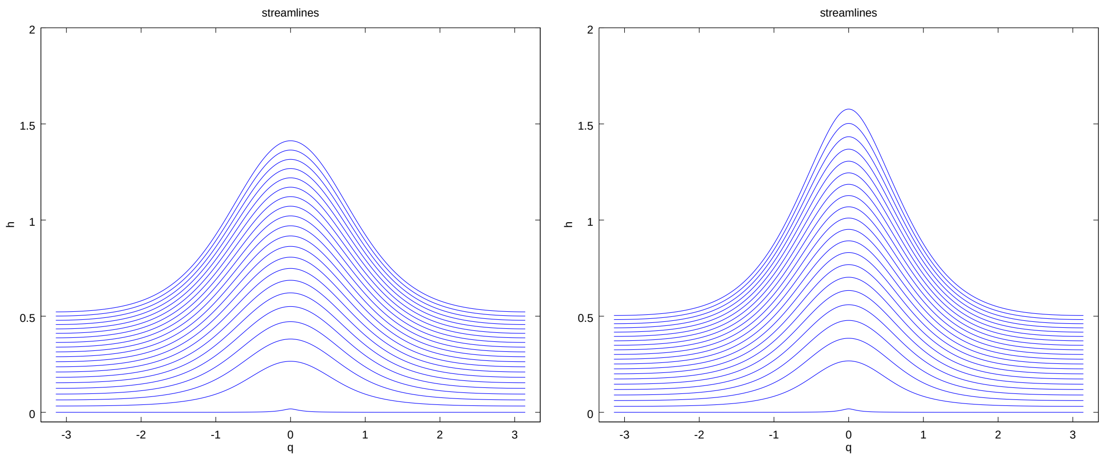

(a) Below the gap (b) Above the gap

Figure 3.16: Streamline for $\gamma = -3$ just below and above the gap.

3.4.3 Examples of non-constant vorticity

An interesting case of non-constant vorticity is the case of vorticity varying linearly with respect to the stream function. A plethora of theoretical results is presented in several recent works. Existence for a variety of families of waves with critical layers is shown in [33, 32, 1], using arguments from bifurcation theory. Moreover, qualitative results for small amplitude waves are presented therein; analogous results for modal waves are presented in [34].

We consider the following distribution of vorticity:

$$\gamma(-p) = -a_1 p + a_0,$$

then the laminar solution is given by

$$H(p;\lambda) = \int_{p_0}^{p} \frac{1}{\sqrt{\lambda - 2\Gamma(s)}} ds = \int_{p_0}^{p} \frac{1}{\sqrt{\lambda + a_1 s^2 - 2a_0 s}} ds.$$

The dispersion relation as given in [49] reads

$$\lambda^* + a_0\sqrt{\lambda^*}F(H(0;\lambda^*)) - gF(H(0;\lambda^*)) = 0$$

with

$$F(d) = \begin{cases} \frac{\tanh(d\sqrt{1+a_1})}{\sqrt{1+a_1}} & \text{if } a_1 > -1 \\ d & \text{if } a_1 = -1 \\ \frac{\tan(d\sqrt{-(1+a_1)})}{\sqrt{-(1+a_1)}} & \text{if } a_1 < -1 \end{cases}.$$

We consider $\gamma_\alpha(-p)$ such that $\gamma_\alpha(-p_0) = 0$ and $\gamma_\alpha(0) = \alpha$ for $\alpha \in \{-1, 0, 1\}$. The analysis of this particular class of examples was motivated by the discussion in [50],

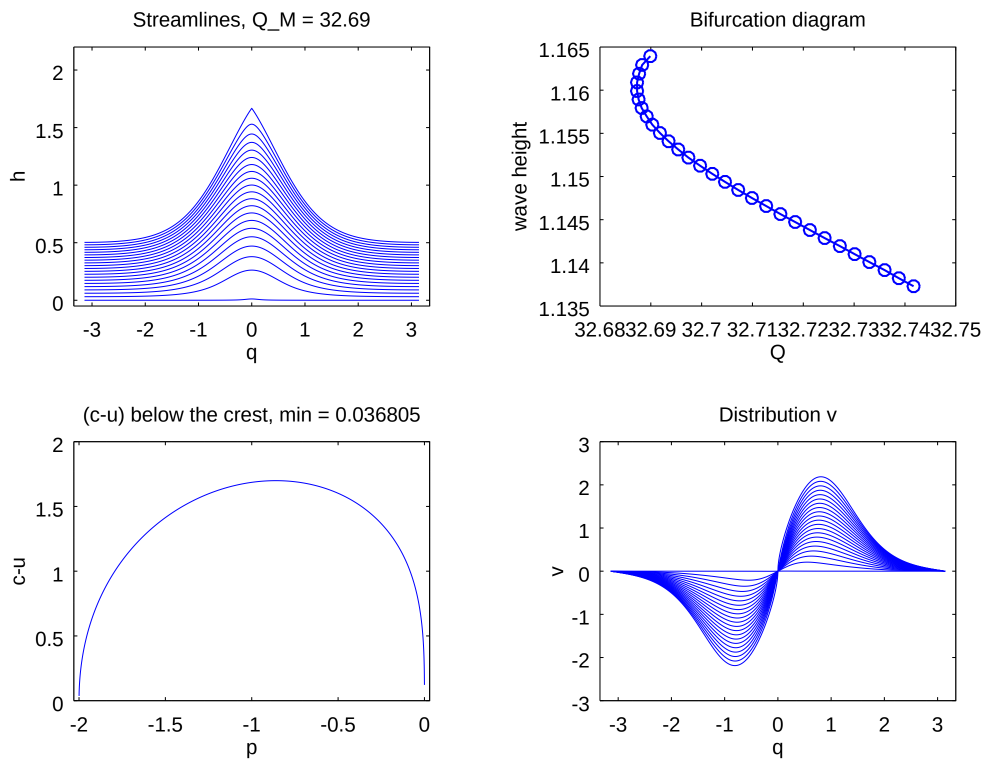

Figure 3.17: Wave for $\gamma = -3.05$ (obtained at $Q = Q_M$) and its bifurcation diagram.

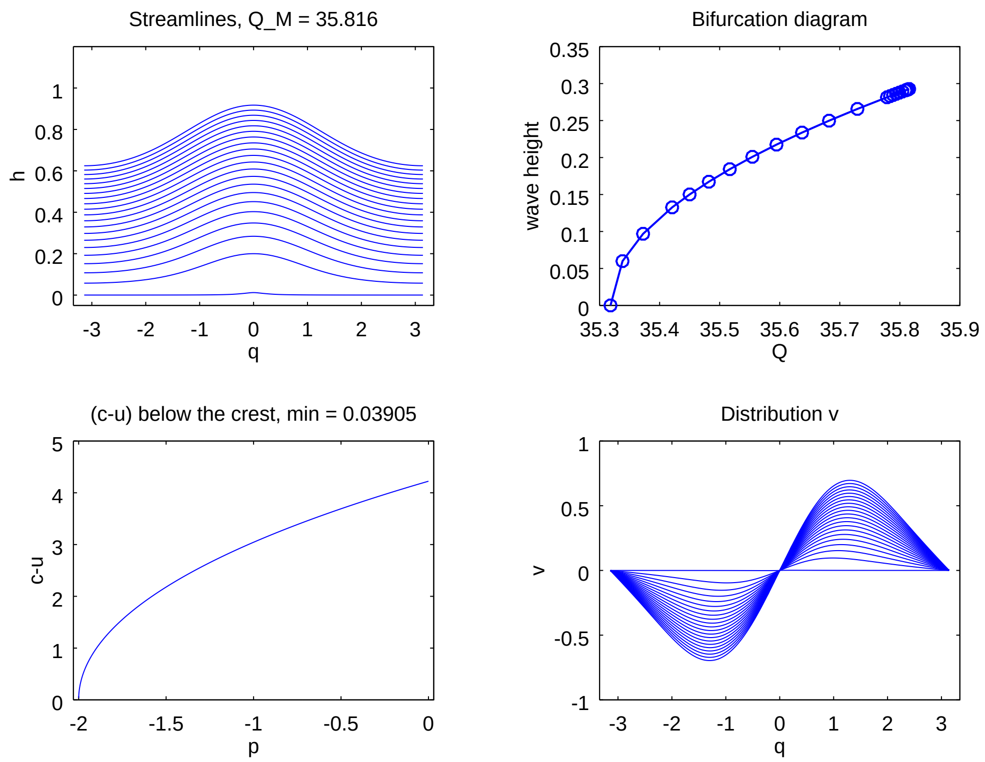

Figure 3.18: Wave for $\gamma = -5$ (obtained at $Q = Q_M$) and its bifurcation diagram.

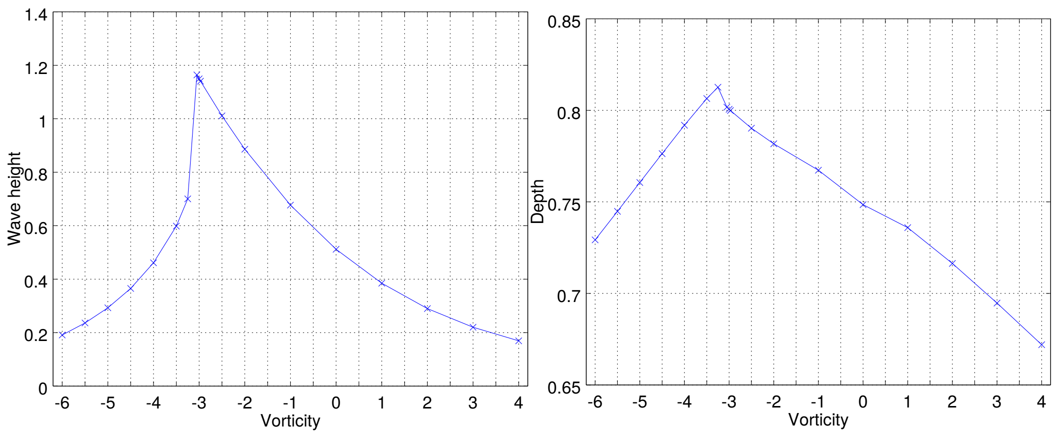

(a) Wave height. (b) Depth

Figure 3.19: Characteristic of the limiting wave for constant vorticity.

where it is mentioned that, from experiments, wind typically has the effect of producing vorticity in the water near the surface. Thus, we discuss a case of non-constant, continuous distribution of vorticity, which vanishes at the bottom, but not at the surface of the fluid. Note, also, that $\alpha = 0$ is the case of a constant zero vorticity which gives us the Stokes' wave as the limiting wave, and we include it here, for comparison with the linear vorticity case.

Similarly to the case of constant vorticity we observe two turning points in Q and monotonously increasing wave heights for $\alpha \in \{-1, 0, 1\}$. Figures 3.20, 3.21 and 3.22 show some characteristics of the wave profile, in particular the free boundary, the velocity $(c - u)$ on the vertical line below the crest and the water pressure at the bottom, respectively, for the different values of α. We note that for the two last quantities we used equation (3.14) and (3.15). In summary we can say that the considered waves display similarities with waves of constant vorticity.

Finally, we have computed a wave for which the vorticity is linearly distributed, taking the value $\alpha = -10$ at the free surface and vanishes at the bottom, see Figure 3.23. For this wave, we observe a different behaviour from the waves of negative constant vorticity $\gamma < \gamma_\ell = -3.062$. Firstly, the wave with linearly distributed vorticity displays a stagnation point at the free surface, while the others display a stagnation point at the bottom. Secondly, the bifurcation curve has two turning points before it reaches a flow with stagnation point. Thirdly, and most striking, the wave with this non-constant vorticity, has a significantly larger wave height compared with other waves with constant negative vorticity.

Finally, we present the results for three more examples of non-constant vorticity in Figure 3.24. Here the vorticity distributions are either linear or quadratic with respect to the stream function and vanish on the bottom while at the free surface it holds $\gamma(0) = -4$. The three considered vorticity functions are

$$\gamma_\ell(-p) = -4\left(1 - \frac{p}{p_0}\right), \quad \gamma_a(-p) = -4\left(1 - \frac{p}{p_0}\right)^2 \quad \text{and} \quad \gamma_b(-p) = -4\left(1 - \frac{p^2}{p_0^2}\right).$$

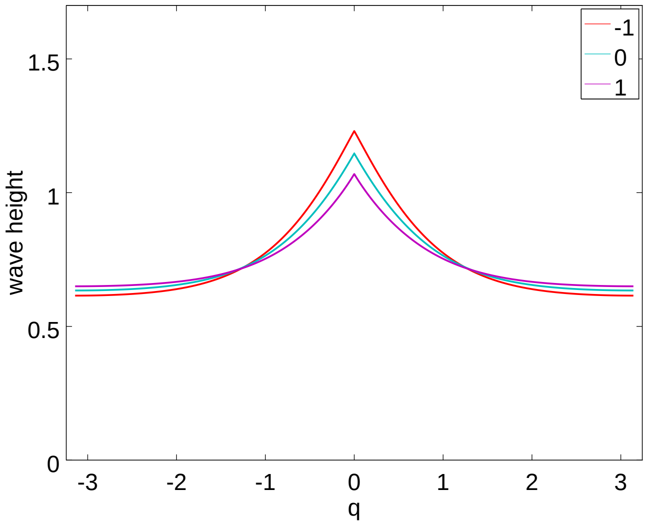

Figure 3.20: The free boundary for linear vorticity with $\gamma_\alpha(0) = \alpha \in \{-1, 0, 1\}$.

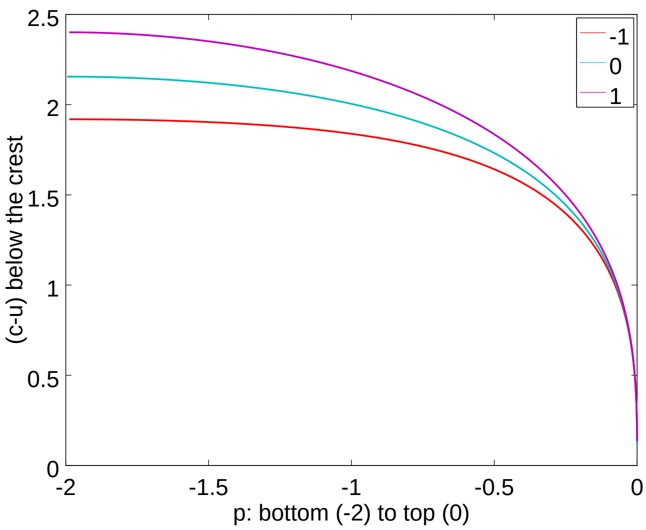

Figure 3.21: The velocity $(c-u)$ below the wave crest for linear vorticity with $\gamma_\alpha(0) = \alpha \in \{-1, 0, 1\}$.

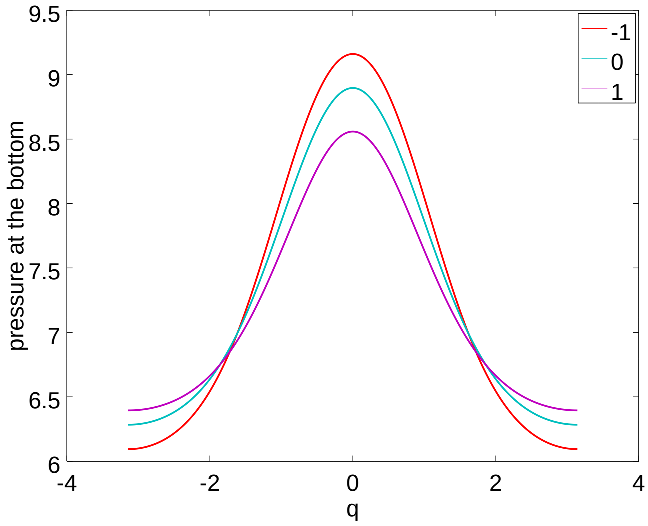

Figure 3.22: The pressure at the flat bottom for linear vorticity with $\gamma_\alpha(0) = \alpha \in \{-1, 0, 1\}$.

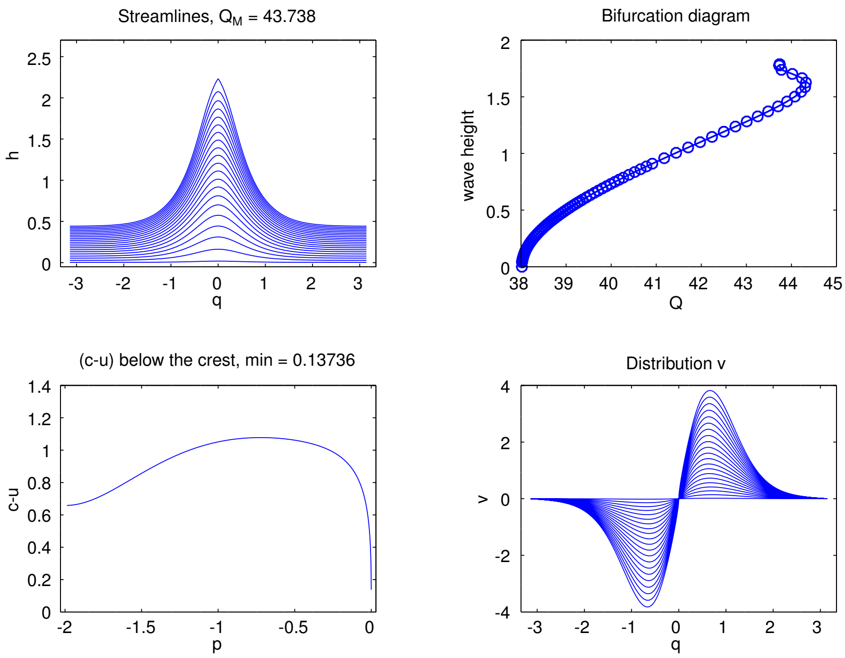

Figure 3.23: The water wave for linear vorticity $\gamma_\alpha(0) = \alpha = -10$.

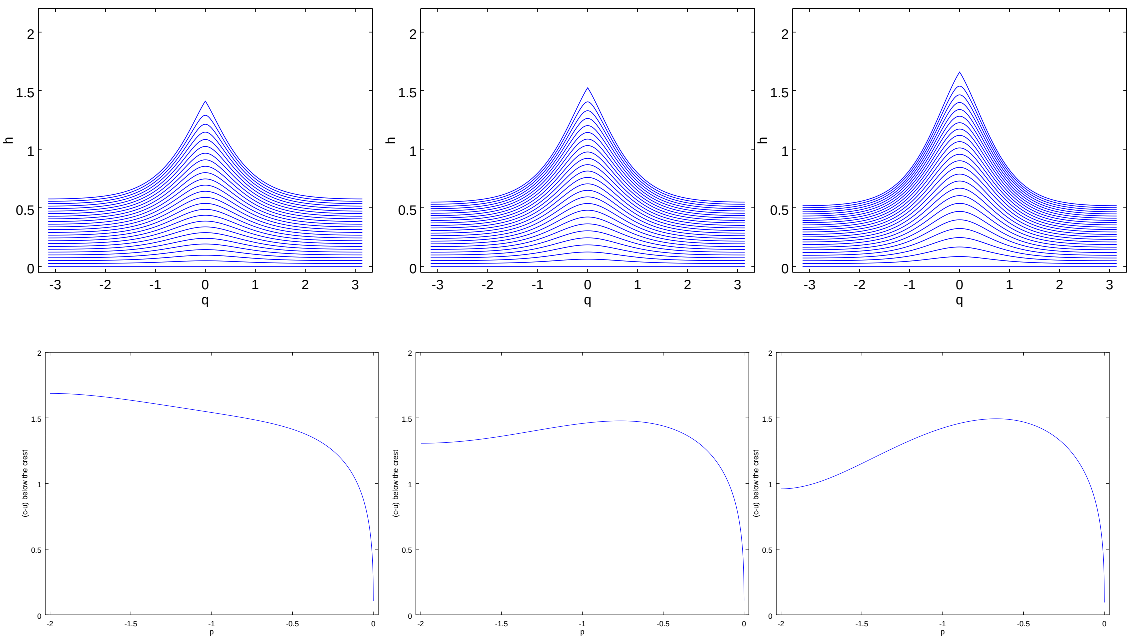

(a) $\gamma_a(-p) = -4\left(1 - \frac{p}{p_0}\right)^2$ (b) $\gamma_\ell(-p) = -4\left(1 - \frac{p}{p_0}\right)$ (c) $\gamma_b(-p) = -4\left(1 - \frac{p^2}{p_0^2}\right)$

Figure 3.24: Streamlines and $(c-u)$ below the crest for waves near stagnation for three quadratic vorticities with $\gamma(0) = -4$ and $\gamma(-p_0) = 0$.

Note that it holds $\gamma_b(-p) < \gamma_\ell(-p) < \gamma_a(-p)$ for $p \in [p_0, 0]$. Figure 3.24 shows the streamlines, as well as $c - u$ below the crest, for a wave near stagnation, for all three vorticity functions. It is notable that the wave height is inversely correlated with the point wise values of the vorticity functions, i.e. γ_a leads to the smallest and γ_b to the largest wave height.

3.5 Conclusions

We presented a detailed analysis of a numerical continuation algorithm to compute water waves. Using this algorithm, we rederived known results, with some results closer to stagnation points, as well as computed new characteristics of the waves, with the most important being:

- A new part of the branch of the bifurcation diagram.
- Limiting waves near stagnation, for the constant vorticity case, with new characteristics; see Section 3.4.2 for more details.
- Maximal waves of much larger amplitude for the case of linear vorticity.

Finally, we showed the performance of the algorithm for some cases of variable vorticity. A more systematic study of the case of general vorticity, through this algorithm, will be presented in future work.

4 Numerical approximation of water waves through a deterministic algorithm

Dominic Amann, Konstantinos Kalimeris

Abstract

Recently, a constructive algorithm based on asymptotic expansions was proposed for computing water waves of large amplitude, in the absence of stagnation points, by one of the authors in [48]. Here, we perform a numerical implementation of this algorithm, verifying the analytical results and, indeed, computing large amplitude waves. Furthermore, we introduce a modification of the existing analytical procedure, which allows the computation of waves with variable vorticity by a straightforward adaptation of the current algorithm. Profiles and other features of water waves are presented for constant and some cases of variable vorticity.

4.1 Introduction

The analysis of the water wave problem dates back to the studies of Newton and Stokes [70]; a detailed review on the origins of water wave theory is given in [27], where the main contributions until the great work of Stokes are presented. Since then, an abundance of work has been appeared. Not in few cases, a detailed insight on the studying of the problem and the properties of its solutions may be extracted through a combined application of analytical and numerical approaches.

In the present work, we study travelling periodic water waves in flows with underlying current of variable vorticity without stagnation points, based on the formulation introduced in [22]; see also [14]. Based on a different viewpoint of the physical parameters of the problem, another formulation was derived in [40]. For waves containing critical layers we refer to [25, 26, 33, 32, 78, 35, 43, 44, 57]. Several numerical works have been made on computing interesting water waves based on the above formulation, see [6, 28, 46, 64].

In [22], starting from Euler's equations for two dimensional, periodic, travelling water waves with variable vorticity, and applying a partial-hodograph transformation, the nonlinear boundary value problem (4.1)-(4.3) was derived. A key role in the analysis of this problem is the occurrence of a bifurcation parameter which is indicative of the total energy of the wave; this parameter, denoted by Q, is called the hydraulic head of the flow.

Based on the above formulation, non-trivial solutions of (4.1)-(4.3) were obtained analytically in the form of asymptotic expansions in [20] and [48], for the case of constant vorticity. The latter work can be viewed as a non-trivial generalization of the former one.

We point out that in the absence of flow reversal, the analysis in [19] ensures the real-analyticity of all the streamlines and thus the convergence of the infinite Taylor expansions, see also [36]. Whereas the available results on regularity for flow reversal, flows with critical layers, are merely of class C^∞, see [26], so that even the existence of suitable high-order approximations is an issue.

We find worth mentioning that the form of this asymptotic expansion exhibits some general features. A similar expansion appears in the analysis of [45] on an essentially different approach of the water wave problem. Furthermore, preliminary results show that special cases of this expansion can be applied to a non-local formulation of the water wave problem; for a detailed analysis of this formulation we refer to [2, 7, 39, 38].

In [48] a constructive algorithm was proposed for the computation of higher order terms of these asymptotic expansions. Moreover, the possibility of extending this algorithm for computing waves with variable vorticity was discussed therein. The above-mentioned algorithm provided a precise way to compute the expansions to all orders, but it involved tedious, though straightforward calculations, which limits computations to the first few order terms.

Thus, the goal of the current work is two-fold:

- Firstly, we provide the numerical implementation of the above algorithm, i.e. we numerically compute higher–order terms of the above asymptotic expansions corresponding to waves of moderate and large amplitude; the details are in section 4. This includes numerical verification that the system (4.8) is satisfied and that the numerical solution of its individual step of the algorithm have the expected convergence.

- Secondly, we introduce a novel transformation in one of the main steps of the analytical procedure which was used in [48]. This allows the extension of the previous analytical solutions to problems with variable vorticity; the details are in section 2.2. Furthermore, this induces a slight modification on the numerical implementation in order to compute high-order expansions of flows with variable vorticity. Following this modification we display some features of such waves in section 4.2.

For the modelling of our problem we follow [22] where the considered problem, finding water waves with a free surface, is reformulated as a fixed–domain system by applying a Dubreil-Jacotin transformation. Then the problem is, for a given constant

$p_0 < 0$ and vorticity function γ, to find $Q \in \mathbb{R}$ and a periodic, even function h satisfying

$$\begin{aligned}
\mathcal{H}[h] :=&(1+h_q^2)h_{pp} - 2h_p h_q h_{qp} + h_p^2 h_{qq} - \gamma(-p)h_p^3 = 0 \quad \text{in } R, && (4.1)\\
\mathcal{B}_0[h,Q] :=& \quad 1 + h_q^2 + (2gh - Q)h_p^2 = 0 \quad \text{for } p = 0, && (4.2)\\
\mathcal{B}_1[h] :=& \quad h = 0 \quad \text{for } p = p_0. && (4.3)
\end{aligned}$$

The mean depth is computed a posteriori, by integrating $h(0,q)$ over a period, see [48]; for an alternative approach, where the depth is a priori fixed, we refer to [40].

One family of solutions are the so called laminar waves or parallel shear flows; those are solutions that only depend on p. With this assumption the system becomes significantly easier and can be solved analytically for a large class of vorticity functions. To emphasize the special character of laminar waves we denote such solutions as H, for example for linear vorticity

$$H(p;\lambda) = \frac{2(p-p_0)}{\sqrt{\lambda - 2\gamma p} + \sqrt{\lambda - 2\gamma p_0}}$$

where $\lambda > 0$ has to satisfy

$$Q = \lambda - \frac{4gp_0}{\sqrt{\lambda} + \sqrt{\lambda - 2\gamma p_0}}.$$

In general, there are no genuine waves in the neighbourhood of a laminar solution $(Q(\lambda), H(\lambda))$, see [22] for constant vorticity. For certain values of λ and Q, denoted as λ_* and Q^* respectively, a branch of non-laminar bifurcates from the curve of laminar flows. The values of λ_* and Q^* are determined by the dispersion relation, see [49].

We present an asymptotic expansion of a solution (Q, h) on the non-laminar branch around the solution $(Q^*, H(\lambda^*))$ for non-constant vorticity. Furthermore, the constructive algorithm for computing the expansion terms can be implemented by only solving one-dimensional differential equations.

This paper is organised as follows: in section 4.2 we review and generalize the expansion algorithm presented in [48]; in section 4.3 we describe the used numerical scheme which is verified by numerical results in section 4.4 where we furthermore present some waves for different distributions of the vorticity.

4.2 Asymptotic Expansion algorithm

In this section we aim to recap the constructive algorithm presented in [48], we refer to the original paper for more details and proofs. The main idea is to find an expansion of the pair (Q, h) around the bifurcation point (Q^*, H). Here and the remainder of this paper H without a specific λ is the laminar flow at the bifurcation point, that is $H(p) = H(p; \lambda_*)$.

We introduce approximations of the pair (Q, h) by the polynomials in $b \in \mathbb{R}$

$$Q \approx Q^{(2N)}(b) \qquad := Q^* + \sum_{k=1}^{N} Q_{2k} b^k \tag{4.4}$$

$$h(q, p; Q) \approx h^{(2N+1)}(q, p; b) := \sum_{k=0}^{2N+1} h_k(q, p) b^k \tag{4.5}$$

with coefficients $Q_{2k} \in \mathbb{R}$ and h_k defined as

$$h_{2k}(q, p) := \sum_{m=0}^{k} \cos(2mq) f_{2m}^{2k}(p), \tag{4.6}$$

$$h_{2k+1}(q, p) := \sum_{m=0}^{k} \cos((2m+1)q) f_{2m+1}^{2k+1}(p) \tag{4.7}$$

where $f_m^k \in C^\infty([p_0, 0])$ for all m, k. The goal is to choose the constants Q_{2k} and functions f_m^k such that $(Q^{(2N)}, h^{(2N+1)})$ satisfies (4.1)–(4.3) up to $\mathcal{O}(b^{2N+2})$, that is

$$\begin{cases} \mathcal{H}[h^{(2N+1)}](q, p) & = \mathcal{O}(b^{2N+2}), \\ \mathcal{B}_0[h^{(2N+1)}, Q^{(2N)}](q) & = \mathcal{O}(b^{2N+2}), \\ \mathcal{B}_1[h^{(2N+1)}] & = 0. \end{cases} \tag{4.8}$$

In this procedure, we assume that the solution for $N = 0$, that is $Q^{(0)}$ and $h^{(1)}$ consisting of Q^*, h_0 and h_1 are known. Indeed, these solutions are known analytically for irrotational waves with zero vorticity and a variety of rotational waves, see [49].

4.2.1 Zero vorticity

For ease of notation we discuss an irrotational case in this section in detail and explain the necessary modifications for more general vorticity in section 4.2.2.

Assume $h^{(2N+1)}$ is known, the goal is to compute additional expansion terms h_{2N+2}, h_{2N+3} and Q_{2N+2}. The algorithm is split into two parts where first we compute h_{2N+2} and then the pair (h_{2N+3}, Q_{2N+2}).

Find h_{2N+2}: Let $h^{(2N+1)}$ be the known solution of our model problem (4.1)–(4.3) up to order b^{2N+2}, then set

$$\hat{h}^{(2N+2)} = h^{(2N+1)} + b^{2N+2} h_{2N+2}.$$

for a yet to be determined function h_{2N+2} of the form (4.6). Apply the operators $\mathcal{H}$ and $\mathcal{B}_0$ to $\hat{h}^{(2N+2)}$ gives us a polynomial in b. For example, the first term of $\mathcal{H}[\hat{h}^{(2N+2)}]$ looks like

$$\left[1 + \left(\hat{h}_q^{(2N+2)}\right)^2\right] \hat{h}_{pp}^{(2N+2)} = \left[1 + \left(\sum_{k=0}^{2N+2} b^k (h_k)_q\right)^2\right] \left(\sum_{\ell=0}^{2N+2} b^\ell (h_\ell)_{pp}\right).$$

We know that by definition all terms up to and including b^{2N+1} are equal to zero. Our goal is to find h_{2N+2} such that the coefficient belonging to b^{2N+2} vanishes as well. Furthermore, h_{2N+2} must satisfy the homogeneous Dirichlet boundary condition at $p = p_0$ and must be of the form (4.6). Setting the coefficients corresponding to b^{2N+2} of $\mathcal{H}[\hat{h}^{(2N+2)}]$ and $\mathcal{B}_0[Q^{(2N)}, \hat{h}^{(2N+2)}]$ to zero and collecting all known data on the right hand side gives us

$$
\begin{aligned}
(h_{2N+2})_{pp} + \frac{1}{\lambda^*}(h_{2N+2})_{qq} &= e^{(R)} && (q,p) \in R,\\
(h_{2N+2})_p - \frac{g}{\lambda_*^{3/2}} h_{2N+2} &= e^{(B)} && p = 0,\\
h_{2N+2} &= 0 && p = p_0.
\end{aligned}
$$

Note that we additionally scaled the boundary condition by $-\frac{1}{2\sqrt{\lambda_*}}$. Furthermore, from [48] we know that $e^{(R)}$ and $e^{(B)}$ can be written as

$$
e^{(R)}(p) = \sum_{m=0}^{N+1} \cos(2mq) e_{2m}^{(R)}(p) \quad \text{and} \quad e^{(B)} = \sum_{m=0}^{N+1} \cos(2mq) e_{2m}^{(B)} \tag{4.9}
$$

and the solution also has the form

$$
h_{2N+2}(q,p) = \sum_{m=0}^{N+1} \cos(2mq) f_{2m}^{2N+2}(p).
$$

The functions f_{2m}^{2N+2} for $m = 0, \dots, N+1$ are found as solutions of the ordinary differential equation

$$
(f_{2m}^{2N+2})_{pp} - \frac{(2m)^2}{\lambda^*} f_{2m}^{2N+2} = e_{2m}^{(R)}(p) \quad p \in (p_0, 0), \tag{4.10}
$$

$$
(f_{2m}^{2N+2})_p - \frac{g}{\lambda_*^{3/2}} f_{2m}^{2N+2} = e_{2m}^{(B)} \quad p = 0 \tag{4.11}
$$

$$
f_{2m}^{2N+2} = 0 \quad p = p_0 \tag{4.12}
$$

Note that one could, as done in [48], already introduce Q_{2N+2} which would results in a different function h_{2N+2}. More precisely f_0^{2N+2} then has the form

$$
f_0^{2N+2} = Q_{2N+2} \hat{f}_0(p) + \widetilde{f}_0^{2N+2}(p)
$$

where $\hat{f}_0 = -\frac{1}{2} \frac{1}{gp_0 + \lambda_*^{3/2}}(p - p_0)$ and $\widetilde{f}_0^{2N+2}$ does not depend on Q_{2N+2}. For every $Q_{2N+2} \in \mathbb{R}$ this provides a function f_0^{2N+2} that solves the system (which would also contain Q_{2N+2}) and we can for the moment choose $Q_{2N+2} = 0$. The parameter Q_{2N+2} will be uniquely determined in the next step and we can update f_0^{2N+2} accordingly.

The so constructed pair $(Q^{(2N)}, \hat{h}^{(2N+2)})$ satisfies the systems (4.1)–(4.3) up to order $\mathcal{O}(b^{2N+3})$.

Find (Q_{2N+2}, h_{2N+3})**:** We set

$$\begin{aligned} h^{(2N+3)} &:= \hat{h}^{(2N+2)} + b^{2N+2} Q_{2N+2} \hat{f}_0 + b^{2N+3} h_{2N+3}, \\ Q^{(2N+2)} &:= Q^{(2N)} + b^{2N+2} Q_{2N+2}. \end{aligned}$$

Here we have to include the contribution of $\hat{f}_0$ that we earlier omitted since otherwise the system we get would not be solvable as observed in [20]. Analogous to before we apply the operators $\mathcal{H}$, $\mathcal{B}_0$ and $\mathcal{B}_1$ to $(Q^{(2N+2)}, h^{(2N+3)})$, set the coefficient belonging to b^{2N+3} to zero and collect all known data in the right hand side $(s^{(R)}, s^{(B)})$. This results in the system

$$(h_{2N+3})_{pp} + \frac{1}{\lambda^*}(h_{2N+3})_{qq} + Q_{2N+2}A(p)\cos(q) = s^{(R)}(q,p) \quad (q,p) \in R, \tag{4.13}$$

$$(h_{2N+3})_p - \frac{g}{\lambda_*^{3/2}} h_{2N+3} + Q_{2N+2} B \cos(q) = s^{(B)} \qquad p = 0 \tag{4.14}$$

$$h_{2k} = 0 \qquad p = p_0 \tag{4.15}$$

The function A and constant B are the contributions related to Q_{2N+2} and thus $\hat{f}_0$. For the case of zero vorticity they are given by

$$\begin{aligned} A(p) &= \frac{1}{\sqrt{\lambda_*}} \frac{1}{g p_0 + \lambda_*^{3/2}} \sinh\left(\frac{p - p_0}{\sqrt{\lambda_*}}\right), \\ B &= \frac{3}{2} \frac{1}{g p_0 + \lambda_*^{3/2}} \cosh \frac{p_0}{\sqrt{\lambda_*}}. \end{aligned}$$

Similar to before the right hand side of (4.13)-(4.15) has the structure

$$s^{(R)}(p) = \sum_{m=0}^{N+1} \cos((2m+1)q) s^{(R)}_{2m+1}(p) \quad \text{and} \quad s^{(B)} = \sum_{m=0}^{N+1} \cos((2m+1)q) s^{(B)}_{2m+1}$$

and so has the solution

$$h_{2N+3}(q,p) = \sum_{m=0}^{N+1} \cos((2m+1)q) f^{2N+3}_{2m+1}(p).$$

Special care has to be taken of $m = 0$, that is the system that includes Q_{2N+2} with $A(p)$ and B. The system reads

$$\begin{aligned} (f_1^{2N+3})_{pp} - \frac{1}{\lambda^*} f_1^{2N+3} + Q_{2N+2} A(p) &= s_1^{(R)}(p) \quad p \in (p_0, 0), \\ (f_1^{2N+3})_p - \frac{g}{\lambda_*^{3/2}} f_1^{2N+3} + Q_{2N+2} B &= s_1^{(B)} \qquad p = 0 \\ f_1^{2N+3} &= 0 \qquad p = p_0. \end{aligned}$$

This system is not solvable for all values of Q_{2N+2}. To find an admissible Q_{2N+2} we consider a function that satisfies the first and third equation of this system. Such a function has the form

$$f_1^{2N+3}(p) = Q_{2N+2}\alpha(p) + \beta(p) + \mathcal{C}_{2N+3} \sinh \frac{p - p_0}{\sqrt{\lambda_*}}$$

for an arbitrary constant $\mathcal{C}_{2N+3}$. The function $\alpha(p)$ depends on $A(p)$ and $\beta(p)$ depends on the right hand side $s_1^{(R)}(p)$. Inserting this into the above Robin boundary condition gives

$$\left(\alpha'(0) - \frac{g}{\lambda_*^{3/2}}\alpha(0)\right) Q_{2N+2} + \beta'(0) - \frac{g}{\lambda_*^{3/2}}\beta(0) + BQ_{2N+2} = s_1^{(B)}.$$

Note that the contribution of the term $\mathcal{C}_{2N+3}\sinh\frac{p-p_0}{\sqrt{\lambda_*}}$ is zero. From this equation we see that Q_{2N+2} has to satisfy an equation of the form

$$\widetilde{\mathcal{C}}_1 Q_{2N+2} = \widetilde{\mathcal{C}}_2.$$

The constant $\tilde{\mathcal{C}}_1$ only depends on A and B and thus on the vorticity, but not on N. For the irrotational case it is given by

$$\widetilde{\mathcal{C}}_1 = -\frac{1}{2\lambda_*^{3/2}} \frac{\sqrt{\lambda_*}(2g + p_0\sqrt{\lambda_*})\sinh(\frac{p_0}{\sqrt{\lambda_*}}) + gp_0\cosh(\frac{p_0}{\sqrt{\lambda_*}})}{gp_0 + \lambda_*^{3/2}}.$$

Note that since $\mathcal{C}_{2N+3}$ can be chosen arbitrarily, so f_1^{2N+3} is not uniquely determined. For our numerical implementation we need to introduce and suitable constraint, see section 4.3.3. In our evaluation we considered and compared several strategies for choosing $\mathcal{C}_{2N+3}$, see section 4.4.3, note that for any strategy the resulting functions satisfy (4.1)–(4.3) up to the desired order.

With this last step we determined h_{2N+3} and Q_{2N+2} and hence

$$\begin{aligned} Q^{(2N+2)} &= Q^{(2N+2)} + b^{N+1}Q_{2N+2}, \\ h^{(2N+3)} &= h^{(2N+1)} + b^{2N+2}\left(h_{2N+2} + Q_{2N+2}\hat{f}_0\right) + b^{2N+3}h_{2N+3}. \end{aligned}$$

4.2.2 Non zero vorticity

In this section we discuss how the procedure described in section 4.2.1 can be applied if the vorticity is not equal to zero but a function $\gamma(-p)$. Instead of working with the system as is, we will transform it to an equivalent system of the form (4.10)–(4.12) to unify our numerical considerations. A similar transformation was used in [20, 48], the transformation presented here has the advantage to work for general vorticities $\gamma \in C^1$.

Let $h^{(2N+1)}$ be known, then as in section 4.2, we apply $\mathcal{H}$ and $\mathcal{B}_0$ to $h^{(2N+1)} + b^{2N+2}h_{2N+2}$ for a function h_{2N+2} of the form (4.6). Setting the coefficient belonging to b^{2N+2} to zero gives us the system

$$\begin{aligned} (h_{2N+2})_{pp} - 3\gamma(H')^2(h_{2N+2})_p + (H')^2(h_{2N+2})_{qq} &= e^{(R)} & (q,p) \in R, \\ (h_{2N+2})_p - \frac{g}{\lambda_*^{3/2}}(h_{2N+2}) &= e^{(B)} & p = 0, \\ h_{2N+2} &= 0 & p = p_0. \end{aligned}$$

Here the function H is the solution of the laminar problem, given as the first term of the expansion $h^{(2N+1)}$, namely $H = h_0$, which is a q-independent function; furthermore H' denotes the derivative with respect to p. Employing separation of variables in the above system, and exploiting the structure of the right hand side, as well as the form of h_{2N+2}, see (4.6), we obtain the following system:

$$
\begin{aligned}
(f_{2m}^{2N+2})'' - 3\gamma(H')^2(f_{2m}^{2N+2})' - (2mH')^2 f_{2m}^{2N+2} &= e_{2m}^{(R)}(p) \qquad p \in (p_0, 0), && (4.16)\\
(f_{2m}^{2N+2})' - \frac{g}{\lambda_*^{3/2}} f_{2m}^{2N+2} &= e_{2m}^{(B)} \qquad p = 0, && (4.17)\\
f_{2m}^{2N+2} &= 0 \qquad p = p_0. && (4.18)
\end{aligned}
$$

If there exists a shear flow $H = h_0$ that solves the laminar problem, then it follows from [22] that $H'(p) > 0$ for all $p \in (p_0, 0)$ which allows us the change of variables from p to $H(p)$. With this transformation we define

$$f_{2m}^{2N+2}(p) = \check{f}_{2m}^{2N+2}(H(p))H'(p),$$

which leads to a system that is equivalent to (4.16)–(4.18), namely

$$
\begin{aligned}
\frac{d^2}{dH^2}\check{f}_{2m}^{2N+2}(H) + \left[\frac{d}{dp}\gamma(p(H)) - (2m)^2\right]\check{f}_{2m}^{2N+2}(H) &= \check{e}_{2m}^{(R)}(H) \qquad H \in (0, H(0)),\\
\frac{d}{dH}\check{f}_{2m}^{2N+2}(H) + \frac{\gamma(0)\sqrt{\lambda_*} - g}{\lambda_*}\check{f}_{2m}^{2N+2}(H) &= \check{e}_{2m}^{(B)} \qquad H = H(0),\\
\check{f}_{2m}^{2N+2}(H) &= 0 \qquad H = 0.
\end{aligned}
$$

The right hand side is given by

$$\check{e}_{2m}^{(R)}(H) = \frac{e_{2m}^{(R)}(p(H))}{(H')^3} \qquad \text{and} \qquad \check{e}_{2m}^{(B)} = \lambda_* e_{2m}^{(B)}.$$

In case of linear vorticity the derivative $\frac{d}{dp}\gamma$ is constant and so the system is of the same form as in the zero vorticity case. For more general functions $\gamma(-p)$, like quadratic vorticity, we need the inverse of the transform $p(H)$ which is not readily available analytically but can be obtained numerically for computation purposes. This observation allows us to restrict our numerical considerations to system of the form (4.10)–(4.12).

We note that in the irrotational case considered in section 4.2.1 $\hat{f}_0$, the part of f_0^{2N+2} that depends on Q_{2N+2}, is given analytically. For the case of non-zero vorticity, we define $\hat{f}_0$ as the solution of

$$
\begin{aligned}
\hat{f}_0'' - 3\gamma(H')^2\hat{f}_0' &= 0 \qquad p \in (p_0, 0),\\
\hat{f}_0' - \frac{g}{\lambda_*^{3/2}}\hat{f}_0 &= -\frac{1}{2\lambda_*^{3/2}} \qquad p = 0,\\
\hat{f}_0 &= 0 \qquad p = p_0.
\end{aligned}
$$

Once we computed $\hat{f}_0$ we can apply the operators $\mathcal{H}$ and $\mathcal{B}_0$ which gives us $A(p)$ and B respectively and allows us to compute Q_{2N+2}.

4.3 Numerical Approximation

Given $(Q^{(2N)}, h^{(2N+1)})$, our aim is to compute Q_{2N+2} as well as h_{2N+2} and h_{2N+3} while preserving their structure (4.6) and (4.7) respectively. Thus we need to find approximations of

$$\begin{aligned} &f_{2m}^{2N+2}(p) \qquad m = 0, \ldots, N+1, \\ &f_{2m+1}^{2N+3}(p) \qquad m = 0, \ldots, N+1. \end{aligned}$$

To find these functions, we need to solve systems whose right hand side involve $f_{2m}^{2k}(p)$ and $f_{2m+1}^{2k+1}(p)$ for $k \leq N$ as well as their first and second derivatives, which we must assume are also just approximations. Since the approximations can at best be as good as the input data, i.e. the right hand side, we need to ensure that f and its derivatives up to second order have the same order of convergence.

To summarize, our goal is to find approximations of Q_{2N+2} and

$$\begin{aligned} &f_{2m}^{2N+2}, (f_{2m}^{2N+2})', (f_{2m}^{2N+2})'' \qquad m = 0, \ldots, N+1, \\ &f_{2m+1}^{2N+3}, (f_{2m+1}^{2N+3})', (f_{2m+1}^{2N+3})'' \qquad m = 0, \ldots, N+1. \end{aligned}$$

where all orders of convergence should match. For this we follow the algorithm outlined in section 4.2 and substitute approximations where necessary. section 4.3.1 explains how the right hand side of (4.10)–(4.12) and (4.13)-(4.15) is computed. How to solve the resulting systems is considered in sections 4.3.2 and 4.3.3 for uniquely solvable and singular systems, respectively.

4.3.1 Construction of right hand side

Recalling that the compuation of the right hand side of (4.10)-(4.15) was described in detail in [48], for matters of clarity, we consider only a specific part to illustrate the relevant procedure; the remaining part of the right hand side can be computed accordingly. Let $h^{(2N+1)}$ be known, then we are interested in the b^{2N+2}-coefficient of $\mathcal{H}[h^{(2N+1)}]$, which is the first non-zero coefficient. Here we consider the third term of $\mathcal{H}[h^{(2N+1)}]$, that is

$$h_q^{(2N+1)} h_q^{(2N+1)} h_{pp}^{(2N+1)} = \sum_{k_1=0}^{2N+1} b^{k_1} (h_{k_1})_q \sum_{k_2=0}^{2N+1} b^{k_2} (h_{k_2})_q \sum_{k_3=0}^{2N+1} b^{k_3} (h_{k_3})_{pp}.$$

Since we are only interested in the terms belonging to b^{2N+2}, let K be the set of all tuples (k_1, k_2, k_3) such that $\sum_{i=1}^{3} k_i = 2N+2$ and $0 \leq k_i \leq 2N+1$ for $i = 1, 2, 3$. We must therefore compute

$$\sum_{(k_1,k_2,k_3) \in K} (h_{k_1})_q (h_{k_2})_q (h_{k_3})_{pp}. \tag{4.19}$$

To facilitate the distinction between odd and even cases of k_i we introduce the auxiliary functions

$$N(k_i) = \begin{cases} \frac{k_i - 1}{2} & k_i \text{ odd} \\ \frac{k_i}{2} & k_i \text{ even} \end{cases},$$

$$n_{k_i}(m) = \begin{cases} 2m+1 & k_i \text{ odd} \\ 2m & k_i \text{ even} \end{cases}.$$

Now we consider one term of (4.19) and replace h_k by its definition

$$\begin{aligned}
(h_{k_1})_q(h_{k_2})_q(h_{k_3})_{pp} &= \sum_{m_1=0}^{N(k_1)} \cos'(n_{k_1}(m_1)q) f^{k_1}_{n_{k_1}(m_1)} \sum_{m_2=0}^{N(k_2)} \cos'(n_{k_2}(m_2)q) f^{k_2}_{n_{k_2}(m_2)} \\
&\quad \sum_{m_3=0}^{N(k_3)} \cos(n_{k_3}(m_3)q) \left[f^{k_3}_{n_{k_3}(m_3)} \right]'' \\
&= \sum_{m_1}^{N(k_1)} \sum_{m_2}^{N(k_2)} \sum_{m_3}^{N(k_3)} \Big\{ \sin(n_{k_1}(m_1)q) \sin(n_{k_2}(m_2)q) \cos(n_{k_3}(m_3)q) \\
&\qquad f^{k_1,k_2,k_3}_{m_1,m_2,m_3} \Big\} \\
&= \sum_{\ell=0}^{N+1} \cos(2\ell q) e^{(k_1,k_2,k_3)}_{2\ell}(p).
\end{aligned}$$

In the last step we exploited the known structure of the right hand side (4.9) which means that for all valid values k_i and m_i it holds

$$\sin(n_{k_1}(m_1)q) \sin(n_{k_2}(m_2)q) \cos(n_{k_3}(m_3)q) = \sum_{\ell=0}^{N+1} \cos(2\ell q) c^{k_1,k_2,k_3}_{m_1,m_2,m_3,2\ell}.$$

Now we collect all summands with the same value ℓ to get the desired result. Keeping track of the values k_i and $n_{k_i}(m_i)$ allows us to implement these computations exactly; no approximation in q-direction is necessary.

Finally, (4.19) can be written as

$$\begin{aligned}
\sum_{(k_1,k_2,k_3)\in K} (h_{k_1})_q(h_{k_2})_q(h_{k_3})_{pp} &= \sum_{(k_1,k_2,k_3)\in K} \sum_{\ell=0}^{N+1} \cos(2\ell q) e^{(k_1,k_2,k_3)}_{2\ell}(p) \\
&= \sum_{\ell=0}^{N+1} \cos(2\ell q) e_{2\ell}(p)
\end{aligned}$$

Doing the same for the other two terms of $\mathcal{H}[h^{(2N+1)}]$ and adding all three terms up yields the right hand side of (4.10) in the required series representation. The right hand side of the boundary condition (4.11) can be computed in the same manner but instead of functions $f^{k_i}_{n_{k_i}}$ we have to consider the functions evaluated at $p = 0$.

4.3.2 Solving the system

In this section we analyse systems of the form (4.10)–(4.12) where we applied separation of variables so that we only have to consider one–dimensional systems. These systems will be solved using a finite element approach, for more details on this see [66]. This section aims to be self–contained to avoid confusion due to notation. Where possible, we avoided to reuse symbols but in some cases that is not feasible. The most notable exception is that in this section h denotes the mesh width and not, as in the rest of this work, the wave height.

Let $\Omega = (a, b)$, $e^{(\Omega)} \in C^\infty(\Omega)$, $e^{(b)} \in \mathbb{R}$, $\alpha \geq 0$. Find $u \in H_0^1(\Omega, a)$ as the weak solution of

$$u'' - \alpha u = e^{(\Omega)} \qquad x \in \Omega, \tag{4.20}$$

$$u' - \beta u = e^{(b)} \qquad x = b, \tag{4.21}$$

$$u = 0 \qquad x = a. \tag{4.22}$$

In this section we assume that the system is uniquely solvable. The case of a singular system, see $f_1^{(2k+1)}$, is considered in section 4.3.3. The Dirichlet boundary conditions motivates the trial and test space

$$H_0^1(\Omega, a) := \{v \in H^1(\Omega) : v(a) = 0\}.$$

The associated variational formulation is to find $u \in H_0^1(\Omega, a)$ that satisfies

$$a(u, v) - c(u, v) = -\langle e^{(\Omega)}, v\rangle_{L_2(\Omega)} + e^{(b)} v(b) = F(v) \qquad \forall v \in H_0^1(\Omega, a) \tag{4.23}$$

with

$$\begin{aligned} a(u, v) &:= \int_\Omega u'(x)v'(x)dx + \alpha \int_\Omega u(x)v(x)dx, \\ c(u, v) &:= \beta u(b)v(b). \end{aligned}$$

The symmetric and bounded bilinear form $a(\cdot, \cdot)$ is $H_0^1(\Omega, a)$–elliptic by standard arguments and the non negativity of α. Considering $c(\cdot, \cdot)$, we show in Lemma 1 that the the operator $C : H^1(\Omega) \to H^{-1}(\Omega)$, induced by the symmetric and bounded bilinear form

$$c(u, v) = \langle Cu, v\rangle_{H^1(\Omega)} = \beta u(b)v(b),$$

is compact. Recall that an operator $C : X \to X'$ is compact if, for any bounded sequence $\{u_n\}_{n\in\mathbb{N}} \subset X$, the sequence $\{Cu_n\}_{n\in\mathbb{N}} \subset X'$ contains a Cauchy subsequence.

Regarding the boundedness, let $v \in H_0^1(\Omega, a)$ and $x \in \Omega$ and consider

$$\begin{aligned} v(x) &= \int_a^x v'(s)ds \\ &\leq \int_a^b |v'(s)|ds \\ &\leq \left(\int_a^b |v'(s)|^2 ds \right)^{1/2} |\Omega|^{1/2} \\ &= c|v|_{H^1(\Omega)}. \end{aligned}$$

Then it follows furthermore

$$\|v\|_\infty = \sup_{x\in\Omega} |v(x)| \leq c \, \|v\|_{H^1(\Omega)} . \tag{4.24}$$

Applying this to the definition of the norm of C,

$$\|Cu\|_{H^{-1}(\Omega)} = \sup_{v\in H^1, \|v\|=1} |\langle Cu, v\rangle_{H^1(\Omega)}| = \sup_{v\in H^1, \|v\|=1} |\beta u(b)v(b)|,$$

gives the desired result of boundedness.

Lemma 1. *The operator C is compact.*

Proof. Let $\{v_n\}_n \subset H^1(\Omega)$ be a bounded sequence such that $\|v_n\|_{H^1} \leq M \ \forall n$, then $v_n(b) \leq \|v_n\|_\infty \leq cM$. So $\{v_n(b)\}_n \subset \mathbb{R}$ is a bounded sequence and has, according to Bolzano Weierstrass, a Cauchy subsequence $\{v_{n_\ell}(b)\}_\ell$. For every $\varepsilon > 0$ there exists $N_\varepsilon \in \mathbb{N}$ such that

$$|v_{n_k}(b) - v_{n_\ell}(b)| \leq \varepsilon \qquad \forall k, \ell \geq N_\varepsilon.$$

Let $k, \ell \geq N_\varepsilon$ and consider

$$\begin{aligned}\|Cv_{n_k} - Cv_{n_\ell}\|_{H^{-1}} &= \|C_2(v_{n_k} - v_{n_\ell})\|_{H^{-1}} \\ &\leq c|\beta||v_{n_k}(b) - v_{n_\ell}(b)| \\ &\leq c|\beta|\varepsilon\end{aligned}$$

Thus $\{Cv_{n_\ell}\}_\ell$ is a Cauchy sequence in H^{-1} which proves that C is compact. □

To summarise we have shown $H_0^1(\Omega, a)$–ellipticity of $a(\cdot,\cdot)$ and compactness of $c(\cdot,\cdot)$. Together with the assumed injectivity of (4.20)–(4.22) we can employ Fredholm's alternative that shows unique solvability of the variational formulation (4.23).

We discretize the test and trial space $H_0^1(\Omega, a)$ by the space of piecewise linear, globally continuous functions $S_h^1(\Omega_h)$ with an equidistant grid Ω_h with mesh width h. A standard finite element approximation $u_h \in S_h^1(\Omega_h)$ of u leads to a uniquely solvable discrete system and error estimates [60, 66]

$$\|u - u_h\|_{L_2(\Omega)} \leq ch^2 \|u''\|_{L_2(\Omega)}, \qquad \|u - u_h\|_{L^\infty(\Omega)} \leq ch^2 \ln(h) \|u''\|_{L_2(\Omega)}.$$

As was established in section 4.3.1 we need to ensure convergence rates not only of u but also u' and u''. To this end we introduce the piecewise linear, globally continuous approximations t_h of u' and s_h of u''. Define s_h as a reformulation of (4.20)

$$s_h = e^{(\Omega)} + \alpha u_h. \qquad \in \Omega,$$

then it follows immediately that s_h converges to s in the $L_2(\Omega)$-norm quadratically. The approximation t_h of u' is found by integrating

$$\begin{aligned} t_h' &= s_h & x &\in \Omega, \\ t_h &= e^{(b)} + \beta u_h & x &= b. \end{aligned}$$

Using Simpson quadrature rule and convergence properties of u_h we find that t_h admits the same convergence rates as u_h, that is quadratic in $L_2(\Omega)$ and quadratic up to a logarithmic factor in $L_\infty(\Omega)$.

4.3.3 Solving the singular system

Consider the same problem as in the section 4.3.2, namely (4.20)-(4.22), but without assuming injectivity. Let $\Omega = [a, b]$, $e^{(\Omega)} \in C^\infty$, $e^{(b)} \in \mathbb{R}$, $\alpha \geq 0$ and $b \in \mathbb{R}$. Find $u \in H_0^1(\Omega, a)$ as the weak solution of

$$\begin{aligned} u'' - \alpha u &= e^{(\Omega)} && x \in \Omega, \\ u' - \beta u &= e^{(b)} && x = b, \\ u &= 0 && x = a. \end{aligned}$$

Then the homogeneous variational formulation

$$a(u, v) - c(u, v) = 0 \qquad \forall v \in H_0^1(\Omega, a)$$

has non trivial solutions. In fact, these homogeneous solutions are known, for the zero vorticity case they are of the form $u_0 := \kappa \sinh\left(\frac{p-p_0}{\sqrt{\lambda_*}}\right)$ with $\kappa \in \mathbb{R}$. In particular it holds for all considered vorticities $\int_\Omega u_0 \neq 0$ for $\kappa \neq 0$, so a suitable constraint for the solution u is

$$\int_\Omega u dx = \langle u, 1 \rangle_{L_2(\Omega)} = 0.$$

We incorporate this constraint into our variational formulation as a Lagrange multiplier which gives us a saddle point formulation to find $(u, \eta) \in H_0^1(\Omega, a) \times \mathbb{R}$

$$\begin{aligned} a(u, v) - c(u, v) + \eta \langle v, 1 \rangle_{L_2(\Omega)} &= F(v) \\ \langle u, 1 \rangle_{L_2(\Omega)} &= 0 \end{aligned}$$

Since $u_0 \in H_0^1(\Omega, a)$ we can use it as a test function in the original system (4.23) which gives

$$F(u_0) = a(u, u_0) - c(u, u_0) = a(u_0, u) - c(u_0, u) = 0.$$

Here we used the symmetry of a and c, the fact that $u \in H_0^1(\Omega, a)$ is a valid test function and that u_0 solves the homogeneous system. Now letting u_0 be a test function for the first equation in the Lagrange multiplier formulation reads

$$a(u, u_0) - c(u, u_0) + \eta \langle u_0, 1 \rangle = F(u_0) = 0.$$

Since u_0 solves the homogeneous formulation and $\langle u_0, 1 \rangle_{L_2(\Omega)} \neq 0$ it follows $\eta = 0$. Therefore the saddle point formulation is equivalent to find

$$\begin{aligned} a(u, v) - c(u, v) + \eta \langle v, 1 \rangle_{L_2(\Omega)} &= F(v) \\ \langle u, 1 \rangle_{L_2(\Omega)} - \frac{\eta}{\mu} &= 0 \end{aligned}$$

with a scaling parameter $\mu \in \mathbb{R} \setminus \{0\}$ we can choose freely. In all our numerical experiments we have chosen the value $\mu = 1$. This variational formulation is further equivalent to

$$a(u, v) - c(u, v) + \mu \langle u, 1 \rangle_{L_2(\Omega)} \langle v, 1 \rangle_{L_2(\Omega)} = F(v)$$

This motivates the definition of a new bilinear form

$$\widetilde{a}(u,v) := a(u,v) + \mu\langle u,1\rangle_{L_2(\Omega)}\langle v,1\rangle_{L_2(\Omega)}$$

that is still symmetric, $H_0^1(\Omega,a)$–elliptic and bounded. So the system

$$\widetilde{a}(u,v) - c(u,v) = F(v) \qquad \forall v \in H_0^1(\Omega,a)$$

is still coercive, but now also injective. The remaining analysis of the variational formulation follows as in section 4.3.2.

4.4 Numerical results

For our numerical experiments we choose the parameters in the considered systems (4.1)–(4.3) as $p_0 = -2$ and $g = 9.8$ in accordance with the numerical tests in [48, 20]. To distinguish between analytical and approximate functions and values we mark all approximations with a sub-index h.

The computation domain is either the interval $\Omega = (p_0, 0)$ which is divided into equidistant elements or its transformation as described in section 4.2.2. On this mesh Ω_h we define the space of piecewise linear, globally continuous functions $S_h^1(\Omega)$. All approximate functions, i.e. $f_{m,h}^k \approx f_m^k$, $s_{m,h}^k \approx (f_m^k)'$ and $t_{m,h}^k \approx (f_m^k)''$ are defined as elements of $S_h^1(\Omega)$. If two or more functions are multiplied, then their product is projected back into the space $S_h^1(\Omega)$. The assembly and solution of the finite element system and everything related to it, like the previously mentioned projections, are implemented using the dolfin library [53, 54], part of the FEniCS project.

Note that this algorithm does not include any approximations of the q–dependent trigonometric functions. We simply keep track of the coefficient inside and if its a sin or a cos function. The only computations necessary are integrals of the form

$$\int_{-\pi}^{\pi} \cos(a_0 q)\sin(a_1 q)\sin(a_2 q)\sin(a_3 q)dq$$

which can be done exactly.

4.4.1 Irrotational waves

First we test the convergence of our approximate solution as we increase the number of elements used to discretize Ω. Figure 4.1 shows the relative error of the $f_{m,h}^k$ in the $L_2(\Omega)$-norm as well as the relative error of the constants $Q_{k,h}$. The reference values used are analytical forms given in [48] up to h_5 and Q_4, and approximate solutions computed for 8192 grid points for terms of higher order. We observe the expected quadratic convergence for all $f_{m,h}^k$ and $Q_{k,h}$.

A second consideration is the residual of the operators $\mathcal{H}$ and $\mathcal{B}_0$ as we increase the number of expansion terms. Table 4.1 shows the results when we fix $Q = 22.05$ and use 512 elements. Fixing Q means that for every pair $(Q_h^{(2N)}, h_h^{(2N+1)})$ we have to

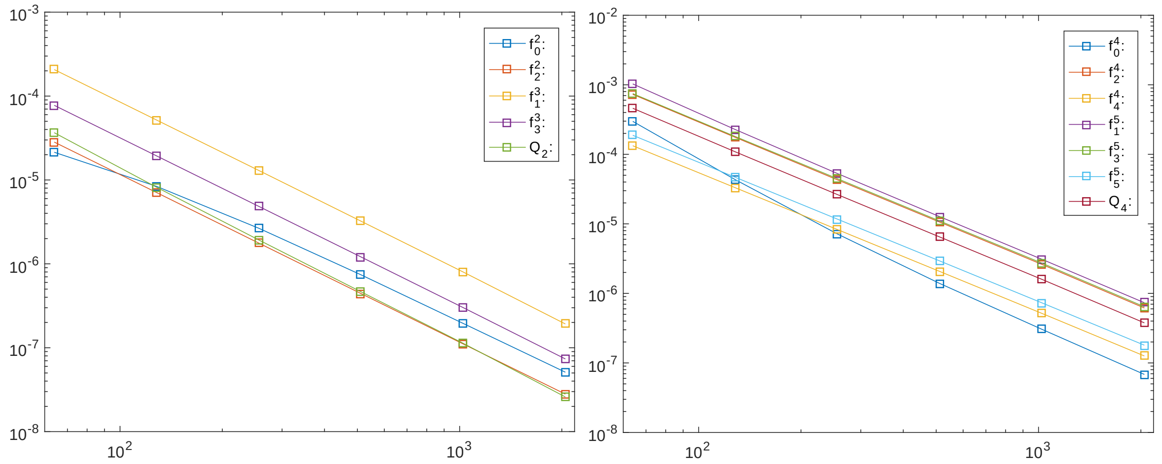

(a) $h_{2,h}, h_{3,h}$ and $Q_{2,h}$ (b) $h_{4,h}, h_{5,h}$ and $Q_{4,h}$

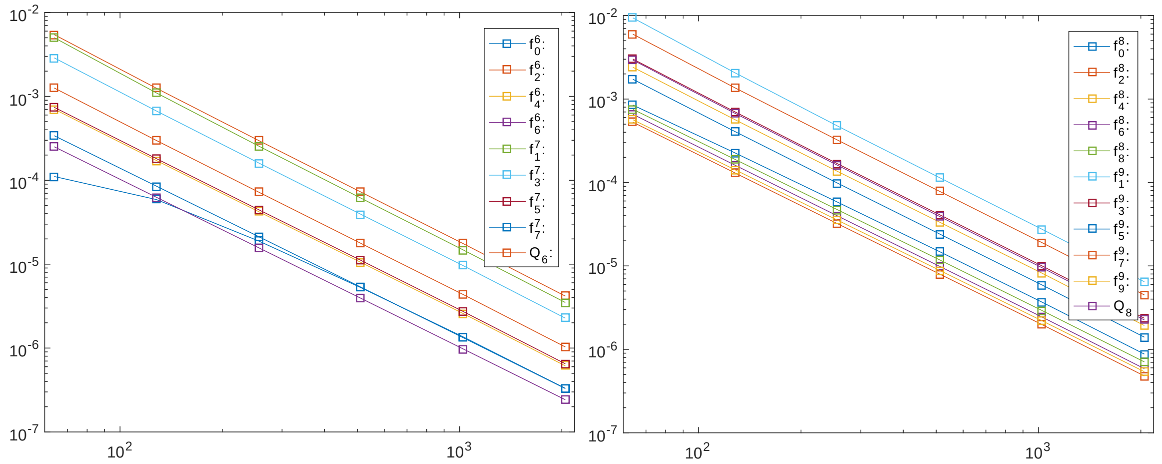

(c) $h_{6,h}, h_{8,h}$ and $Q_{6,h}$ (d) $h_{8,h}, h_{9,h}$ and $Q_{8,h}$

Figure 4.1: $||f_m^k - f_{m,h}^k||_{L_2}$ and $|Q_k - Q_{k,h}|$ vs. degrees of freedom, $\gamma = 0$.

determine b such that $Q_h^{(2N)}(b) = 22.05$, for the shown data it holds $b \in [0.1309, 0.1409]$. As one would expect, the residuals decrease as more expansion terms are added. This behaviour is not guaranteed and depends on the considered Q, values closer to Q^* lead to smaller values of b and a steeper decline, see Table 4.2, while for too large values of Q the residuals might diverge.

The third column in Table 4.1 is the relative low order error. Applying the operator $\mathcal{H}$ to the approximate solution $h_h^{(2N+1)}$ yields a polynomial in b, namely $\mathcal{H}[h_h^{(2N+1)}] = \sum_{k=0}^{6N+3} b^k r_k$. For an analytical solution it holds $r_k = 0$ for $k \leq 2N+1$ and r_{2N+2} is the first non-zero term. This motivates the definition of the error

$$E_{\mathrm{LO}}\left(h_h^{(2N+1)}\right) = \max_{k=0,\dots,2N+1} \frac{\|r_k\|_{L_2}}{\|r_{2N+2}\|_{L_2}} \tag{4.25}$$

where r_k is defined as above. Note that the contribution of this error to the total error is very small since it is additionally multiplied with b^k. We observe in Table 4.1 that the terms up to order $2N+1$ are almost zero as we would expect.

	$\|\|\mathcal{H}[h_h^{(2N+1)}]\|\|_{L_2}$	$\|B_0[h_h^{(2N+1)}, Q_h^{(2N)}]\|$	$E_{\text{LO}}(h_h^{(2N+1)})$
$Q_h^{(2)}, h_h^{(3)}$	4.51E-03	5.29E-03	1.14E-16
$Q_h^{(4)}, h_h^{(5)}$	8.50E-04	8.97E-04	2.15E-16
$Q_h^{(6)}, h_h^{(7)}$	1.63E-04	1.74E-04	3.27E-16
$Q_h^{(8)}, h_h^{(9)}$	6.35E-05	6.08E-05	2.19E-16
$Q_h^{(10)}, h_h^{(11)}$	1.49E-05	1.32E-05	3.35E-16
$Q_h^{(12)}, h_h^{(13)}$	3.31E-06	3.50E-06	3.07E-16
$Q_h^{(14)}, h_h^{(15)}$	1.12E-06	1.08E-06	4.40E-16
$Q_h^{(16)}, h_h^{(17)}$	3.66E-07	2.99E-07	2.47E-16
$Q_h^{(18)}, h_h^{(19)}$	8.85E-08	7.27E-08	3.04E-16
$Q_h^{(20)}, h_h^{(21)}$	2.18E-08	2.15E-08	5.32E-16
$Q_h^{(22)}, h_h^{(23)}$	7.67E-09	6.78E-09	4.70E-16
$Q_h^{(24)}, h_h^{(25)}$	2.24E-09	2.18E-09	3.42E-16
$Q_h^{(26)}, h_h^{(27)}$	6.91E-10	6.40E-10	6.17E-16
$Q_h^{(28)}, h_h^{(29)}$	2.21E-10	1.81E-10	4.95E-16

Table 4.1: Residual of the differential and boundary operator for $Q = 22.05$ and the relative low order error E_{LO} (4.25), $\gamma = 0$

After confirming our algorithm and implementation, we display some characteristics of the irrotational wave. Figure 4.2 shows the bifurcation diagrams for the wave height and depth as we take more expansion terms into account. Figure 4.3a shows the streamlines of the irrotational wave at $Q = 22.05$, that is the same wave as studied in Table 4.1 with wave height ≈ 0.216.

For Figure 4.5 we fixed the residual at 10^{-4} and displayed the waves we observe for different values of N. The residual was chosen rather large so that for the first order approximation a distinction from the shear flow is still visible. We see that higher order approximations allow for far larger waves while maintaining a similar residual.

4.4.2 Rotational waves

Here we present a similar result as in section 4.4.1 but for non-zero vorticity. Figure 4.6 shows the relative errors for $\gamma = 1$ as we decrease the mesh width. As in the irrotational case we observe the expected quadratic convergence rate.

Table 4.2 displays residuals of the operators $\mathcal{H}$ and $\mathcal{B}_0$ for the vorticity function $\gamma(-p) = p$. Notable is that the residuals decrease significantly faster than the ones in Table 4.1. One reason for this is that the considered value $Q = 20.69$ is relatively close to Q^* and thus the values of $b \in [0.0843, 0.0860]$ smaller than in the considered irrotational case. As expected we observe that the error of low order terms, displayed in the third column, is insignificant compared to the residual of high order terms.

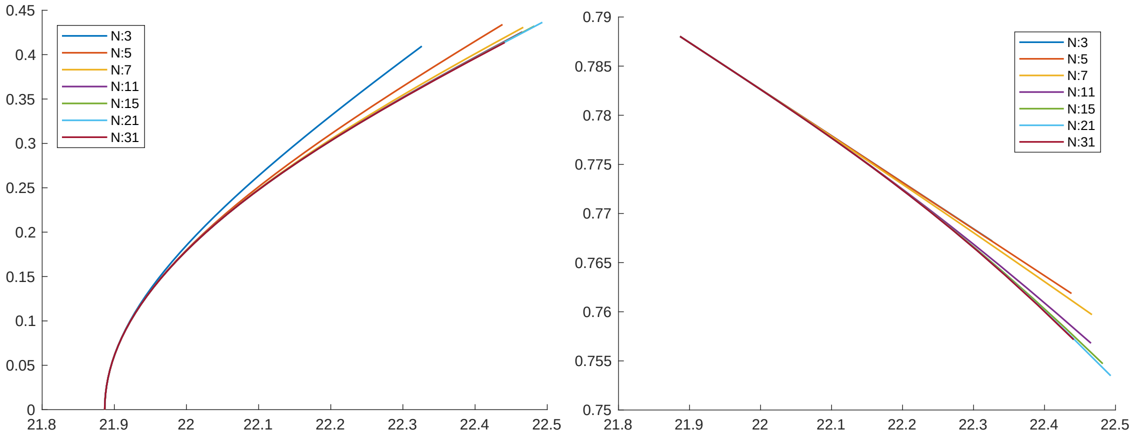

(a) Q, wave height (b) Q, depth

Figure 4.2: Bifurcation diagrams for expansions $(Q_h^{(N-1)}, h_h^{(N)})$, $\gamma = 0$.

	$\|\|\mathcal{H}[h_h^{(2N+1)}]\|\|_{L_2}$	$\|B_0[h_h^{(2N+1)}, Q_h^{(2N)}]\|$	$E_{\mathrm{LO}}(h_h^{(2N+1)})$
$Q_h^{(2)}, h_h^{(3)}$	3.37E-04	4.67E-04	8.15E-09
$Q_h^{(4)}, h_h^{(5)}$	3.02E-05	3.47E-05	8.00E-09
$Q_h^{(6)}, h_h^{(7)}$	2.18E-06	2.35E-06	9.35E-09
$Q_h^{(8)}, h_h^{(9)}$	3.11E-07	3.22E-07	6.12E-09
$Q_h^{(10)}, h_h^{(11)}$	2.67E-08	2.42E-08	7.52E-09
$Q_h^{(12)}, h_h^{(13)}$	2.06E-09	2.16E-09	8.75E-09
$Q_h^{(14)}, h_h^{(15)}$	2.40E-10	2.33E-10	7.15E-09
$Q_h^{(16)}, h_h^{(17)}$	2.70E-11	2.20E-11	6.26E-09
$Q_h^{(18)}, h_h^{(19)}$	2.26E-12	1.90E-12	6.90E-09
$Q_h^{(20)}, h_h^{(21)}$	1.92E-13	1.87E-13	7.86E-09
$Q_h^{(22)}, h_h^{(23)}$	2.27E-14	1.96E-14	6.69E-09
$Q_h^{(24)}, h_h^{(25)}$	2.25E-15	2.21E-15	6.91E-09
$Q_h^{(26)}, h_h^{(27)}$	2.36E-16	2.17E-16	7.02E-09
$Q_h^{(28)}, h_h^{(29)}$	2.49E-17	2.02E-17	7.24E-09

Table 4.2: Residual of the differential and boundary operator for $Q = 20.69$ and the relative low order error E_{LO} (4.25), $\gamma(-p) = p$

Finally we give some examples of the influence of vorticity on wave characteristics. The waves are chosen such that the residual is of same magnitude where the reference was the irrotational wave with $Q = 22.05$. In Figure 4.4 we observe that negative vorticities allow for larger waves while maintaining the same error.

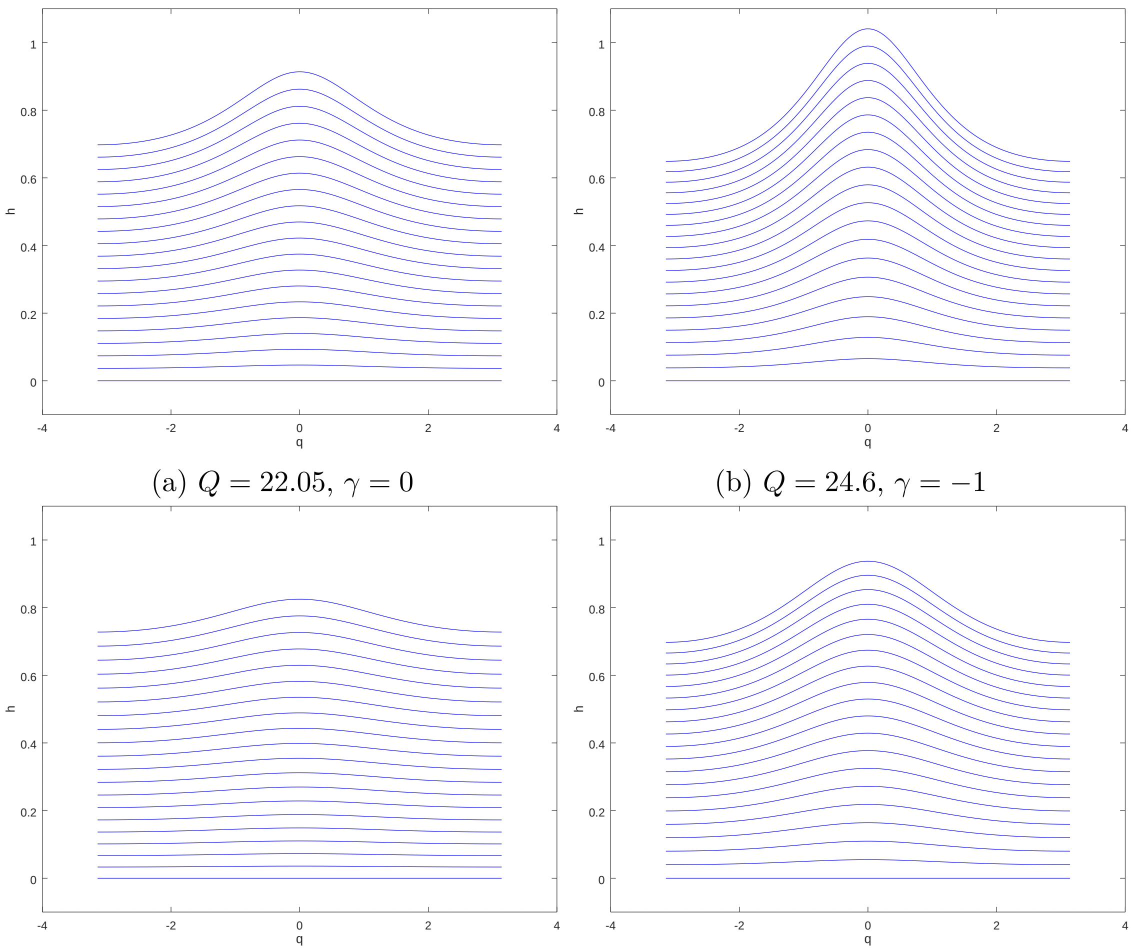

(a) $Q = 22.05$, $\gamma = 0$

(b) $Q = 24.6$, $\gamma = -1$

(c) $Q = 20.69$, $\gamma(-p) = p$

(d) $Q = 24.95$, $\gamma(-p) = p_0 - p$

Figure 4.3: Streamlines of $h_h^{(21)}$ for waves with different distributions of vorticity. The waves displayed at (a) and (c) are considered in Tables 4.1 and 4.2, respectively.

4.4.3 On the choice of $\mathcal{C}_{2k+1}$

As discussed in section 4.2.1 the function f_1^{2k+1} for $k > 1$ has the form

$$f_1^{2k+1}(p) = \tilde{f}_1^{2k+1}(p) + \mathcal{C}_{2k+1} f_1^*(p)$$

where $\mathcal{C}_{2k+1}$ is an arbitrary constant. For our numerical considerations we introduce an additional constraint to make the problem uniquely solvable, in particular we enforce

$$\int_{p_0}^{0} f_1^{2k+1}(s)ds = 0.$$

This uniquely determines f_1^{2k+1}, we denote this solution as $\hat{f}_1^{2k+1}$, and fixes $\mathcal{C}_{2k+1}$ to an unknown value. Since the function f_1^* is known we are able to compute new solutions $\hat{f}_1^{2k+1} + \alpha_{2k+1} f_1^*$ where α_{2k+1} can be any constant.

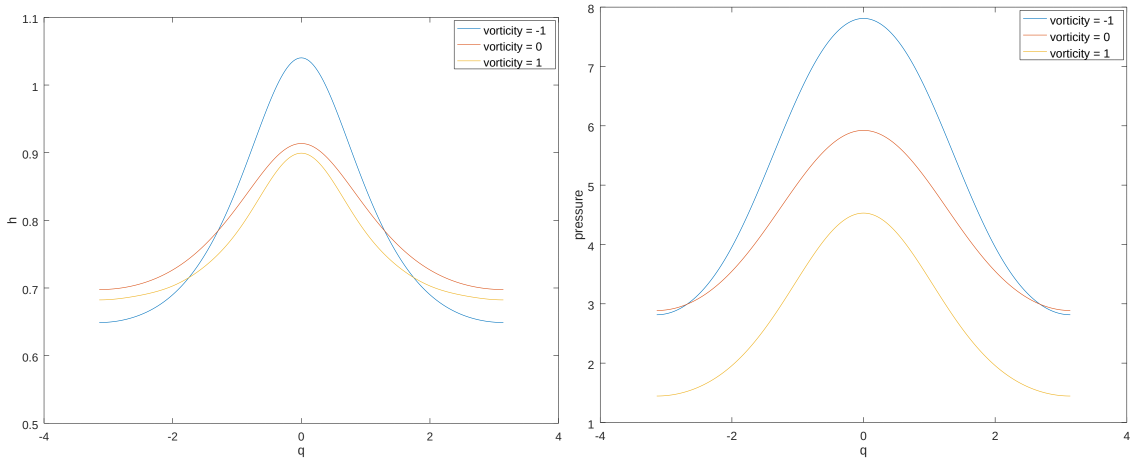

(a) Waveprofile (b) Pressure at $p = p_0$

Figure 4.4: Comparison of three waves with constant but different γ. Waves are chosen such that the residual are similar, reference was $\gamma = 0$ with $Q = 22.05$.

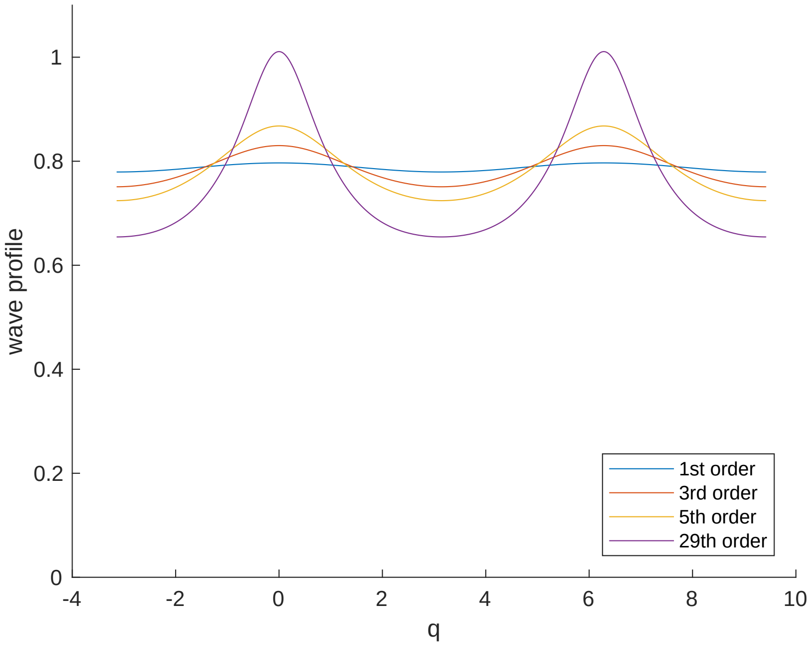

Figure 4.5: Waveprofiles for waves with residual of same magnitude, $\gamma = 0$.

In this section we introduce and compare two strategies on how to choose α_{2k+1}. The first idea, denoted as min_{L_2}, is to minimise the norm of the f_1^{2k+1}, that means choose α_{2k+1} for $k > 1$ such that the term

$$||\hat{f}_1^{2k+1} + \alpha_{2k+1} f_1^*||_{L_2(p_0,0)}$$

is minimised.

The second considered strategy min_{BC} is to choose α_{2N+1} such that the residual of

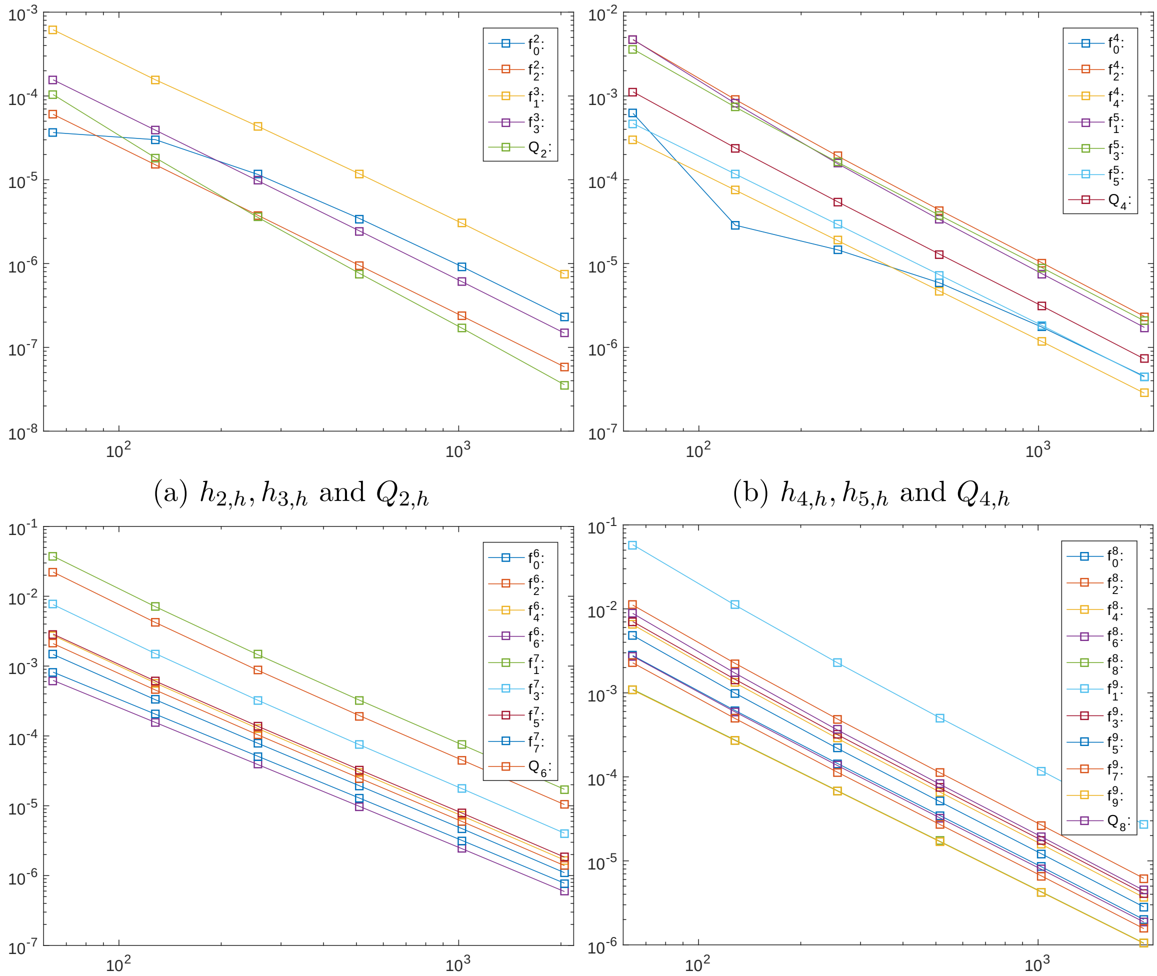

(a) $h_{2,h}, h_{3,h}$ and $Q_{2,h}$ (b) $h_{4,h}, h_{5,h}$ and $Q_{4,h}$

(c) $h_{6,h}, h_{8,h}$ and $Q_{6,h}$ (d) $h_{8,h}, h_{9,h}$ and $Q_{8,h}$

Figure 4.6: $||f_m^k - f_{m,h}^k||_{L_2}$ and $|Q_k - Q_{k,h}|$ vs. degrees of freedom, $\gamma = 1$.

the Robin boundary condition

$$||\mathcal{B}_0[h_h^{(2N+1)}, Q_h^{(2N)}]||_{L_2(-\pi,\pi)}$$

is minimised. Note that we only minimise this term for α_{2N+1}, all terms with lower order, those are α_{2k+1} with $k < N$, are fixed.

Table 4.3 shows the residual for both strategies for the first few expansion terms. Both min_{L_2} and min_{BC} give similar behaviour and no significant difference can be seen. Next we look at the corresponding values of Q_k in Table 4.4. Here the two schemes show a remarkable difference, in particular that some of the values Q_k are negative for in the min_{BC} case, this allows for turning points along the bifurcation graph. For the strategy min_{L_2}, which minimises the function norms, all observed terms of the expansion Q are positive.

In Table 4.5 and Table 4.6 we compare wave characteristics of the two strategies, namely the wave height, at two points along the bifurcation curve. Comparing the two tables we see that the difference between the strategies is larger for larger waves. This agrees with the fact that larger waves indicate larger values of b and thus more influence of higher order terms. Finally, we observe the common characteristic in both tables that by taking more expansion terms into consideration, the difference in wave height of the two strategies becomes smaller.

	min_{L_2}		min_{BC}	
	$\|\|\mathcal{H}[h_h]\|\|_{L_2}$	$\|B_0[h_h, Q_h]\|$	$\|\|\mathcal{H}[h_h]\|\|_{L_2}$	$\|B_0[h_h, Q_h]\|$
$Q_h^{(2)}, h_h^{(3)}$	4.51E-03	5.29E-03	3.51E-03	2.59E-03
$Q_h^{(4)}, h_h^{(5)}$	8.50E-04	8.97E-04	8.79E-04	7.16E-04
$Q_h^{(6)}, h_h^{(7)}$	1.63E-04	1.74E-04	1.45E-04	1.35E-04
$Q_h^{(8)}, h_h^{(9)}$	6.35E-05	6.08E-05	6.76E-05	5.57E-05
$Q_h^{(10)}, h_h^{(11)}$	1.49E-05	1.32E-05	2.28E-05	1.94E-05

Table 4.3: Residuals for different strategies, $Q = 22.05$

	Q_0	Q_2	Q_4	Q_6	Q_8	Q_{10}
min_{L_2}	21.89	10.99	69.89	1133.48	12877.58	298475.54
min_{BC}	21.89	10.99	-66.49	736.28	-18413.69	43759.28

Table 4.4: Q_k for different strategies

	min_{L_2}	min_{BC}
$Q_h^{(2)}, h_h^{(3)}$	0.135867	0.130997
$Q_h^{(4)}, h_h^{(5)}$	0.133470	0.133438
$Q_h^{(6)}, h_h^{(7)}$	0.133268	0.133269
$Q_h^{(8)}, h_h^{(9)}$	0.133256	0.133292
$Q_h^{(10)}, h_h^{(11)}$	0.133253	0.133292

Table 4.5: Wave heights for different strategies and expansion orders, $Q = 21.95$

	min_{L_2}	min_{BC}
$Q_h^{(2)}, h_h^{(3)}$	0.226957	0.206786
$Q_h^{(4)}, h_h^{(5)}$	0.217876	0.218021
$Q_h^{(6)}, h_h^{(7)}$	0.216199	0.215739
$Q_h^{(8)}, h_h^{(9)}$	0.216000	0.216508
$Q_h^{(10)}, h_h^{(11)}$	0.215913	0.216528

Table 4.6: Wave heights for different strategies and expansion orders, $Q = 22.05$

Bibliography

[1] A. Aasen and K. Varholm. Traveling gravity water waves with critical layers. *Journal of Mathematical Fluid Mechanics*, pages 1–27, 2017.

[2] M. Ablowitz, A. S. Fokas, and Z. Musslimani. On a new non-local formulation of water waves. *Journal of Fluid Mechanics*, 562:313–343, 2006.

[3] E. L. Allgower and K. Georg. *Introduction to numerical continuation methods*, volume 45. SIAM, 2003.

[4] D. Amann. On recent numerical methods for steady periodic water waves. In *Nonlinear Water Waves*, pages 139–149. Springer, 2019.

[5] D. Amann and K. Kalimeris. Numerical approximation of water waves through a deterministic algorithm. *Journal of Mathematical Fluid Mechanics*, Sep 2018.

[6] D. Amann and K. Kalimeris. A numerical continuation approach for computing water waves of large wave height. *European Journal of Mechanics - B/Fluids*, 67:314 – 328, 2018.

[7] A. C. Ashton and A. Fokas. A non-local formulation of rotational water waves. *Journal of Fluid Mechanics*, 689:129–148, 2011.

[8] S. Balay, S. Abhyankar, M. F. Adams, J. Brown, P. Brune, K. Buschelman, L. Dalcin, A. Dener, V. Eijkhout, W. D. Gropp, D. Kaushik, M. G. Knepley, D. A. May, L. C. McInnes, R. T. Mills, T. Munson, K. Rupp, P. Sanan, B. F. Smith, S. Zampini, H. Zhang, and H. Zhang. PETSc Web page, 2021. https://petsc.org/.

[9] B. Buffoni and J. Toland. *Analytic theory of global bifurcation.* Princeton University Press, 2003.

[10] W. Choi. Nonlinear surface waves interacting with a linear shear current. *Mathematics and Computers in Simulation*, 80(1):29–36, 2009.

[11] D. Clamond. New exact relations for easy recovery of steady wave profiles from bottom pressure measurements. *Journal of Fluid Mechanics*, 726:547–558, 2013.

[12] D. Clamond and A. Constantin. Recovery of steady periodic wave profiles from pressure measurements at the bed. *Journal of Fluid Mechanics*, 714:463–475, 2013.

[13] A. Constantin. The trajectories of particles in stokes waves. *Inventiones mathematicae*, 166(3):523–535, 2006.

[14] A. Constantin. *Nonlinear Water Waves with Applications to Wave-Current Interactions and Tsunamis*, volume 81. SIAM, 2011.

[15] A. Constantin. On the modelling of equatorial waves. *Geophysical Research Letters*, 39(5), 2012.

[16] A. Constantin. Estimating wave heights from pressure data at the bed. *Journal of Fluid Mechanics*, 743:R2, 2014.

[17] A. Constantin, M. Ehrnström, E. Wahlén, et al. Symmetry of steady periodic gravity water waves with vorticity. *Duke Mathematical Journal*, 140(3):591–603, 2007.

[18] A. Constantin and J. Escher. Symmetry of steady periodic surface water waves with vorticity. *Journal of Fluid Mechanics*, 498:171–181, 2004.

[19] A. Constantin and J. Escher. Analyticity of periodic traveling free surface water waves with vorticity. *Annals of Mathematics*, pages 559–568, 2011.

[20] A. Constantin, K. Kalimeris, and O. Scherzer. Approximations of steady periodic water waves in flows with constant vorticity. *Nonlinear Analysis: Real World Applications*, 25:276–306, 2015.

[21] A. Constantin, K. Kalimeris, and O. Scherzer. A penalization method for calculating the flow beneath traveling water waves of large amplitude. *SIAM Journal on Applied Mathematics*, 75(4):1513–1535, 2015.

[22] A. Constantin and W. Strauss. Exact steady periodic water waves with vorticity. *Communications on Pure and Applied Mathematics*, 57(4):481–527, 2004.

[23] A. Constantin and W. Strauss. Rotational steady water waves near stagnation. *Philosophical Transactions of the Royal Society of London A: Mathematical, Physical and Engineering Sciences*, 365(1858):2227–2239, 2007.

[24] A. Constantin and W. Strauss. Pressure beneath a stokes wave. *Communications on Pure and Applied Mathematics*, 63(4):533–557, 2010.

[25] A. Constantin, W. Strauss, and E. Vărvărucă. Global bifurcation of steady gravity water waves with critical layers. *Acta Mathematica*, 217(2):195–262, 2016.

[26] A. Constantin and E. Varvaruca. Steady periodic water waves with constant vorticity: regularity and local bifurcation. *Archive for rational mechanics and analysis*, 199(1):33–67, 2011.

[27] A. D. Craik. The origins of water wave theory. *Annual review of fluid mechanics*, 36, 2004.

[28] A. T. Da Silva and D. Peregrine. Steep, steady surface waves on water of finite depth with constant vorticity. *Journal of Fluid Mechanics*, 195:281–302, 1988.

[29] B. Deconinick and K. Oliveras. The instability of periodic surface gravity waves. *Journal of Fluid Mechanics*, 675:141–167, 5 2011.

[30] E. J. Doedel. *Numerical Continuation Methods for Dynamical Systems: Path following and boundary value problems*, chapter Lecture Notes on Numerical Analysis of Nonlinear Equations, pages 1–49. Springer Netherlands, Dordrecht, 2007.

[31] M. L. Dubreil-Jacotin. *Sur la détermination rigoureuse des ondes permanentes périodiques d'ampleur finie.* PhD thesis, Gauthier-Villars, 1934.

[32] M. Ehrnström, J. Escher, and G. Villari. Steady water waves with multiple critical layers: interior dynamics. *Journal of Mathematical Fluid Mechanics*, 14(3):407–419, 2012.

[33] M. Ehrnström, J. Escher, and E. Wahlén. Steady water waves with multiple critical layers. *SIAM Journal on Mathematical Analysis*, 43(3):1436–1456, 2011.

[34] M. Ehrnström and E. Wahlén. Trimodal steady water waves. *Arch. Ration. Mech. Anal.*, 216:449–471, 2015.

[35] J. Escher, A.-V. Matioc, and B.-V. Matioc. On stratified steady periodic water waves with linear density distribution and stagnation points. *Journal of Differential Equations*, 251(10):2932–2949, 2011.

[36] J. Escher and B.-V. Matioc. Analyticity of rotational water waves. In *Elliptic and Parabolic Equations*, pages 111–137. Springer, 2015.

[37] A. S. Fokas and K. Kalimeris. Water waves with moving boundaries. to appear *in Journal of Fluid Mechanics*.

[38] A. S. Fokas and K. Kalimeris. A novel non-local formulation of water waves. In T. J. Bridges, M. D. Groves, and D. P. Nicholls, editors, *Lectures on the Theory of Water Waves*, pages 63–77. Cambridge University Press, 2016. Cambridge Books Online.

[39] A. S. Fokas and A. Nachbin. Water waves over a variable bottom: a non-local formulation and conformal mappings. *Journal of Fluid Mechanics*, 695:288–309, 2012.

[40] D. Henry. Large amplitude steady periodic waves for fixed-depth rotational flows. *Communications in Partial Differential Equations*, 38(6):1015–1037, 2013.

[41] D. Henry. On the pressure transfer function for solitary water waves with vorticity. *Mathematische Annalen*, 357(1):23–30, 2013.

[42] D. Henry. Steady periodic waves bifurcating for fixed-depth rotational flows. *Quarterly of Applied Mathematics*, 71(3):455–487, 2013.

[43] D. Henry and A.-V. Matioc. Global bifurcation of capillary–gravity-stratified water waves. *Proceedings of the Royal Society of Edinburgh Section A: Mathematics*, 144(4):775–786, 2014.

[44] D. Henry and B.-V. Matioc. On the existence of steady periodic capillary-gravity stratified water waves. *Ann. Sc. Norm. Super. Pisa Cl. Sci. (5)*, 12:955–974, 2013.

[45] D. Henry and G. P. Thomas. Prediction of the free-surface elevation for rotational water waves using the recovery of pressure at the bed. *Philosophical Transactions of the Royal Society of London A: Mathematical, Physical and Engineering Sciences*, 376(2111), 2018.

[46] V. M. Hur. Shallow water models with constant vorticity. *European Journal of Mechanics - B/Fluids*, 2017.

[47] R. S. Johnson. *A modern introduction to the mathematical theory of water waves.* Number 19. Cambridge university press, 1997.

[48] K. Kalimeris. Asymptotic expansions for steady periodic water waves in flows with constant vorticity. *Nonlinear Analysis: Real World Applications*, 2017.

[49] P. Karageorgis. Dispersion relation for water waves with non-constant vorticity. *European Journal of Mechanics-B/Fluids*, 34:7–12, 2012.

[50] J. Ko and W. Strauss. Effect of vorticity on steady water waves. *Journal of Fluid Mechanics*, 608:197–215, 2008.

[51] J. Ko and W. Strauss. Large-amplitude steady rotational water waves. *European Journal of Mechanics - B/Fluids*, 27(2):96 – 109, 2008.

[52] F. Kogelbauer. Recovery of the wave profile for irrotational periodic water waves from pressure measurements. *Nonlinear Analysis: Real World Applications*, 22:219–224, 2015.

[53] A. Logg and G. N. Wells. Dolfin: Automated finite element computing. *ACM Transactions on Mathematical Software (TOMS)*, 37(2):20, 2010.

[54] A. Logg, G. N. Wells, and J. Hake. Dolfin: A c++/python finite element library. *Automated Solution of Differential Equations by the Finite Element Method*, pages 173–225, 2012.

[55] M. Longuet-Higgins and M. Tanaka. On the crest instabilities of steep surface waves. *Journal of Fluid Mechanics*, 336:51–68, 1997.

[56] D. V. Maklakov. Almost-highest gravity waves on water of finite depth. *European Journal of Applied Mathematics*, 13(1):67–93, 2002.

[57] B.-V. Matioc. Global bifurcation for water waves with capillary effects and constant vorticity. *Monatshefte für Mathematik*, 174(3):459–475, 2014.

[58] P. A. Milewski, J.-M. Vanden-Broeck, and Z. Wang. Dynamics of steep two-dimensional gravity–capillary solitary waves. *Journal of Fluid Mechanics*, 664:466–477, 2010.

[59] A. Nachbin and R. Ribeiro-Junior. A boundary integral formulation for particle trajectories in stokes waves. *Discrete Contin. Dyn. Syst*, 34:3135–3153, 2014.

[60] J. Nitsche. L inifity-convergence of finite element approximations. *Mathematical aspects of finite element methods*, pages 261–274, 1977.

[61] K. Oliveras and V. Vasan. A new equation describing travelling water waves. *Journal of Fluid Mechanics*, 717:514–522, 2013.

[62] K. L. Oliveras, V. Vasan, B. Deconinck, and D. Henderson. Recovering the water-wave profile from pressure measurements. *SIAM Journal on Applied Mathematics*, 72(3):897–918, 2012.

[63] R. Quirchmayr. On irrotational flows beneath periodic traveling equatorial waves. *Journal of Mathematical Fluid Mechanics*, 19(2):283–304, 2017.

[64] R. Ribeiro, P. A. Milewski, and A. Nachbin. Flow structure beneath rotational water waves with stagnation points. *Journal of Fluid Mechanics*, 812:792–814, 2017.

[65] L. Schwartz and J. Fenton. Strongly nonlinear waves. *Annual review of fluid mechanics*, 14(1):39–60, 1982.

[66] H. R. Schwarz. *Methode der finiten Elemente: eine Einführung unter besonderer Berücksichtigung der Rechenpraxis*, volume 47. Springer-Verlag, 2013.

[67] R. Seydel. *Practical bifurcation and stability analysis*, volume 5. Springer Science & Business Media, 2009.

[68] J. A. Simmen and P. Saffman. Steady deep-water waves on a linear shear current. *Studies in Applied Mathematics*, 73(1):35–57, 1985.

[69] M. Souli, J. Zolesio, and A. Ouahsine. Shape optimization for non-smooth geometry in two dimensions. *Computer methods in applied mechanics and engineering*, 188(1):109–119, 2000.

[70] G. G. Stokes. On the theory of oscillatory waves. *Trans Cambridge Philos Soc*, 8:441–473, 1847.

[71] W. Strauss. Steady water waves. *Bulletin of the American Mathematical Society*, 47(4):671–694, 2010.

[72] G. Thomas. Wave–current interactions: an experimental and numerical study. part 2. nonlinear waves. *Journal of Fluid Mechanics*, 216:505–536, 1990.

[73] G. Thomas and G. Klopman. *Gravity Waves in Water of Finite Depth*, chapter Wave-current interactions in the near shore region, pages 255–319. Computational Mechanics Publications, 1997.

[74] J. F. Toland. On the existence of a wave of greatest height and stokes's conjecture. *Proceedings of the Royal Society of London. A. Mathematical and Physical Sciences*, 363(1715):469–485, 1978.

[75] E. Varvaruca. On the existence of extreme waves and the stokes conjecture with vorticity. *Journal of Differential Equations*, 246(10):4043–4076, 2009.

[76] V. Vasan and B. Deconinck. The inverse water wave problem of bathymetry detection. *Journal of Fluid Mechanics*, 714:562–590, 2013.

[77] V. Vasan and K. Oliveras. Pressure beneath a traveling wave with constant vorticity. *Discrete Contin. Dyn. Syst*, 34:3219–3239, 2014.

[78] E. Wahlén. Steady water waves with a critical layer. *Journal of Differential Equations*, 246(6):2468–2483, 2009.

[79] S. Walsh. Steady stratified periodic gravity waves with surface tension ii: global bifurcation. *Discrete Contin. Dyn. Syst*, 34(8):3287–3315, 2014.

[80] V. E. Zakharov. Stability of periodic waves of finite amplitude on the surface of a deep fluid. *Journal of Applied Mechanics and Technical Physics*, 9(2):190–194, 1968.